Addis Ababa University
Addis Ababa Institute of Technology
African Railway Center of Excellence

Ground Penetrating Radar Simulation for Estimating Track Bed Thickness and Material Characterization.

A research submitted to the African Railway Center of Excellence (ARCE) in partial fulfillment of the requirements for the Addis Ababa Institute of Technology's Masters of Science in Railway Engineering (Civil Infrastructure)

Prepared By: Samuel Hailemariam
GSR/0617/14
Advisor: Dr. Fiseha Nega (PhD)

Date: July, 2024
Addis Ababa, Ethiopia

ADDIS ABABA UNIVERSITY
SCHOOL OF GRADUATE STUDIES
ADDIS ABABA INSTITUTE OF TECHNOLOGY
African Railway Centre of Excellence

Ground Penetrating Radar Simulation for Estimating Track Bed Thickness and Material Characterization.

By:

Samuel Hailemariam

Approved by Board of Examiners

	Name	Signature	Date
Advisor	Dr. Fiseha Nega (PhD.)	_____	_____
Internal Examiner:		_____	_____
External Examiner:-		_____	_____
Director of ARCE:-		_____	_____

DECLARATION

This is to declare that the work presented here in this thesis with the title "***Ground penetrating radar simulation for estimating track bed thickness and material characterization***" is original, has not been presented for a degree of any other university and all the resource of materials used for this thesis have been suitably cited.

Samuel Hailemariam. _____

Name Signature

The thesis has been submitted for examination with my approval as a university advisor.

Dr. Fiseha Nega(PhD). _____

Advisor Name Signature

ABSTRACT

One of the most important substructures is the railway, which is a vital component of a country and demands significant investment. A railway track bed's surface layer is a multilayered structure. Three sublayers are often present: the top surface layer, known as ballast, the intermediate surface layer, sometimes known as sub-ballast, and the subsequent surface layer (Subgrade).

An essential instrument for evaluating the status of railroad track beds is ground penetrating radar (GPR), which makes it possible to estimate the thickness of the track bed and classify the materials. . However, accurate interpretation of GPR data is challenged by the resolution limitations of GPR and the similar permittivity of track material sublayers. This study aims to verify and optimize GPR simulations using GprMax to improve the accuracy of determining track bed thickness and characterizing materials within railway infrastructure.

The research methodology involves simulating various parametric conditions such as ballast fouling, variable track bed layer thicknesses, and different moisture content scenarios (wet and dry conditions). A structured approach is employed, starting with the establishment of study area characteristics, followed by configuring the geometry and materials in GprMax. The appropriate GPR antenna and frequency settings are then defined, and simulation settings and boundary conditions are established to ensure numerical stability and accuracy.

Simulations are conducted, and the results are analyzed through post-processing techniques to examine the impact of parameter changes on GPR responses. Visualization capabilities of GprMax are utilized to compare simulated GPR scans under different conditions. The simulated results are validated against known field data or theoretical expectations to verify the simulation setup and parameters.

The study concludes that GPR simulations in GprMax can effectively model the impact of ballast fouling, layer thickness variations, and moisture content on GPR signals. These simulations provide valuable insights into improving GPR data interpretation, promoting cost-effective maintenance strategies by reducing the need for extensive physical testing. This research contributes to enhancing the reliability and efficiency of GPR in railway infrastructure maintenance.

Key words: Ground Penetrating Radar (GPR), Track bed, GprMax software, Post-processing and Numerical modeling (Simulation).

ACKNOWLEDGMENT

First and foremost, I would want to express my gratitude to God, the Almighty, for His many gifts that enabled me to successfully complete my studies.

I would like to thank my advisor, Dr. Fisha Nega Birhane, for their invaluable guidance and support. Their expertise and insights have been instrumental in shaping this research and improving its quality. I am truly grateful for their patience, availability, and dedication to my academic development.

I would like to acknowledge the support and assistance provided by African Railway Center of Excellence. Their provision of resources, access to data, and financial support have been crucial in conducting this research. I am grateful for their collaboration and willingness to contribute to the advancement of knowledge in this field.

I would like to express my gratitude to my colleagues and friends who have provided valuable insights, discussions, and moral support throughout this journey. I am thankful for their willingness to share their expertise and engage in thought-provoking conversations.

Furthermore, I would like to thank the GprMax Google Group participants of this study for their time, cooperation, and willingness to share their experiences and guidance.

Lastly, I would like to acknowledge the unwavering support of my family. Their understanding, patience, and encouragement have been a constant source of motivation during challenging times. I am deeply grateful for their belief in me and their unwavering support throughout this thesis journey.

In conclusion, I am truly grateful to all those who have contributed to the successful completion of this thesis. Their support, guidance, and assistance have been invaluable, and I am honored to have had the opportunity to work with such remarkable individuals and organizations.

Samuel Hailemariam

July, 2024

TABLE OF CONTENTS

LIST OF TABLES

LIST OF FIGURES

LIST OF ACRONYMS

ε_r- RELATIVE ELECTRIC PERMITTIVITY

μ_r- RELATIVE MAGNETIC PERMEABILITY

ABC - ABSORBING BOUNDARY CONDITIONS

CAD - COMPUTER AID DRAFTING

CB - CLEAN BALLAST

CMP - COMMON MIDPOINT TEST

CRIM - COMPLEX REFRACTIVE INDEX METHOD

CRS - COMMON REFLECTION SURFACE TEST

FDTD - FINITE-DIFFERENCE TIME-DOMAIN

FFB - FULLY FOULED BALLAST

FI - FOULING INDEX

GPRMAX – SOFTWARE TOOL (GROUND PENETRATING RADAR AND MAXWELL EQUATION)

GSSI - GEOPHYSICAL SURVEY SYSTEMS, INC.

GUI - GRAPHICAL USER INTERFACE

NDT – NON DESTRUCTIVE TEST

PEC - PERFECTLY ELECTRIC CONDUCTOR

PFB - PARTIALLY FOULED BALLAST

PML - PERFECTLY MATCHED LAYER

RX – RECEIVER ANTENNA

SNR - SIGNAL-TO-NOISE RATIO

SRC - SURFACE REFLECTION COEFFICIENT

STFT - SHORT TIME FOURIER TRANSFORM

TWTT - TWO-WAY TRAVEL TIME

TX – TRANSMITTER ANTENNA

(σ) - ELECTRICAL CONDUCTIVITY

1. INTRODUCTION

1.1. Background

Railway convoys use both ballasted and non-ballasted tracks to transport large numbers of commuters, freight, and bulk products every day. The function of railroads in linking residential and production areas has grown increasingly important over time, leading to significant advancements in the technological performance of the convoys, which in turn depend on the track beds for sufficient support. To guarantee appropriate safety and operational conditions at the network level, railway track beds require more efficient and timely maintenance. [1]

Currently, two important factors need to be considered. “Initially designed for lower loads and speeds, the increased axle loads and traffic speeds on pre-existing buildings However, climate changes are important factors that can damage the structure due to high temperatures or severe rains.” These cause faster track deterioration, which has the knock on effect of lowering performance and service quality. On the other hand, the construction industry contributes significantly to national growth and job creation in developing countries such. But a variety of obstacles are impeding and testing the sector's management methods. Numerous studies agreed that the industry's shoddy construction management system contributes to shoddy construction. These days, the main focus of track monitoring is the assessment of metrics pertaining to rail wear and track geometry. Among the real causes of inadequacies that this monitoring technique misses are subgrade settlements, unclean ballast, transition problems, inadequate drainage, and ballast pockets. [1]; [2].

Thus, the evaluation of the substructure condition is a crucial component in the maintenance choice. A popular geophysical method called ground penetrating radar (GPR) uses data from the propagation of electromagnetic (EM) waves to examine pertinent underlying structures. [3]. The electromagnetic (EM) impulse that is partially transmitted and partially back-reflected at every specific dielectric contrast found across the medium is emitted by a source inside the GPR system.

Understanding the components required to build a simple simulator could be a very helpful method of understanding the nature and content of GPR radiograms for a particular GPR signal. The simulator would assist explain how concealed target structures are converted into recorded reflection profiles and offer a way to anticipate radiograms taken across candidate models of the

ground. The simulator can demonstrate the shortcomings of this remote sensing technique while also showcasing GPR's potential and the subsurface conditions in which it can and cannot operate at its best.

In order to estimate recorded reflections over the model, the simulator must take into consideration both the engineering design of the simulated GPR equipment and the theory of electromagnetic radar wave propagation. Earth Model, Reflection, Transmission Refraction, Attenuation, and Antenna Pulse are among the fundamental parameters that must be specified and incorporated into the simulator. [4]

1.2. Problem Statement

Currently, organizations in the railway industry use a destructive method to measure the thickness and characteristics of the track bed layer: they remove the track substructure cores. Since cores are normally taken at intervals of between 50 and 100 meters, this approach gives very little data, is time-consuming, dangerous, and requires traffic management, but it also yields thickness measurements that are fairly accurate.

In order to support the traffic of revenue trains, railroad track engineers are concentrating on cost effective track maintenance. Therefore, to increase efficiency, it is necessary to recognize railway track repair needs effectively and organize maintenance actions. Identification and diagnosis of track support issues is one area that needs to be improved to guarantee safe train operations and effective maintenance. So Using Ground penetrating radar (GPR) survey is efficient process survey method for track bed defect investigation and characterization.

Track bed thickness and material classification can be estimated from Ground Penetrating Radar (GPR) data. However, because of the limited GPR resolution and the identical permittivity of the track material sublayer, estimating thickness and classifying the material type are difficult tasks.

The basic challenge of interpreting GPR data is the complexity and variability of the signals received. GPR signals can be affected by various factors such as the type of subsurface material, moisture content, presence of objects or anomalies, and the depth of the target.

These factors can cause variations in signal amplitude, frequency, and shape, making it difficult to accurately interpret the data. Additionally, GPR signals can be affected by noise and interference from other sources, further complicating the interpretation process. Therefore, interpreting GPR data requires expertise and experience in understanding the characteristics of different materials and their corresponding signatures in GPR signals.

1.3. Research Objectives

1.3.1 General Objective

This study's primary goal is to verified and optimize ground penetrating radar (GPR) simulations in GprMax for accurately determining trackbed thickness and characterizing materials within railway infrastructure.

1.3.2 Specific Objectives

This thesis's particular goals are:

- Evaluate how varying degrees of ballast fouling affect GPR signal penetration and reflection characteristics. By using numerical modelling, develop more advanced ballast fouling condition models to be as close as possible to reality.
- Investigate how changes in ballast layer thicknesses influence GPR detection capabilities and compare different antennas to ensure they meet the requirements of the project.
- Assess the effects of ballast moisture content (wet vs. dry conditions) on GPR signal propagation and reflection characteristics.
- Verified the capability of GPR simulations to accurately predict trackbed layer thicknesses under varying conditions.
- The intention is to eliminate the need for cost-effective physical models by enabling professionals and academics to mathematically experiment with GPR on their computers.

1.4. Research Questions

This thesis's particular goals are:

- How can the dielectric constant of various materials be estimated?
- How thick is the track bed layer estimated?
- How can different ballast fouling conditions classified based on non-destructive testing such as GPR?
- What kind of GPR antennas are more effective for accurate interpretation?
- Which kind of track bed material negatively affects the performance of the GPR antenna more?
- What kind of simulation model environments is good homogeneous or heterogeneous model representative?

1.5. Significance of the Study

The study's conclusions are significant for the global railway sector. A popular geophysical method called ground penetrating radar (GPR) uses data from the propagation of electromagnetic (EM) fields to examine pertinent subsurface railroad characteristics. However, handling GPR signal data that has a lot of noise at a location with complicated ground conditions frequently requires the expertise of specialists, and accurate analysis is challenging. The simulator would assist explain how concealed target structures are converted into recorded reflection profiles and offer a way to anticipate radiograms taken across candidate models of the ground. The simulator can demonstrate both the advantages and disadvantages of this remote sensing technique.

1.6. Research Methodology

The Ground Penetrating Radar simulation structured methodology can be used with GprMax to simulate the study area of a parametric condition are ballast fouling situations, variable trackbed layer thicknesses investigation, and varying ballast wet and dry conditions. Establish the characteristics and study area first. These are Give precise instructions on the size and configuration of the trackbed area which are modeling. Indicate the composition and densities of the various levels (such as subgrade, ballast, and sub ballast). Ascertain the differences in fouling levels and ballast moisture content in both wet and dry circumstances.

Second, configure GprMax's geometry and materials, which Using GprMax, create a 2D model of the trackbed. Define the dimensions in light of the research field and Give each layer a material property designation (e.g., ballast, sub ballast, subgrade). Dielectric constants, electrical conductivity, and density are a few examples of these that might change depending on the fouling level and moisture content.

Third, indicate the type of ground-penetrating radar (GPR) antenna (such as a dipole or horn) and its location in relation to the layers of the trackbed. Based on the required depth of penetration and resolution for identifying various materials and circumstances, choose the right frequencies. Describe the GPR system's waveform properties, such as the Gaussian pulse.

Fourth, include simulation settings and boundary conditions. Set up boundary conditions to reduce reflections at model boundaries, such as perfectly matched layers (PML). To guarantee numerical stability and accuracy, choose a suitable time step for the simulation based on the GPR waveform's highest frequency component. Based on the anticipated arrival times of reflections from deeper layers, calculate the total simulation time.

Fifth, carry out simulations and examine the outcomes. Use GprMax to run the simulations for every scenario that has been defined. Using post processing, one can examine the output data, such as frequency-domain spectra and time-domain signals, to understand how parameter changes impact GPR responses. Create images of simulated GPR scans using GprMax's visualization capabilities, then compare them in various contexts.

Finally, verify and interpret the results. Compare the simulated results with known field data or theoretical expectations to verify the simulation setup and parameters. Draw conclusions about the sensitivity of GPR to various trackbed conditions (fouling, layer thickness, and moisture content) based on simulation outcomes.

By following this methodology in GprMax, you can effectively simulate and analyze the impact of ballast fouling conditions, different trackbed layer thicknesses, and varying ballast wet and dry conditions on GPR signals within your selected study area.

1.7. Scope and Limitation of the Study

1.7.1. Scope of the Study

This study employs the open-source, Python-based gprMax code to present a numerical modeling technique that can quantitatively simulate the GPR signal characteristics based on the degree of fouling, track bed layer thickness estimation, and dry and wet track bed material condition.

1.7.2. Limitation of the Study

This research is restricted to confirm the accuracy of the simulation model which can provide valuable insights into the signal response of different ballast conditions, track bed layer thickness and moisture content, to validate these findings through field investigations in real-world scenarios.

1.8. Thesis Structure

This study is divided into six chapters after an introduction. The introduction to the thesis is covered in Chapter 1, along with the basic overview of GPR numerical modeling simulation, problem formulation, objectives, methodology, study scope and limitations, and the study's importance.

Chapter two includes a summary of the reviewed literature, forming the foundation for this simulation model. A general review about railway track bed, track bed ballast, GPR theory and properties, GPR studies and railway applications. Modelling GPR using gprMax was also described.

Chapter three briefly illustrates the study area and model simulation environment. This section focuses on three specific aspects of the study area selection: layer thickness estimation, ballast fouling condition, and ballast water content/anomaly investigation.

Chapter four discusses the identified results of model simulation output data. The discussion assesses comparing different GPR antennas, Estimating dielectric constant, estimating layer thickness and investigating dry and wet ballast water condition.

Chapter Five verified the simulated results with known laboratory experimental data or theoretical expectations to verify the simulation setup and parameters.

Chapter six conclude the research conclusions based on the simulation result and gives further recommendations.

2. LITERATURE REVIEW

2.1 Overview

The thorough literature review for ground penetrating radar properties and railway track-bed characterization is compiled in this chapter. First, the definition and characterization of the railway track-bed are emphasized. For a deeper comprehension of the railway system, the primary manuals and specifications pertaining to railway infrastructure are examined. Additionally, this chapter provides an overview of other studies of a comparable nature as well as the Multi Criteria Decision Making methods used in the Ground Penetrating Radar.

2.2. Definition of Track bed

Different countries, design standards, literature, and academics use different terms to refer to track-bed layers. It is referred to as "Track Pavement" layers in certain texts and as "Subsystem of Superstructure" in others. Track-bed as components of a ballast-less track made of reinforced concrete, regular concrete, or asphalt foundations. [5]

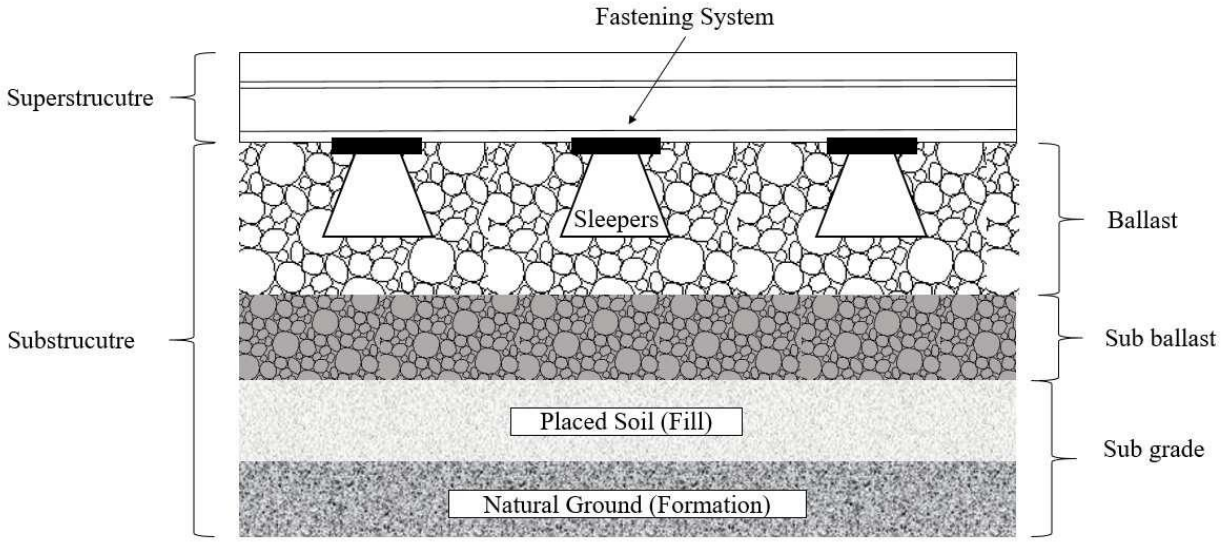

Figure 2.1. An example of many track element terms from literature [6]

There are two primary reasons why track-bed terminology is used:

1. Whether to regard the sub and protection layers as part of the substructure and just consider the track-bed on the superstructure portion (ballast, concrete, or asphalt layer) or
2. To consider all of the layers beneath sleepers up to the top of the subsoil as a track-bed layer.

The second definition is applied in this study. As a result, the track-bed of a ballasted track system may include subgrade, protective layers, ballast, and subballast. In contrast, the track-bed of a ballast-less track system may have a concrete slab, foundation, and/or formation layers, including subgrade, asphalt, unbound granular material, protection layer, and concrete treated base. The design requirements, including major geological and subsurface conditions, permanent way design, traffic and train loading, geographical and climatic conditions (topography, temperature changes, frost action, and rain intensity), water table level, drainage system, and a few other minor factors, all influence the composition of track-bed layers. The use of various material kinds, variations in the stiffness, and the thickness of the track-bed layers are all topics covered in the numerous research projects that have been conducted thus far. [7]

2.3. Track bed Ballast

"Ballasted train lines use a ballast layer of crushed granule material between the sleepers and the subgrade. The ballast layer must perform several vital functions in order to maintain the track body's geometric stability and ensure the railway runs safely and dependably." [8]

2.3.1. Objective and Features

Most significantly, the ballast resists longitudinal, lateral, and vertical stresses, disperses pressure from the sleepers to acceptable levels for the subgrade, helps absorb shocks from dynamic loads, and permits water to promptly drain through the ballast away from the rails and sleepers. [8]

The ballast needs to preserve a number of intrinsic qualities in order to carry out these functions. The most widely employed hard, angular particles of high-strength rocks provide the ballast body with strength and internal friction while also allowing enough void space between the particles to allow drainage. But eventually, the ballast will begin to lose its empty spaces and strength. Either the aggregate material deteriorates mechanically or other contaminants (fines, fluids, organic material, etc.) are introduced into the ballast, contaminating it.

Four zones can be distinguished in the ballast body, as determined by [8]:

- Crib - substance in "between sleepers"
- Shoulder - Beyond the sleeper, the material descends to the ballast layer's bottom.
- Top ballast - the top part of the ballast layer that is disturbed by tamping.
- Bottom ballast - lowest part of the supporting ballast layer, which is typically the more polluted part and is not disturbed by tamping

2.3.2. Faults and Deterioration of Ballast

The fundamental reasons and processes that lead to ballast failures and deterioration are a broad topic. We are concentrating on a few specific scenarios in this study that have been shown to degrade the track body's or ballast's structural qualities. [9].

2.3.2.1 Fouling of Ballast

Ballast fouling, which is used to indicate contamination by fines, can take several forms and have a variety of reasons. It is thought to be the primary cause of ballast issues. [8]; [9] categorized the fouling causes into five groups, each of which had a different contribution.

- Breakdown of ballast (75 %)

In addition to some material wear from tamping, initial transport, and handling, ballast breakdown happens when the angular edges of the ballast material break off into smaller pieces as a result of repetitive cyclic pressure from track traffic. [10]

- Penetration from the granular layers underneath (14 %)

The upward migration of particles from lower ballast layers is referred to as infiltration from underlying granular layers.

- Ballast surface infiltration (6 %)

When spilled particles from passing trains (such coal or mineral ore) or air or water debris get inside the ballast surface.

- Infiltration of the subgrade (4 %)

When the finer subgrade grains go higher into the ballast, it's known as subgrade infiltration. The most frequent correlation between this procedure and the track body's undrained water content.

- Wearing sleepwear (1 %)

Sleeper wear is caused by the degradation of the sleepers under cyclic traffic loading. . The fouling materials, particularly when combined with water, not only fill the vacuum areas used for drainage, but they also lubricate the contact interface between the angular rocks.

2.3.2.2 Pockets of Ballast Caused by Subgrade Depressions

Under the repetitive stress of passing wheel loads, loose or fine-grained soils with excessive moisture content can cause subgrade depressions. A ballast pocket is created when a depression appears in the top formation or subgrade beneath the rails. [11] This depression will begin to collect water because it can no longer drain correctly, eventually filling the ballast pocket and weakening the subgrade even more.

2.3.2.3 Burrows of Animals

The presence of wildlife beside the track poses a number of difficulties for railroad operations. Smaller animals creating tunnels or dens in the subgrade of embankments is one such problem. According to Ralcorp Network and Network Rail, this kind of animal infestation is a common issue in some parts of the world and might jeopardize the track body drainage system's ability to function and, eventually, the stability of the embankments. .[11]

2.3.2.4 Moisture/Water Retention

Water will begin to build up in the track body if the drainage system isn't working properly. The ballast's shear strength and stiffness are decreased, and the deterioration and fouling process is accelerated, when trapped water is present. . [10]

According to [9], “causes of restricted drainage may include”:

- Formation of ballast pockets due to subgrade settlement
- Ballast shoulder that is fouled
- Low permeability border near the ballast's edge
- Lack of a ditch to remove water from the track as it exits the ballast causes ponding of water next to the track.
- The sub ballast surface's lateral slope is insufficient to channel water to the track's side.

2.4. GPR Properties and Theory

Ground Penetrating Radar (GPR) is a technique that detects reflections from subsurface structures by moving electromagnetic antennae across a surface.[3] [12] initially tried the idea as a means of determining the water table in the desert of Egypt. The idea found new uses during the following thirty years, such as archeological surveys and measures of ice thickness. Beginning in the late 1980s, as computational power increased rapidly, GPR began to be recognized as a promising technology for a growing number of uses, leading to the diverse applications and research that are currently being conducted. . [13]

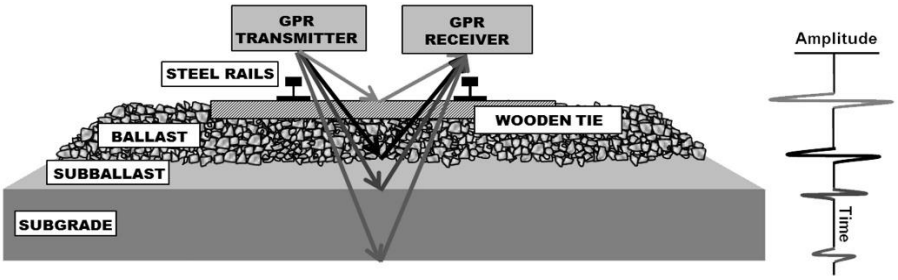

Figure 2.2: GPR is utilized to evaluate railroad ballast. . [14]

A continuous profile of the track-bed structure can be obtained by using ground penetrating radar, a non-destructive technique for scanning a section of track. . [15] This offers substantial benefits over the conventional method of subjective eye assessment and sample drilling. Track GPR scans offer quantifiable and objective information on the ballast/formation interface and track bed anomalies. Its use allows for the assured prioritizing of planned maintenance, cutting down on wasteful spending by only performing work where it is required. . [16]

2.4.1. Theory

To provide an approximate image of the subsurface without affecting the scanned region, GPR surveying uses the propagation of electromagnetic waves and, therefore, the magnetic and electric characteristics of the materials in the ground. .

2.4.2. Dielectric Properties

The underlying materials are often called dielectrics, and the permittivity and conductivity parameters that affect the electric and magnetic fields are called the dielectric characteristics. These characteristics are crucial for GPR applications since they aid in determining the substance, form, and depth of buried barriers. [2]

Equation below is used to compute relative magnetic permeability (,-$\boldsymbol{r}$.) and relative electric permittivity (,$\boldsymbol{\varepsilon}$-$\boldsymbol{r}$.) in relation to the dielectric characteristics of free-space. There are no physical dimensions to the relative dielectric characteristics. The relative permeability of non-magnetic materials is 1. .[17]

$$\varepsilon_r = \frac{\varepsilon_s}{\varepsilon_0} \qquad\qquad \mu_r = \frac{\mu_s}{\mu_0}$$

Where:

ε_r = Permittivity of relative static

ε_s= F/m, or static permittivity

ε_0= Free-space permittivity (,8.854 x 10-−12.F/m)

μ_r = permeability of relative static

μ_s= Permeability of statics (H/m)

μ_0 = Permeability of free space (,4π x 10-−7.H/m)

2.4.2.1. Relative permittivity (ε_r)

A material's ability to store electrical energy in an electric field is gauged by its relative permittivity, sometimes referred to as its dielectric constant. The symbol εr is used to symbolize it. In the context of GPR, The term "relative permittivity" describes a material's capacity to either transmit or reflect electromagnetic waves. Different materials have different relative permittivity values, which affects the speed at which electromagnetic waves travel through them. For example, materials with high relative permittivity, such as water or moist soil, tend to slow down the propagation of electromagnetic waves, while materials with low relative permittivity, such as air or dry soil, allow waves to travel faster. [2]

2.4.2.2. Relative Permeability (μ_r)

Relative permeability, on the other hand, is a measure of how easily a material can store magnetic energy in a magnetic field. It is represented by the symbol μr. In GPR, relative permeability is less significant compared to relative permittivity because the majority of GPR applications use non-magnetic materials such as soil, concrete, or asphalt. However, in certain cases where magnetic materials are present, such as in the detection of buried metallic objects, relative permeability can affect the behavior of electromagnetic waves. [2]

2.4.2.3. Electrical Conductivity (σ)

The attenuation of the signal is influenced by the electrical conductivity (σ), which is a measurement of the free charge flow in the material. A large portion of the electromagnetic energy will be lost as heat by conduction in a material with a high value of σ. Because of this, surveying in high-electric conductivity mediums (such as metals, saline solutions, or environments rich in clay) results in substantial signal attenuation and effectively restricts the depth of signal

penetration. They are referred to as "loss" materials. . [18] Additionally, it reduces the intensity of reflected signals, making the GPR essentially useless in these conditions. Both material conductivity and antenna frequency increase signal attenuation. [2]

Up to about 19 GHz, the signal attenuation caused by free water will rise as the signal frequency increases. The effect is already apparent at 1-2 GHz, despite the fact that this is much outside the frequency range of GPR radars. This implies that high-frequency surveys conducted on specific kinds of wet materials may have even less penetration depth. . [13]; [2]

2.4.3. GPR Data Presentation Types

There are three ways to represent GPR data: Three scans: A, B, and C .

- A-Scan

A-Scan, often known as a trace, is a one-dimensional graphic. It shows a time variation of the recorded signal amplitude and is a series of sample points gathered by the GPR at a fixed antenna position. [19]. It plots the time histories of the currents and electric and magnetic field components for each receiver in a model (each receiver gets a separate figure window)

- B-Scan

As GPR travels in a straight line above the ground, the B-Scan is a two-dimensional map that shows an ensemble of A-scans. The vertical axis shows the range or amount of time it took for the pulse to return, while the horizontal axis shows the scan length or number of traces. . [19]

- C-Scan

A three-dimensional representation of GPR data, known as a C-Scan, is produced by stacking B-scans side by side. It can also be shown as a set of horizontal slices, each of which represents a different depth or sample point. [19]

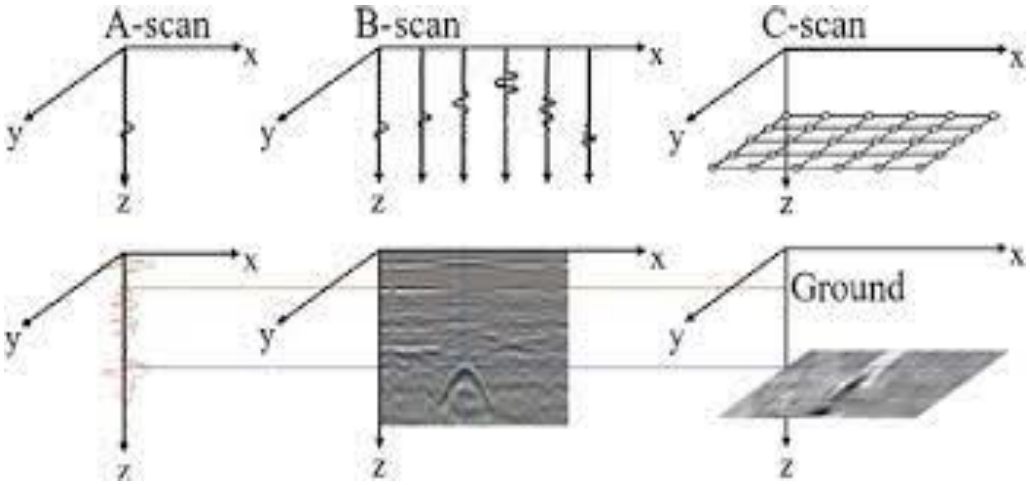

Figure 2.3: Co-ordinate systems for scan description [19]

1.5. GPR Research and Use in Railroads

Numerous studies have been conducted on the subject as a result of the high expense of track maintenance today and the enormous potential that GPR technology offers. GPR has only recently been used for railway track surveys, and further study is needed to fully map its capabilities and accuracy in this application. An overview of some of the most pertinent applications and research on the topic is provided below.

1.5.1. Assessing the Thickness of the Ballast Layer

Maintenance workers can evaluate the general performance and condition of an operational rail line by being aware of the track ballast layer's thickness . To disperse the loads from the sleepers across the contact between the ballast and the subgrade, the layer must be a specific thickness; if the layers are too thin in some places, the sections will be more vulnerable to adverse riding conditions and faster ballast deterioration.

Variations in the thickness of the ballast layer along a track are not unusual. The ballast/subgrade contact cannot be expected to stay at a consistent depth over a track's length due to local repairs following derailments or embankment failures, fluctuating ballast levels brought on by lower-quality ballast, or similar circumstances.

Several studies have used GPR surveying data to successfully determine the thickness of continuous ballast layers with a high degree of precision. [16]; [20] This can be detected thanks to the distinct interface reflection provided by the ballast-to-subgrade transition. The actual thickness

of the ballast layer can be ascertained by calculating the signal velocity and its depth. To use this strategy accurately, there are a few requirements, though.

- A clear interface e

Although there is typically a considerable interface reflection from the ballast/subgrade contact, this depends on the media having a large dielectric permittivity difference. It will be more challenging to determine the precise depth of the ballast layer if the ballast has degraded or gradationally fouled close to the bottom of the track bed (for example, due to subgrade infiltration). This will result in a considerably less defined interface signature. [15]; [23] Therefore, a failure to accurately identify the ballast/subgrade contact on GPR scans could be an indication of ballast fouling on its own.

- Precise signal propagation speed y

A crucial component of depth calculation is signal propagation velocity, which varies depending on the investigated medium's dielectric characteristics. For uniform materials with well-known dielectric characteristics, this is not an issue; nevertheless, the dielectric permittivity of ballast will change depending on factors like moisture content, void content, and fouling level. [22] According to research on the topic, ballast's degree of fouling can be used to predict signal propagation velocities. Combining the efforts of [22] and [23] gives the values in table 2.1.

Material	***Er, Annan and Davis (1989)***	***Er; Daniels (1996)***	***Velocity (m/ns)***	***Velocity (ft/ns)***
Air	*1*	*1*	*0.3*	*0.98*
Distilled water	*80*		*0.03*	*0.11*
Fresh water	*80*	*81*	*0.03*	*0.11*
Sea water	*80*		*0.03*	*0.49–0.57*
Fresh water ice	*3–4*	*4*	*0.15–0.17*	*0.35–0.49*
Sea water ice		*4–8*	*0.11–0.15*	*0.28–0.35*
Snow		*8–12*	*0.09–0.11*	*0.35–0.50*
Permafrost		*4–8*	*0.11–0.16*	*0.40–0.57*
Sand, dry	*3–5*	*4–6*	*0.12–0.17*	*0.18–0.31*
Sand, wet	*20–30*	*10–30*	*0.05–0.09*	*0.57–0.70*
Sandstone, dry		*2–3*	*0.17–0.21*	*0.31–0.44*
Sandstone, wet		*5–10*	*0.09–0.13*	*0.35–0.49*
Lime stones	*4–8*		*0.11–0.15*	*0.37*

Limestone, dry		*7*	*0.11*	*0.35*
Limestone, wet		*8*	*0.11*	*0.25–0.44*
Shales	*5–15*		*0.08–0.13*	*0.33–0.40*
Shale, wet		*6–9*	*0.10–0.12*	*0.18–0.44*
Silts	*3–30*		*0.05–0.13*	*0.16–0.44*
Clays	*5–40*		*0.05–0.13*	*0.16–0.44*
Clay, dry		*2–6*	*0.12–0.21*	*0.40–0.70*
Clay, wet		*15–40*	*0.05–0.08*	*0.16–0.25*
Soil, sandy dry		*4–6*	*0.12–0.15*	*0.40–0.49*
Soil, sandy wet		*15–30*	*0.05–0.08*	*0.18–0.25*
Soil, loamy dry		*4–6*	*0.05–0.08*	*0.40–0.49*
Soil, loamy wet		*15–30*	*0.07–0.09*	*0.22–0.31*
Soil clayey dry		*4–6*	*0.12–0.15*	*0.40–0.49*
Soil, clayey wet		*10–15*	*0.08–0.09*	*0.25–0.31*
Coal, dry		*3.5*	*0.16*	*0.53*
Coal, wet		*8*	*0.11*	*0.35*
Granites	*4–6*		*0.12–0.15*	*0.40–0.49*
Granite, dry		*5*	*0.13*	*0.44*
Granite, wet		*7*	*0.11*	*0.37*
Salt, dry	*5–6*	*4–7*	*0.11–0.15*	*0.37–0.49*

Table 2.1: Properties of electromagnetic fields under various ballast circumstances.

A testament to the differing qualities of various material kinds and compositions in the ballast types utilized is the difference in value between the two sources for ballast in the same category ("Dry clean"). The table illustrates the relationship between moisture content and fouling level and signal propagation velocity. .

- Because fouled or "spent" ballast contains more fines than clean ballast, it has fewer voids. Electromagnetic waves will move more quickly in clean ballast than in spent ballast because air carries them more quickly than ballast material. [24]
- Dielectric constants for "saturated clean ballast" and "saturated spent ballast" differ not just because spent ballast has a smaller void content but also because spent ballast has a greater capacity to store water than clean ballast. [25]; [24]

- Common Reflection Surface Test (CRS)/Common Midpoint Test (CMP))

The Common Midpoint test, also known as the Common Reflection Surface test, is a rapid and precise technique for determining the signal propagation velocity of GPRs that use movable

antennas or many antennas in an array. Moving a transmitter and a receiver apart is known as a CMP test, whereas using an array of several static antennas is known as a CRS test. [26]

Since the distance between the antennas is known, information on variations in signal travel time can be obtained by measuring a common point with several or mobile antennas. The signal propagation velocity at that particular location on the track stretch can then be determined using these data. [16]; [25]

High-accuracy measurements of ballast layer thickness are made possible by GPR, however for best results, calibrations and transparent layer interfaces are still necessary. Although there are some issues with thickness measurements due to variations in signal propagation velocity throughout a track, the technique is still better than existing approaches. [18]

2.5.2. Finding the Level of Ballast Fouling

Managing track maintenance resources requires accurate and up-to-date information about the ballast quality on the railway network. Ballast cleaning or renewal is a costly and time-consuming process, yet unnoticed areas of low ballast quality can eventually damage rolling stock and track condition. It will be simpler to prevent unnecessary renewals and focus maintenance efforts where they are most needed if the track ballast condition is well understood. There are multiple methods for identifying and measuring the extent of ballast fouling using GPR technology. [27]

- Using the dielectric constant to show fouling

Shifts in the dielectric constant of ballast can be detected using the same electromagnetic methods that are used to measure the thickness of the ballast layer. This can assist in locating regions where ballast quality deviates from intended values because the degree of fouling has a direct impact on the dielectric constant. .

When surveying a section of track with high-quality ballast, regions with low-quality ballast will show up as having a thicker layer of ballast on GPR scans. This occurs when the electromagnetic signal travels longer through fouled ballast than through clean ballast because it propagates more slowly through the former. It is crucial to remember that these changes in transit time could also be caused by locally increased water content or by thicker ballast layers (as water also decreases signal propagation velocity) [27]. Furthermore, the limits of gradational fouling are not obviously

shown by this approach. Therefore, the two-way travel time of the GPR signal alone should not be used to evaluate ballast fouling.

- Ballast fouling detection using scattering from voids

By utilizing the EM-scattering characteristics of ballast vacancies, ballast fouling could also be evaluated. Significant electromagnetic signal dispersion occurs when the wavelength of the signal is comparable to the size of the voids. [28] When surveyed with a 2 GHz antenna, the air holes in clean ballast create significant signal dispersion since their size is similar to the wavelength of 2 GHz signals. [28] On the other hand, data from fouled ballast should result in very little, if any, signal scattering. [29]

More control data is required to confirm the method's limitations and the extent of its applicability, however practical field tests have shown encouraging results and consistency with real data. For starters, the approach will struggle to distinguish between the contributions of fouling material content and water content. [28]; [30]

- Short Time Fourier Transform(STFT)

"The frequency analysis of the reflected signals, which is related to the rate of signal energy attenuation across the medium, provides the basis for a third method of conducting ballast fouling surveys using GPR. By converting some time-domain data to frequency-domain data, the Short Time Fourier Transform tracks how the frequency spectrum changes over time and, consequently, with depth". [25]; [28]

Even in the absence of well-defined interfaces, the frequency variations enable the differentiation of different ballast fouling situations and the presence of moisture. In essence, what is produced is an ongoing examination of the subsurface material properties. [31]

The technique may be regarded as better than conventional core sample gradation tests, which simply gather data for the entire sample as a whole, since it will provide information about ballast quality in relation to depth. [28]

Other fouling detection techniques that are presently being developed are not discussed here but are detailed in:

- "Discrete Wavelet Transform" [32]

- "System based on magnitude spectrum analysis and support vector machine" [31]

2.5.3. Finding Hidden Items or Facilities

The ballast and subgrade are still comparatively homogenous materials, despite fouling changing their dielectric characteristics. Even in the majority of ballast fouling situations, this facilitates the identification of foreign objects or the tracking of associated utilities on a GPR scan. [33] Because of their high conductivity and powerful signal reflection, metals in particular are easily detectable with GPR. Objects formed of different materials will have varying dielectric characteristics. [10]; [33]

When examined using GPR, plastic pipes also produce distinctive scattered signal forms, albeit the signal is far weaker than that of metals. The higher the moisture content, the harder it is to tell them apart. This is particularly valid for soils that have a high intrinsic permittivity. Although it weakens the signal strength of their reflection, "the loss nature of the high moisture soil does not obscure the signature of the metallic and plastic pipes. Therefore, filtering the data by deducting the clutter from the received signal is necessary for their detection." [33]

The GPR's capacity to identify subsurface objects is also impacted by the antenna frequency. Radar gram resolution is improved and finer texture is obtained at frequencies of around 1 GHz and above. Nevertheless, these frequencies cause gaps in the ballast to produce scattering signals, or noise, which makes it challenging to identify foreign items and layering. [10]

2.5.4. Detecting Ballast Anomalies

As a technique for identifying the existence and extent of rail bed abnormalities such as subsurface penetration, layer deformation, or mud pumping, GPR has also shown encouraging results. [31]; [34]

"Radar measurements will show these kinds of mistakes as local abnormalities in the ballast bed reflection that deviate from the scan's overall pattern. However, since the ballast bed interface may not always show up as a straight and even line, identifying these could be challenging." [34]

- penetration of the subgrade

In one investigation, the presence and size of regions where subsoil has migrated into the ballast were accurately identified by [34]. Subgrade penetration will be apparent by distinctive forms in

the reflection of the ballast bed interface as long as there is a contrast to the dielectric constant of the ballast.

- Pockets for ballast

If the size of the ballast pockets is large enough to differentiate them from the surrounding trend, they can be identified on radar images as depressions in the reflection of the ballast/subgrade interface. The same is true for other oddities in the track-bed, such as the subgrade's slow slumping. It will be more challenging to discover ballast pockets in their early phases of development, despite the significant advantages of early detection (enabling for repair with smaller precision draining efforts). “To precisely target drainage measures, GPR is a useful technique for figuring out the depth and lowest point of ballast pockets.” [35]

- Mud pumping

“When the ballast's ability to support loads diminishes, a slurry of water and particles is pumped upward through the ballast body by the cyclical loading of passing trains.” This phenomenon is known as mud pumping. The water and penalties help to contaminate the ballast, which lowers the speed at which the signal travels. Since the integrity of the ballast/subgrade contact will be jeopardized by the upward migration of particles from the subgrade, identification based only on this characteristic may prove challenging. [36]

2.5.5. Exposing the Moisture and Water Content

Moisture will have a notable impact on GPR survey results because water has a far higher dielectric constant than ballast and fouling elements combined. Radar-gram textures of features will be more intense when surveying a section in wet conditions than when it is dry, particularly if the materials hold moisture better than the clean permeable ballast. [10]; [37]. If pockets of water are within the signal range depth, they should also be easily discernible on GPR scans. [38] Accurate water detection has also been achieved experimentally using the amplitude envelope method and the Short Time Fourier Transform method. [28]; [29].

GPR is a practical inspection technique, according to studies on the identification of leaks from water and sewage pipes. [39] Not just to find leaks but also to map the distribution and dissipation of water in the soil. To get the best findings, a three-dimensional ground survey requires an array of antennas.

1.6. Ground Penetrating Radar modelling with gprMax

To get the most out of gprMax for modeling GPR, you should understand the Finite-Difference Time-Domain (FDTD) approach, which forms the foundation of the program.

Some fundamental ideas of the FDTD technique and GPR modeling are covered in this section. The pertinent literature contains a wealth of further information. This article explains how FDTD is specifically applied to the GPR forward problem. [40]

1.6.1. Fundamental Ideas in GPR Modeling

The well-known Maxwell's equations describe all electromagnetic phenomena on a macroscopic level. The relationships between the basic electromagnetic field quantities and how they depend on their sources are expressed by these first-order partial differential equations.

$$\nabla \times E = -\frac{\partial B}{\partial t}$$

$$\nabla \times H = \frac{\partial B}{\partial t} + J_c + J_s$$

$$\nabla . E = 0$$

$$\nabla . D = q_v$$

“Where t is time (seconds), E is the strength of the electric field, H is the strength of the magnetic field, and y is the volume electric charge density (coulombs/ cubic meter). It is assumed that the field vectors in Maxwell's equations are continuous, bounded, single-valued functions of time and position. The preceding equations must be solved, taking into account the problem's geometry and beginning conditions, in order to mimic the GPR response from a specific target or group of targets.” [40]

The GPR forward problem is classified as an initial value-open boundary problem due to its nature. Since there is no precise boundary limiting the problem's geometry or the range of values at which the electromagnetic fields can take, a solution must be found by defining an initial condition (i.e., excitation of the GPR transmitting antenna) and permitting the resulting fields to propagate through space, reaching a zero value at infinity. The second portion is difficult to handle with a limited computational space, even though the first part (i.e., source specification) is simple to accommodate. [41]

1.6.2. Finite-Difference Time-Domain (FDTD)

Both the space and time continua are discretized in the FDTD method of numerically solving Maxwell's equations. Therefore, the temporal Δt steps and the spatial Δx, Δy, and Δz discretization stages are crucial. Because the FDTD model is more accurate in representing the problem the smaller they are. However, because computers have a finite amount of storage and a finite processing speed, the values of the discretization stages must always be finite.

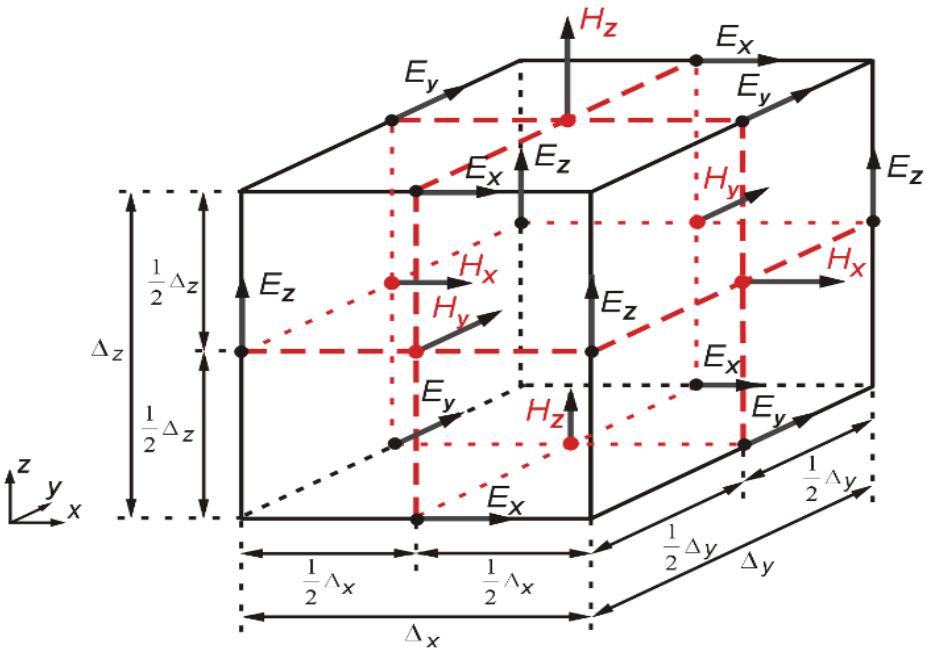

Figure 2.4: The 3D FDTD Yee cell [41]

"As a result, the FDTD model is a condensed and small representation of the actual problem. The Yee cell—named for Kane Yee, the man who invented the FDTD method—is the fundamental component of this discretized FDTD grid. Figure 2.4 provides an illustration of this for the 3D situation."

"Complex shaped targets can be readily incorporated into the models by allocating suitable constitutive parameters to the positions of the electromagnetic field components. On the other hand, a staircase approximation is used to depict things having curving bounds." [40]

Each FDTD cell applies a discretized version of Maxwell's curl equations, which yields the numerical solution directly in the time domain. The solution is found iteratively because these equations are discretized in both space and time. Every iteration corresponds to an elapsed

simulated time of one Δt, and the electromagnetic fields progress (propagate) in the FDTD grid. Therefore, one may tell "the FDTD solver to simulate the fields for a certain time window by indicating the number of iterations."

The inability to assign the values of Δx, Δy, Δz, and Δt individually is the cost of employing the FDTD approach to achieve a solution directly in the time domain. FDTD is a numerical procedure that is conditionally stable. The stability condition is known as the CFL condition after the initials of Courant, Freidrichs and Lewy and is

$$\Delta t \leq \frac{1}{c\sqrt{\frac{1}{(\Delta x)^2}+\frac{1}{(\Delta y)^2}+\frac{1}{(\Delta z)^2}}}$$

"Where c is the speed of light. Hence Δt is bounded by the values of Δx, Δy and Δz. The stability condition for the 2D case is easily obtained by letting $\Delta z \to \infty$."

1.6.3. File Format, Scripting, and User Interface

"gprMax employs a text-based input file where users enter pre-defined commands to determine all of the simulation's parameters, including model size, discretization, time frame, geometry, materials, and excitation. We thought about making a graphical user interface (GUI) for gprMax that was based on CAD or a pure programming interface, but we ultimately decided against both of these choices. This design choice was based on three guiding concepts, two of which are comparable to those listed in First, in order to solve or optimize a certain problem, users typically run a number of related simulations with different parameters; Thirdly, we determined that the greatest use of our limited resources was to construct sophisticated modeling elements for GPR within software that could readily interact with other tools. Second, we wanted users to be able to generate models with little to no programming knowledge or experience".[41]

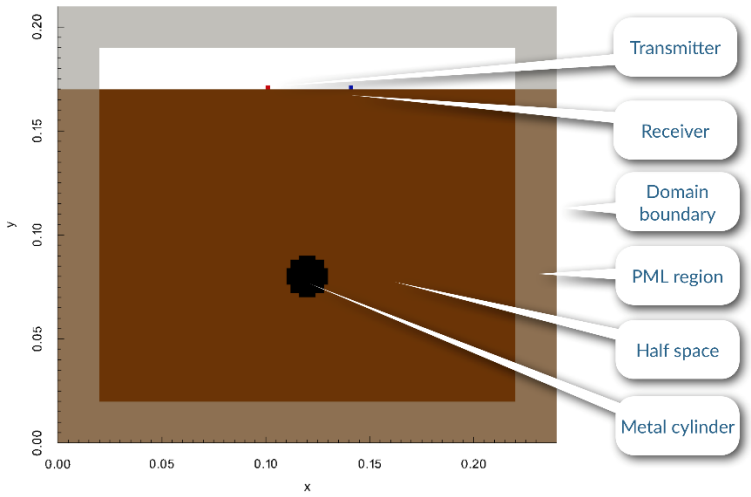

Figure 2.5: FDTD mesh of metal cylinder buried in a lossless dielectric half-space. [41]

```
1.  #title: B-scan from a metal cylinder buried in a dielectric half-space
2.  #domain: 0.240 0.210 0.002
3.  #dx_dy_dz: 0.002 0.002 0.002
4.  #time_window: 3e-9
5.  #material: 6 0 1 0 half_space


6.  #waveform: ricker 1 1.5e9 my_ricker
7.  #hertzian_dipole: z 0.040 0.170 0 my_ricker
8.  #rx: 0.080 0.170 0
9.  #src_steps: 0.002 0 0
10. #rx_steps: 0.002 0 0


11. #box: 0 0 0 0.240 0.170 0.002 half_space
12. #cylinder: 0.120 0.080 0 0.120 0.080 0.002 0.010 pec
```

Figure 2.6: Input file for a simple 2D GPR simulation of a metal cylinder buried in a lossless dielectric half-space.

"When producing a series of simulations or when simulations incorporate heterogeneities, such as a model of a soil with stochastically shifting electrical properties, a CAD-based GUI becomes more difficult to use, even though it is helpful for creating single simulations." [41]

1.6.4. Advanced GPR Modeling Features

Many strong and adaptable capabilities for modeling GPR are included in gprMax. A few of the newly created and sophisticated capabilities are highlighted in this section.

2.6.3.1. Library of Antenna Models

The past 20 years have seen the sporadic inclusion of antenna models with differing levels of realism in numerical simulations of GPR. A library of pre-defined antenna types that function similarly to commercial antennas is now included in gprMax. “At this time, antenna models that resemble the 1.5 GHz (Model 5100) antenna from Geophysical Survey Systems, Inc. (GSSI) (http://www.geophysical.com) and MALA Geoscience (http://www.malags.com/) There is a 1.2 GHz antenna provided.” [40]

2.6.3.2. Absorbing Boundary Conditions

“As more study is being done on quantitative amplitude information from GPR, simulations now need to feature Perfectly Matched Layer (PML) absorbing border conditions that are more effective and perform better (ABC). PML ABCs based on the uniaxial PML (UPML) formulation have been available in gprMax since 2005. Now, a PML for gprMax has been created using a recursive integration method to the complex frequency shifted PML.” [40]

2.6.3.3. Materials

“GPR is employed in a variety of complicated, heterogeneous situations that include materials having dispersive qualities. As a result, we have concentrated on creating new features and enhancing the software's simulation and creation of materials.” [40]

2.6.3.3.1. Anisotropic Materials

“Anisotropic objects can be modeled in a simulation using gprMax. It is now possible to describe materials more precisely, including fiber-reinforced composites and wood, which are frequently scanned using GPR. This is accomplished by allowing up to three material identifiers to be specified for each volumetric geometry object.” [41]

2.6.3.3.2. Dispersive Materials

“Using a single-pole Debye model to depict dispersive materials has always been possible with gprMax. With this method, a wide variety of materials can be suitably represented for the usual GPR frequency ranges. Nonetheless, the electric sensitivity of materials like water is frequently simulated using multi-pole De-bye, Drude, and Lorenz functions.” [41].

2.6.3.3.3. Soil Models and Topography

For many GPR simulations, it is crucial to use enhanced soil models. Now, soils with more realistic geometrical and dielectric characteristics can be produced with gprMax. The dielectric characteristics of the soil are described using a semi-empirical model that was first proposed by. "The model relates relative the permittivity of the soil to its bulk density, sand particle density, sand fraction, clay fraction and volumetric water fraction."

"For example, to create a soil with bulk density, ρb = 2 g/cm3, sand particle density, ρs= 2:66 g/cm3, sand fraction, S = 0:5, clay fraction, C = 0:5, and a volumetric water fraction in the range {0.001-0.25}, the command #soil_peplinski: 0.5 0.5 2 2.66 0.001 0.25 soil_properties would be used." [41]

In summary, the literature underscores the importance of maintaining track beds, particularly ballast track beds, for railway stability. GPR is a valuable tool for non-destructive evaluation of track conditions, with extensive research validating its effectiveness. GprMax enhances GPR studies by enabling precise simulations, contributing to more accurate and cost-effective railway maintenance strategies. GprMax is an open-source software widely used for simulating GPR responses. It allows for the creation of detailed numerical models that replicate real-world conditions, enabling researchers to study the interaction between GPR signals and different subsurface materials.

2. METHODOLOGY

3.1 Overview

This chapter will present about the Ground Penetrating Radar simulation model presented in this study demonstrates it's potential for estimating track bed thickness and characterizing underlying materials in railway infrastructure. The simulation provides valuable insights into the capabilities and limitations of GPR, aiding in decision-making processes related to track maintenance, rehabilitation, and construction.

GPR (Ground Penetrating Radar) is frequently used for subsurface imaging and non-destructive testing. It can be used to gauge the degree of ballast fouling, or the presence of small impurities or contaminants within the ballast layer, on railroad tracks. Determining the water content or void in the track bed and measuring the thickness of the track bed. It would need to specify the characteristics of the ballast layer, such as its dielectric permittivity and thickness, in order to replicate GPR readings for ballast fouling estimation using gprMax (a well-known open-source GPR simulator). It might also mention the presence of fouling substances with various dielectric characteristics.

A synthetic GPR response that simulates the interaction between the antenna's electromagnetic waves and the subsurface layers can be obtained by running the simulation. This response's interpretation can reveal details regarding the track bed layer, substructure water content, and the existence and severity of ballast fouling.

Dividing the data processing system into smaller subsystems could simplify the process of automating the interpretation of GPR data. The inputs and outputs of these subsystems are the sole things that connect them. This configuration allows the performance of each subsystem to be evaluated as if it were a standalone module. Moreover, it allows for the evaluation of any combination of consecutive subsystems. Another advantage of this configuration is the possibility of distributing the data processing over multiple processors to speed up the analysis.

Figure 3.1 shows the technique data analysis system's flowchart. The following elements are part of the system

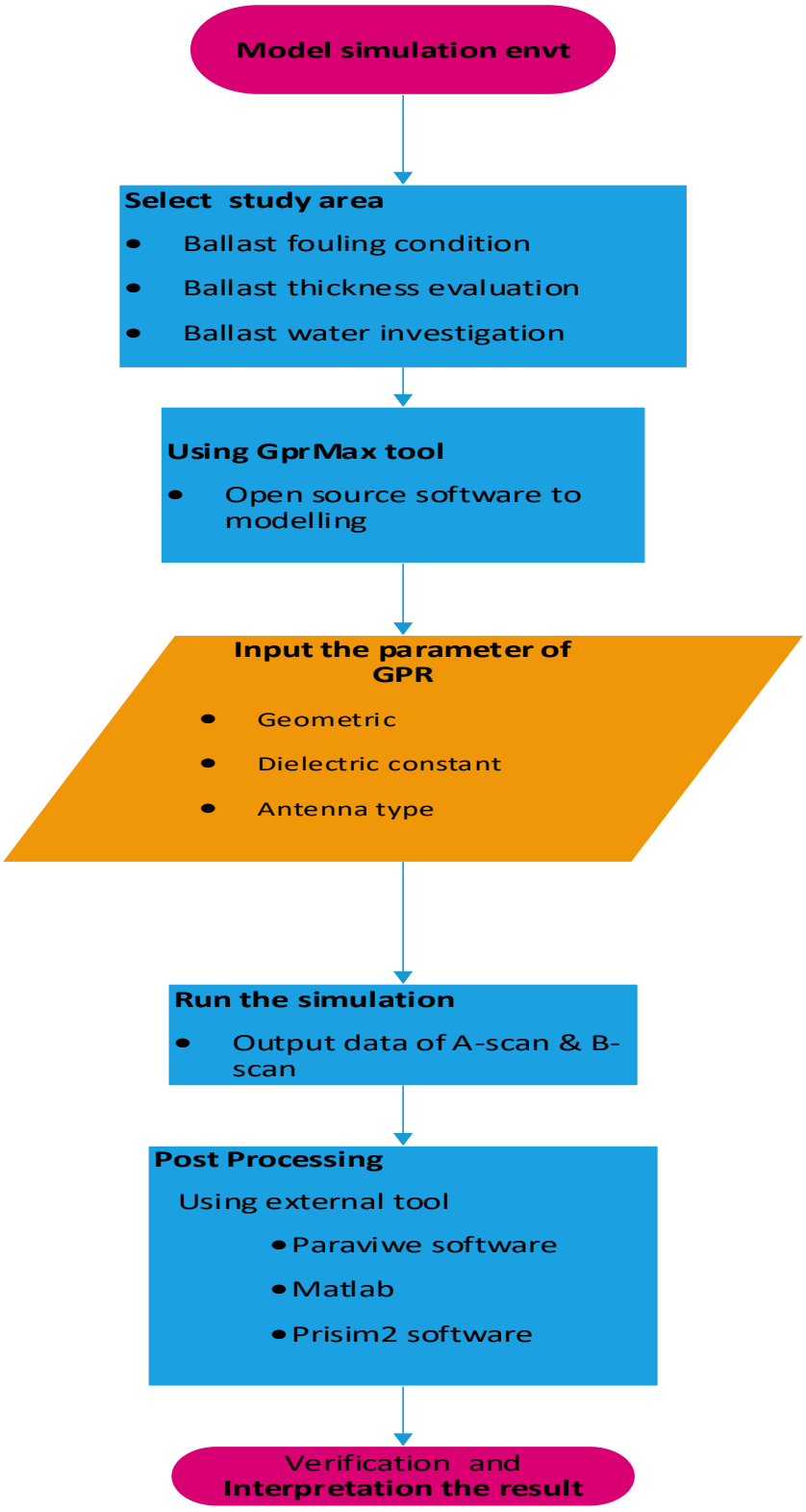

Figure 3.1 the flowchart of the proposed data analysis

3.2 Simulation Model Environment

In the simulation methodology for Ground Penetrating Radar (GPR), the selection of a suitable study area is crucial for accurate estimation of track bed thickness and material characterization. This section focuses on three specific aspects of the study area selection: layer thickness estimation, ballast fouling condition, and ballast water content/anomaly investigation.

3.3 Ballast Fouling Estimation:

Ballast fouling refers to the accumulation of fine particles and debris within the ballast layer, which can affect its drainage properties and overall stability. In the study area selection, it is important to include sections with varying degrees of ballast fouling. This allows for the simulation of GPR profiles that can detect and characterize the presence and extent of fouling within the ballast layer.

Three ballast boxes with different fouling levels were used to mimic the ballast tracks in the "Finite Difference Time Domain (FDTD)" model simulation. The stages of fouling on a ballast track are represented by the three ballast boxes in figure 3.1: (1) clean (Box a); (2) slightly fouled (Box b); and (3) fully fouled (Box c). Before the boxes are filled, "the fouling material is always combined with the ballast aggregate in specified ratios."

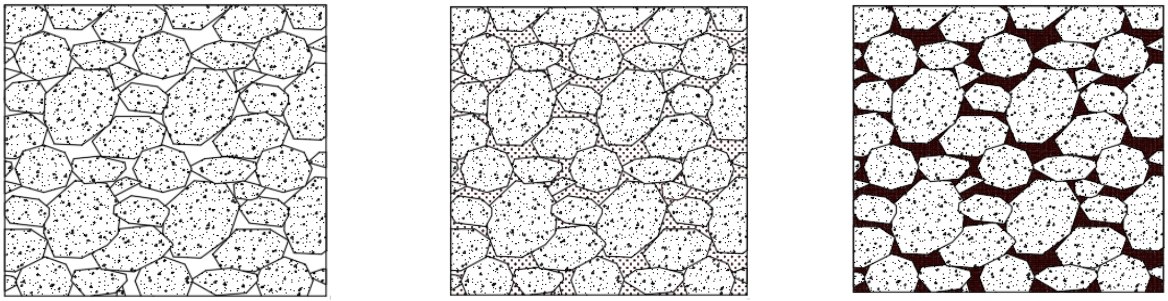

a) Clean Ballast b) Partially Fouled Ballast C) fully fouled Ballast

Figure 3.2. Schematic drawing of ballast fouling condition [42]

Material Type	Ratio of fouling material to clean ballast	Fouling Index
Clean Ballast	*0%*	0.4
Partially Fouled Ballast	*50%*	34.23
Fully fouled Ballast	*100%*	51.15

Table 3.1 Model simulation Track Ballast Boxes with Various Fouling Levels [42]

Ballast mixture	Material	Relative permittivity
Air	*Air*	*~ 1*
Ballast	*Granite*	*(5-7)*
	Limestone	*(4-8)*
Fouling Composition	*Water*	*80 + (related to the wave frequency)*
	Sands	*(3-6)*
	Soil	*(2-19)*
	Coal	*(3-4)*

Table 3.2 Dielectric constants of common materials in ballast layer.

3.3.1. Homogeneous Two Dimensional Model

The original ballast model's design was presented as a 2D homogeneous model in order to maintain the framework's simplicity. The model was updated to a more sophisticated version that more closely resembles an actual ballast combination as the study project developed.

The homogeneous model in gprMax assumes that the subsurface being studied is composed of a single material with uniform properties. This means that the electromagnetic wave propagates through the same medium without encountering any changes in its composition or properties. In this model, the entire subsurface is represented by a single layer with consistent material properties such as permittivity and conductivity. This simplifies the simulation process as there are no variations or interfaces to consider within the subsurface. It was wise to begin with a simple homogeneous model that had few reflections from within homogeneities, as this made it easier to understand the output response and determine the received wavelet. The Complex Refractive Index Method provides a table 3.3 that details the input GPR parameter and domain size for the gprMax software in the event of different ballast circumstances, such as clean ballast, somewhat fouled ballast, and entirely fouled ballast (CRIM). The thicknesses of the pec and ballast inside the domain are 0.05 and 0.30 meters, respectively. It served as a gprMax input. (Appendix A1).

3.3.1.1 Permittivity Calculation of Complex Model

Ballast particles and fouling found in ballast voids combine to form the ballast layer. The Complex Refractive Index Method is typically used to determine the dielectric constant of a mixed medium, which is made up of two or more anisotropic materials (CRIM) [43], as shown in

$$\varepsilon_b = \left(\sum \rho_i \, \varepsilon_i^{\alpha}\right)^{\frac{1}{\alpha}} \dots\dots\dots\dots\dots\dots\dots\dots\dots\dots (3.1)$$

"Where ε_b is the dielectric constant of the mixture, ρ_i is the volume percentage of each material of the mixture, ε_i is the dielectric constant of each component, and α is a parameter that depends on the spatial structure and the angle between the mixture and the electric field, generally α is taken to be 0.5."

In the case of ballast mixture material the CRIM formula are derivative

$$\varepsilon_b = \left(V_b\varepsilon_b^{\alpha} + V_a\varepsilon_a^{\alpha} + V_f\varepsilon_f^{\alpha} + V_w\varepsilon_w^{\alpha}\right)^{\frac{1}{\alpha}} \ldots\ldots\ldots\ldots\ldots\ldots\ldots\ldots\ldots (3.2)$$

Where in (3.2):

ε_b = Ballast mixture's bulk permittivity

V_b= ballast volume

ε_b= aggregate's relative permittivity

V_a = air-void volumetric fraction

ε_a = Free space's relative permittivity

V_f = volumetric portion of the fine substance

ε_f= relative permittivity of fine material

V_m = volumetric moisture content portion

ε_m= relative moisture content permittivity

α = shape factor = 0.5

Type	Parameter	value	unit
Domain Size (Model Frame)	*0.4 X 0.45m*		
Air	*default parameter "free _space"*		
Clean ballast	*Relative Permittivity , ∑r**	*3.24*	*_*
	Electric Conductivity, α	*0.01*	*Siemens/meters*
	Relative permeability, μ	*1*	*_*
	*Magnetic Loses ,α**	*0*	*ohms/meter*
Partially Fouled Ballast	*Relative Permittivity , ∑r**	*5.09*	*_*
	Electric Conductivity, α	*0.01*	*Siemens/meters*
	Relative permeability, μ	*1*	*_*
	*Magnetic Loses ,α**	*0*	*ohms/meter*
Fully Fouled Ballast	*Relative Permittivity , ∑r**	*7*	*_*
	Electric Conductivity, α	*0.01*	*Siemens/meters*
	Relative permeability, μ	*1*	*_*
	*Magnetic Loses ,α**	*0*	*ohms/meter*

Note: - Relative Permittivity ∑r* Results come from CRIM, which Detailed Chapter Four.

Table 3.3 Parameter used in the homogenous model for GPRmax

3.3.1.2 Specification of Simulation Antenna

Three ground coupled antennas (1,600MHz, 900MHz, and 400MHz) were employed in a synthetic GPR data collecting unit to create the 'Gaussian waveform' of the graphical waveform. We considered that the 400 MHz antenna, 900 MHz antenna and 1.6 GHz antenna should use 40 ns time window. The number of sampling points (trace) for each GPR signal is uniformly 5. This antenna and sample trace parameter also the same on heterogeneous model.

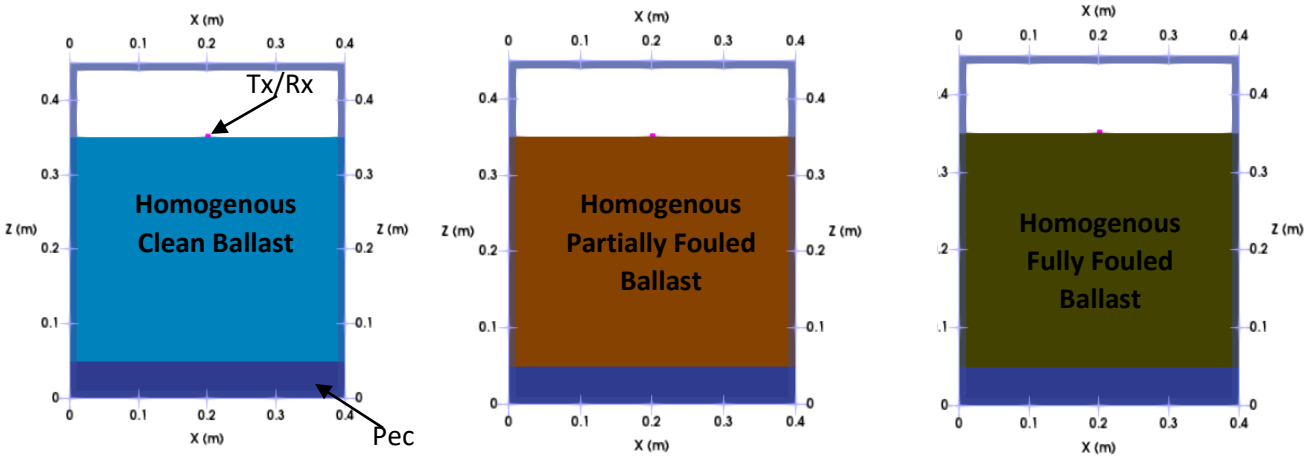

Figure 3.2 Paraview. vti rendering output homogeneous two-dimensional ballast condition simulation model.

3.3.2. Heterogeneous Model

The heterogeneous model in gprMax accounts for the presence of multiple materials or layers with different properties within the subsurface. This model allows for a more realistic representation of the subsurface, as it considers variations in material composition, permittivity, and conductivity. In this model, the subsurface is divided into multiple layers or regions, each with its own set of properties. These layers can represent different materials, interfaces, or structures within the subsurface. The electromagnetic wave propagates through these layers, experiencing changes in its behavior at each interface or transition between materials.

Following its successful generation, this design was entered into gprMax. (Appendix A2). Larger or coarser ballast aggregates, typically with a radius of 0.325 to 0.50 mm, are produced first in this case. “The radius was lowered to fit more circles that produced fine aggregates since the model runs out of room to create a circle with a big radius. Figure 3.3 displays the process's outcome.

The aggregates with random positions and radius's were created in a background medium (clean and fouling materials)."

With the help of the aforementioned tables 3.1 and 3.2, the GPR parameter is used to model three distinct ballast conditions: clean, partially fouled, and fully fouled. The dielectric constants for each material are entered into the gprMax program in Python, which creates non-overlapping circles and adds A single window frame containing arbitrary radiuses .

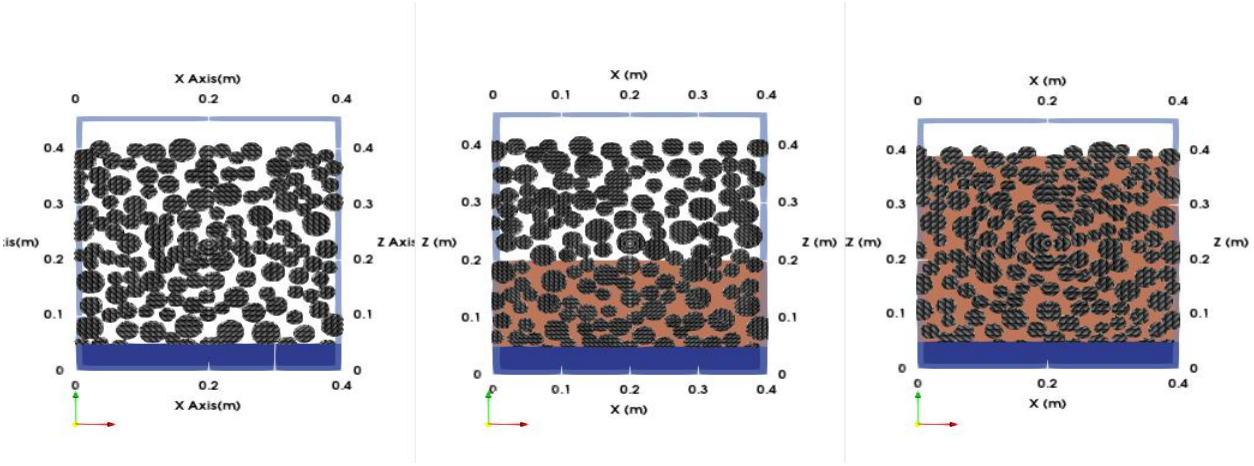

Figure 3.3 Paraview .vti rendering output heterogeneous two-dimensional ballast condition simulation model.

As per Selig and Waters, the fouling index can be computed using Equation (4.1), where FI stands for fouling index, P-4 represents the mass percentage of the sampled ballast material that is finer than the 4.75 mm (No. 4) sieve, and P-200 represents the mass percentage that is finer than the 0.075 mm (No. 200) sieve.

$$FI = P^4 + P^{200} \dots\dots\dots\dots\dots\dots\dots\dots\dots\dots\dots\dots (3.3)$$

3.4. Layer Thickness Estimation:

To accurately estimate the track bed thickness using GPR, the study area should encompass a range of layer thicknesses commonly encountered in railway construction. This can include variations in the thickness of the ballast layer, sub-ballast layer, and subgrade layer. By simulating different layer thicknesses, the GPR data can be analyzed to assess its ability to accurately determine the track bed thickness based on reflection patterns.

As shown in table 2.1, the GPR system employed in this study works on the basis of transmitting an electromagnetic pulse to the train surface via an antenna and then recording the reflected pulses from the internal interfaces, where the dielectric characteristics differ. . The thickness of the surveyed layer can be obtained by combining the dielectric characteristics of the layer with the time difference between the reflected pulses.

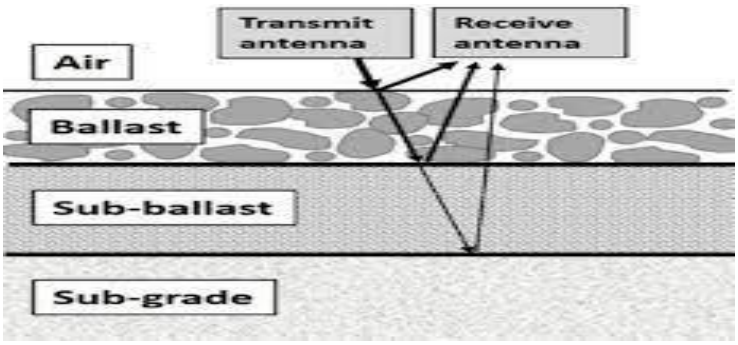

Figure 3.4: Typical GPR Reflection from Track-bed Sub-system [37]

GPR systems can be either ground-coupled or air-coupled, depending on how the antennas are employed. "For operating at train speeds (about 120 km/h to 60 km/h), the antennas (generally horn antennas) in air-coupled systems are suspended above the railroad surface and are normally deployed 150–500 mm above the surface. The depth of penetration is constrained, though, since the track bed surface reflects back some of the electromagnetic energy that the antenna sends." [25]

"In contrast, a ground-coupled systems antenna is the antennas must have a close contact to ground of a few centimeter with no need to have a direct contact which gives a higher depth of penetration (at the same frequency) but limits the speed of the survey."

Must choose the appropriate layer thickness and provide material qualities from the standpoint of electrical properties (i.e., dielectric values) in order to mimic the simulation environment. use the dielectric values from Table 2.1 and the thickness values from Table 3.4.

This three layer are called ballast, sub ballast and subgrade. Sub ballast material are sometimes the same characteristic's with blanket so for this study we proposed the same material for sub-ballast, capping and blanket layer. Depth of blanket depends upon the depth of ballast penetration. The subgrade material are allows to use a mixing model for soils proposed by Soil_Peplinski from

gprMax library. The purpose of the command is to create soils with realistic geometric and dielectric properties by combining it with the #fractal box command.

Track bed Layer	Thickness(mm)	length(m)	Antennas	Gprmax input type
Ballast	300	2	Ground-coupled deployed 1 mm from the surface using 400MHz and 1600MHz ricker wave form	heterogeneous model
	200			
	100			
Sub Ballast	200	2		heterogeneous model
Subgrade	300	2		#soil_peplinski(from gprmax library)

Table 3.4 Simulation input parameter of railway layer estimation

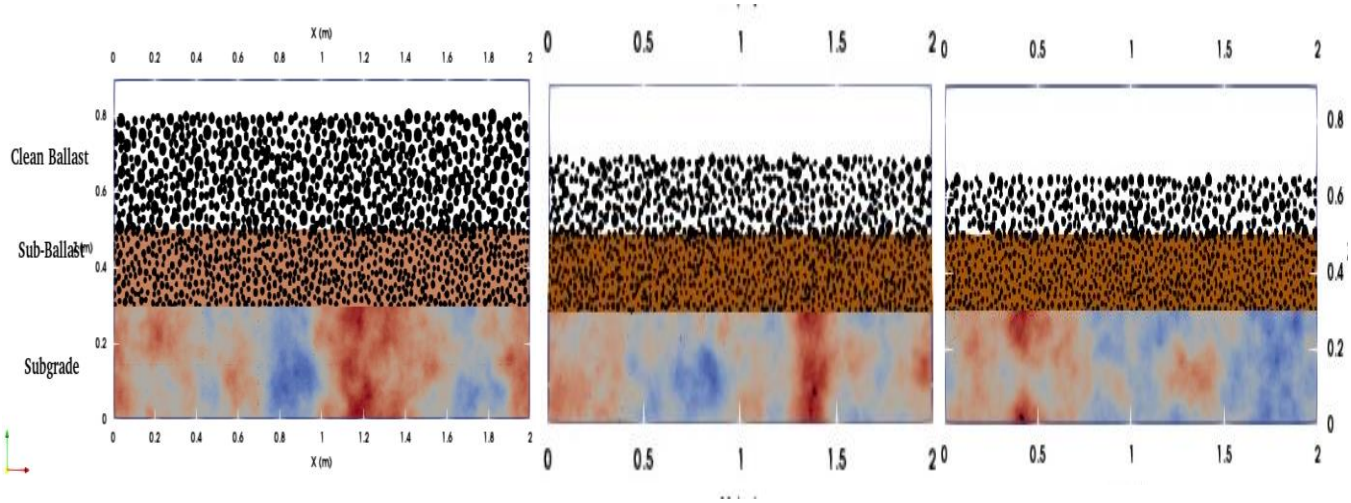

Figure 3.5 Paraview .vti rendering output typical section of railway track bed simulation model of 300mm, 200mm and 100mm thick respectively..

Model different ballast thickness of track bed layer to understand the individual impact of each parameters.

To mimic a ground-coupled antenna, the GPR system is positioned at ground level. Placed 20 mm apart, the transmitter (Tx) and receiver (Rx) could be regarded as monostatic. The EM wave is absorbed and the boundary's reflection is reduced using a perfect matched layer (PML) boundary.

The program automatically selected the time step, and the computing region is spatially discretized into 1 mm by 1 mm squares. Each B-scan contains 60 traces, and the excitation source used to simulate real GPR pulses is the Ricker wavelet, which has a core frequency of 400 MHz and 1600 MHz. The gprMax input files are shown on (Appendix A3)

3.4.1. Layer Thickness Estimation Methods

"The inverse modeling techniques used to predict the track bed properties—specifically, the surface reflection coefficient—are explained in this section (SRC)." [44]

3.4.1.1. The Surface Reflection Coefficient Method

"An effective technique for determining the medium relative permittivity of the surface layer (,-r,1) is the surface reflection coefficient (SRC) method. Given this electromagnetic characteristic and the assumption of straight ray propagation, the following formula can be used to calculate the layer's thickness (h1)":

$$h1 = \frac{C\Delta t}{2\sqrt{E_{r,1}}} \dots\dots\dots\dots\dots\dots\dots\dots\dots\dots\dots\dots\dots\dots\dots\dots (3.4)$$

"Where C and Δt stand for the two-way travel time (TWTT) of the wave propagating within the track-bed layer and the speed of light in empty space (3.x10-8. m/s), respectively. For the majority of rail road materials in the GPR frequency range, the low-loss layer assumed by Eq. (3.3) seems to be rather plausible. The method used to calculate E-r,1 based on the SRC approach involves comparing each measurement's amplitude to a calibration measurement taken over a perfect reflector."

"Based on the surface reflection coefficient R_0, the relative permittivity $E_{r,1}$ can be calculated using the following equation:"

$$E_{r,1} = \frac{(1+R_0)^2}{(1-R_0)^2} = \frac{(1+\frac{A_0}{A_{calib}})^2}{(1-\frac{A_0}{A_{calib}})^2} \dots\dots\dots\dots\dots\dots\dots\dots\dots\dots\dots\dots\dots\dots\dots\dots (3.5)$$

To determine "the values of the dielectric constant, we needed the amplitudes of the surface reflected pulses, A-0, and the GPR incident signal, A-$calib$. However, only the amplitudes of the surface-reflected pulses could be identified. Thus, we designed a calibration experiment to get the incident signal." The GPR was powered on and set up on a sizable metal plate. In this instance,

the incident signal's amplitude might be equated with the reflected signal's amplitude to determine the dielectric constant. [45]

It follows that the reflection from the bottom of the first layer should match the maximum amplitude of the generated signal. Thus, it is possible to determine the peak-to-peak amplitude of this reflection, A-1. At a two-way travel time known as t-1, the reflection is captured.

The parameters A_1 andt_1. Can be used to estimate the relative permittivity of the second layer using the following equation:

$$E_{r,2} = E_{r,1}\left(\frac{\left((1+\frac{A_0}{A_{calib}})\right)^2 e^{-\frac{n_0\sigma_1 t_1 c}{2E_{r,1}}} + \frac{A_1}{A_{calib}}}{\left((1-\frac{A_0}{A_{calib}})\right)^2 e^{-\frac{n_0\sigma_1 t_1 c}{2E_{r,1}}} - \frac{A_1}{A_{calib}}}\right) \ldots\ldots\ldots\ldots\ldots\ldots\ldots\ldots\ldots\ldots\ldots\ldots\ldots (3.6)$$

"Where n_0 is the wave impedance of free space ($n_0 \approx 120\pi\Omega$) and σ_1 represents the conductivity of the first material. This conductivity cannot be calculated from the measured traces and has either to be assumed negligible or to be estimated by the user. Furthermore, the estimation of $E_{r,2}$ in Eq. (3.5) suffers from the approximations made during the evaluation of $E_{r,1}$ and t_1."

- Percentage Relative Error

"The relative error represented as a percentage represents the measurement's percent of error. Because it compares each inaccuracy in terms of 100, the percent of error can be used to compare various measurements. The amount of the error is compared to the size of the object being measured using relative error. Percent error is the term used when relative error is expressed as a percentage."

$$Percentage\ Relative\ Error = \frac{Absolute\ Error}{True\ value}\ x\ 100 \ldots\ldots\ldots\ldots\ldots\ldots\ldots (3.7)$$

- Relative Error

The formula for Relative error can be written as,

$$Relative\ Error = \frac{Absolute\ Error}{AcceptedValue} \ldots\ldots\ldots\ldots\ldots\ldots\ldots\ldots\ldots\ldots\ldots\ldots (3.8)$$

$$AbsoluteError\ =\ TrueValue - ApproximateValue \ldots\ldots\ldots\ldots\ldots\ldots\ldots\ldots\ldots\ldots (3.9)$$

3.5. Ballast Water Content/Anomaly Investigation:

Water content within the ballast layer can significantly impact its mechanical properties and stability. In addition, the presence of anomalies such as voids or areas of high moisture content can also affect track performance. Therefore, the study area selection should include sections with varying ballast water content and potential anomalies. By simulating GPR profiles in these areas, the ability of GPR to estimate water content and identify anomalies within the ballast layer can be evaluated.

In this instance, the same dimension was developed through layer estimate, but different material properties were used to simulate an environment with water and a hollow in the railroad track bed. The output render simulation model environment for the track bed is shown below.

<table>
<tr><th>Track bed Layer</th><th>Thickness(mm)</th><th colspan="2">length(m)</th><th>Antennas</th><th>gprMax input type</th></tr>
<tr><td>Ballast</td><td>300</td><td>(0-1m)Dry clay fully fouling</td><td>(1m-2m)Wet clay fully fouling</td><td rowspan="4">air-coupled deployed 150 mm from the surface using 400MHz and 1600MHz ricker wave form</td><td>heterogeneous model</td></tr>
<tr><td>Sub Ballast</td><td>200</td><td>(0-1m)Dry sandy gravel</td><td>(1m-2m)Wet clay sandy gravel</td><td>heterogeneous model</td></tr>
<tr><td>Subgrade</td><td>300</td><td colspan="2">2m (73% sand fraction and 27% clay fraction soil)</td><td>#soil_peplinski(from gprmax library)</td></tr>
<tr><td>Cavity</td><td colspan="3">40mm radius of two cavity both dry and wet side</td><td>free_space(Air)</td></tr>
</table>

Table 3.5 Model simulation parameters of ballast water content and void inspection

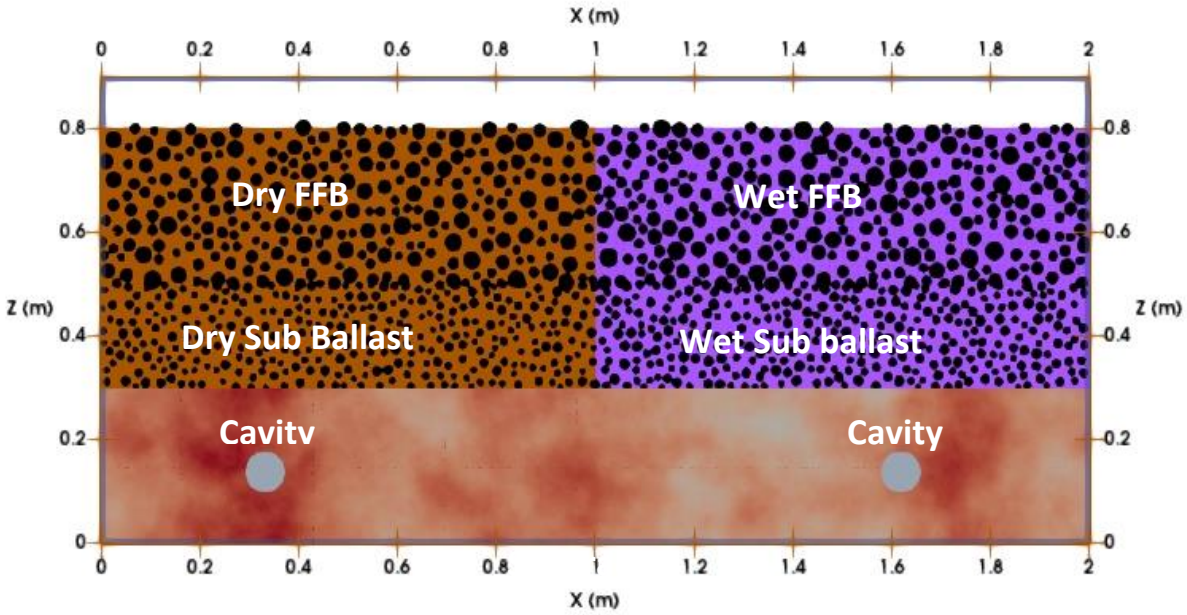

Figure 3.6 Paraview .vti rendering output typical section of railway track bed simulation model in the case of Ballast Water Content/Anomaly.

This conceptual model has 60 trace A-scan and using 400MHz and 1600MHz antenna for comparison. gprMax input file are depicted on (Appendix A4)

The results of the mentioned above gprMax simulation model approach will be examined and discussed in the next chapter.

3. RESULT AND DISCUSSION

4.1 Introduction

The gprMax model has been used to simulate the relationship between attenuation factors and the different parameters of the railway track bed layer. These are the outcomes.

Three specific parts of the study area selection are predicated on the simulation results for a railway track bed layer and material characteristics: layer thickness estimation, ballast fouling condition, and ballast water content/anomaly identification. Time-domain or frequency-domain signals that describe the movement of electromagnetic waves through the subsurface layers are frequently included in the output of a gprMax model simulation. These signals can be used to analyze numerous characteristics of interest and provide useful information about the subsurface conditions. Analyzing the signal characteristics and obtaining pertinent data are necessary for interpreting the output result. Introduce homogeneous and heterogeneous models in the framework of simulation environment. Analyzing the signal characteristics and obtaining important information are necessary for interpreting the output result. Typical interpretations include the following:

Reflections: By analyzing the amplitude and timing of reflections in the signals, it is possible to identify interfaces between different subsurface layers. This can help in determining the depth and thickness of these layers, as well as detecting any anomalies or structures within them.

Attenuation: The attenuation of the signals can provide insights into the electrical conductivity of the subsurface materials. Higher attenuation indicates higher conductivity, which can be indicative of moisture content or the presence of conductive materials.

Signal quality: Examining the signal-to-noise ratio and the overall quality of the received signals can help assess the effectiveness of the GPR system and its ability to penetrate and detect subsurface features accurately.

Signal processing: Additional signal processing techniques, such as filtering, or migration, can be applied to enhance the clarity and resolution of the output signals. These processed signals can provide a clearer representation of subsurface features and aid in further analysis

Using the mentioned interpretation will depend on the precise goals of the analysis and the qualities of the output necessary for the desired outcome. In this research, three study-specific areas (ballast fouling condition, track-bed layer estimation, and identification of anomalies in the water content of the ballast) are each given a different interpretation.

4.2 Result of Model Simulation

The simulation model environment approach and the parameter to use for creating the necessary output data for three study areas are described in the preceding section. Here is an analysis of the results in accordance with what was said above.

4.2.1 Ballast Fouling Condition

A comparison was performed between 400MHz, 900MHz and 1600MHz frequency antenna and three ballast fouling condition of dielectric properties of the material on homogenous and heterogeneous model environment. CRIM is creating the homogenous model of the material characteristics parameter for the ballast condition (Complex Refractive Index Method). It has been extensively used for GPR applications and is the most widely used method for calculating the bulk permittivity of heterogeneous materials.

Here is how to calculate the bulk permittivity output for each ballast situation using these permittivity values and a certain fraction of the material mix to create standard ballast mixtures.

- In case of Clean Ballast the volume of voids within new/clean ballast constitutes approximately 45% of the total volume of ballast within track . So here is:-

Clean Ballast			
V_b= volume of ballast	55%	ε_f= The fine material's relative permittivity	8
ε_b= aggregate's relative permittivity e	6	V_m = section on volumetric moisture content	0%
V_a = air-void volumetric fraction	45%	ε_m= relative moisture content permittivity	80
ε_a =Free space's relative permittivity	1	**α** = factor of shape	0.5
V_f = volumetric portion of the fine substance	0%	ε_b = Ballast mixture's bulk permittivity	?

$$\varepsilon_b = \left(V_b\varepsilon_b^{\alpha} + V_a\varepsilon_a^{\alpha} + V_f\varepsilon_f^{\alpha} + V_w\varepsilon_w^{\alpha}\right)^{\frac{1}{\alpha}}$$

$$\varepsilon_b = (0.55 * 6^{0.5} + 0.45 * 1^{0.5} + 0 * 8^{0.5} + 0 * 6^{0.5})^{\frac{1}{0.5}}$$

$$\varepsilon_b = (1.35 + 0.45 + 0 + 0)^{\frac{1}{0.5}}$$

$$\varepsilon_b = (1.8)^{\frac{1}{0.5}}$$

$$\varepsilon_b = 3.24$$

- **The bulk permittivity of the clean ballast is 3.24**

- The volume of voids within new, clean ballast is filled with some fine particle material in cases when the ballast is partially fouled. Approximately 50% of the total volume of the void is filled by fine

Partially Fouled Ballast			
V_b= volume of ballast	55%	ε_f= The fine material's relative permittivity	8
ε_b= aggregate's relative permittivity e	6	V_m = section on volumetric moisture content	0%
V_a = air-void volumetric fraction	20%	ε_m= relative moisture content permittivity	80
ε_a =Free space's relative permittivity	1	α = factor of shape	0.5
V_f = volumetric portion of the fine substance	25%	ε_b = Ballast mixture's bulk permittivity	?

$$\varepsilon_{bulk} = \left(V_b\varepsilon_b^{\alpha} + V_a\varepsilon_a^{\alpha} + V_f\varepsilon_f^{\alpha} + V_w\varepsilon_w^{\alpha}\right)^{\frac{1}{\alpha}}$$

$$\varepsilon_{bulk} = (0.55 * 6^{0.5} + 0.20 * 1^{0.5} + 0.25 * 8^{0.5} + 0 * 6^{0.5})^{\frac{1}{0.5}}$$

$$\varepsilon_{bulk} = (1.35 + 0.2 + 0.707 + 0)^{\frac{1}{0.5}}$$

$$\varepsilon_{bulk} = (2.257)^{\frac{1}{0.5}}$$

$$\varepsilon_{bulk} = 5.09$$

- **The bulk permittivity of the partially Fouled ballast is 5.09.**

- According to our model simulation, the ratio of gravel ballast and fine fouling material is 50% each in the event of fully fouled ballast, where the volume of voids within new/clean ballast are fully filled by

Fully Fouled Ballast			
V_b= volume of ballast	50%	ε_f= The fine material's relative permittivity	8
ε_b= aggregate's relative permittivity e	6	V_m = section on volumetric moisture content	0%
V_a = air-void volumetric fraction	0%	ε_m= relative moisture content permittivity	80
ε_a =Free space's relative permittivity	1	α = factor of shape	0.5
V_f = volumetric portion of the fine substance	50%	ε_b = Ballast mixture's bulk permittivity	?

$$\varepsilon_{bulk} = \left(V_b\varepsilon_b^{\alpha} + V_a\varepsilon_a^{\alpha} + V_f\varepsilon_f^{\alpha} + V_w\varepsilon_w^{\alpha}\right)^{\frac{1}{\alpha}}$$

$$\varepsilon_{bulk} = (0.5 * 6^{0.5} + 0 * 1^{0.5} + 0.5 * 8^{0.5} + 0 * 6^{0.5})^{\frac{1}{0.5}}$$

$$\varepsilon_{bulk} = (1.225 + 0 + 1.414 + 0)^{\frac{1}{0.5}}$$

$$\varepsilon_{bulk} = (2.646)^{\frac{1}{0.5}}$$

$$\varepsilon_{bulk} = 7.00$$

- **The bulk permittivity of the Fully Fouled ballast is 7.**

"Numerous investigations have shown that the dielectric permittivity increases as fouling increases" [42]. The impact of the fouling index on the bulk dielectric permittivity determined at the ballast boxes is illustrated by comparing the CRIM and FI in Figure 4.1. The relevant fouling indices for every ballast box, which are displayed in Table 3.1, approve the results.

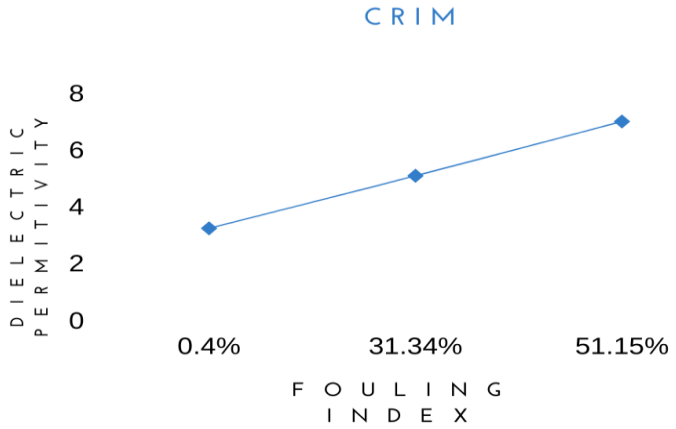

Figure 4.1 Dielectric permittivity vs. the fouling level

Therefore the homogenous ballast fouling condition are model according to the CRIM result with a pec (metallic object) layer at the bottom and here in Figure 4.2 illustrated…

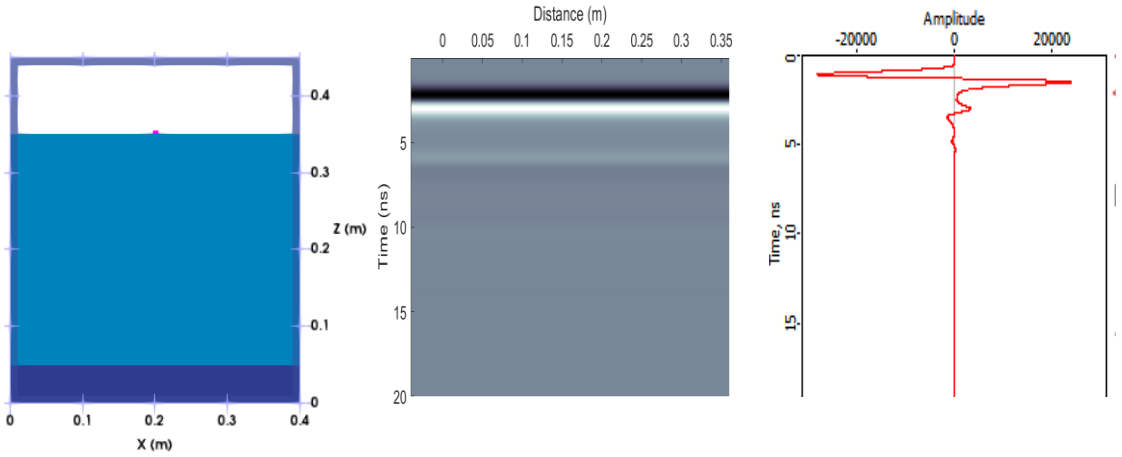

(a) (b) (c)

Figure 4.2 Forward simulation results of clean ballast, (a) homogenous CB with 0.05m thick pec material (b) show the B-Scan grayscale images of 400 MHz antenna and (C) show the A-Scan image single trace of 400 MHz antenna.

The simulation results for a clean ballast are shown in Figure 4.2. Additional results for 900 MHz and 1600 MHz antenna simulation output results for three different ballast conditions (clean, moderately fouled, and totally fouled) are annexed in (Appendix B1). Figure 4.3(a) compares each A-scan 400MHz on three different ballast conditions. Here, the PEC reflection occurs at the same

frequency but with different dielectric materials. Additionally, utilizing 900MHz and 1600MHz antennas produced the same results, which are shown in the (appendix).

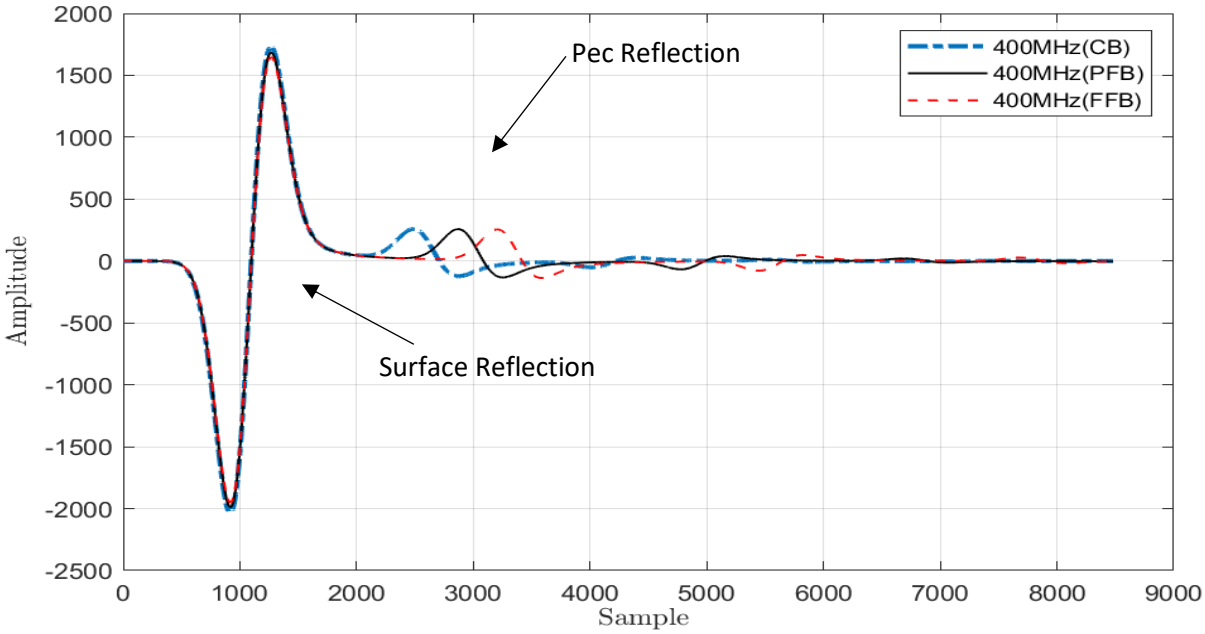

a) Amplitude vs Number of Sample A-san 400MHz Antenna (CB, PFB and FFB).

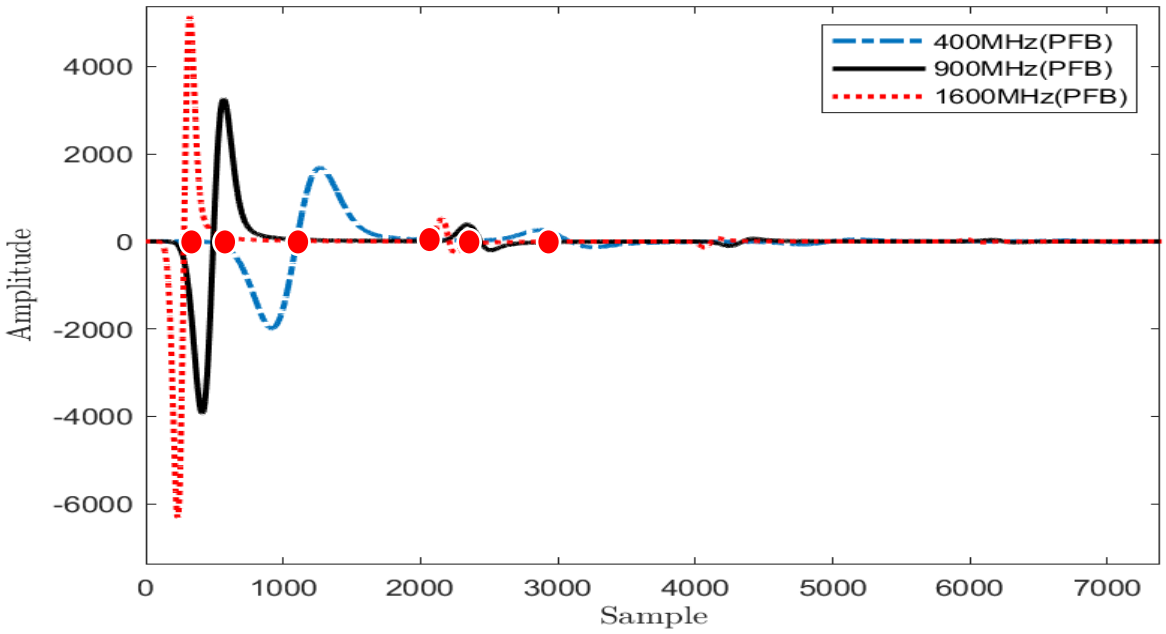

b) Amplitude vs Number of Sample A-san Partially Fouling Ballast (400MHz, 900MHz, and 1600MHz).

Figure 4.3 Comparison between different dielectric materials and different GPR antenna.

Figure 4.3 (b) displays the signal characteristics of antennas at various frequencies. The 400 MHz frequency antenna has much less signal axis crossings than the 1600 MHz antenna (i.e., the crossings of the signal amplitude curve and the coordinate axis in the ballast layer represented by red dots in square box). There are fewer 900 MHz axis crossings than there are at 1600 MHz this indicates that the signal qualities of the 1600 MHz antenna perform better than the 400 MHz and 900 MHz antennas (to reflect information about the ballast layer). The heterogeneous simulation model makes this concept much clear.

"Where, C is the propagation speed of electromagnetic waves in a vacuum (i.e. the speed of light = ($3 \times 10^8\ m/s$)." So calculate each velocity of CB, PFB, and FFB are $1.67 \times 10^8\ m/s$, $1.32 \times 10^8\ m/s$ and $1.13 \times 10^8\ m/s$ respectively. So the figure 4.3(a) are proof which ballast condition is reflect the pec first. If the velocity propagation of a given material known we can calculate ε (dielectric constant) but in real data both are difficult to know so using by the reflection method we can estimate (dielectric constant).

The peak reflections from the pec plate and ballast layer surface at the same position were captured in the GPR image using the areas with distinct signal reflections. The time needed to return was then computed. The dielectric constants are computed using Eq. in conjunction with the results of the ballast thickness (3.3).

Here is the case of heterogeneous simulation model can calculate dielectric constants and estimating ballast fouling condition of CB, PBF and FFB. The model are composed by different material which list on the methodology (3.3.2 Heterogeneous Model). Here is the output are on Figure 4.4.

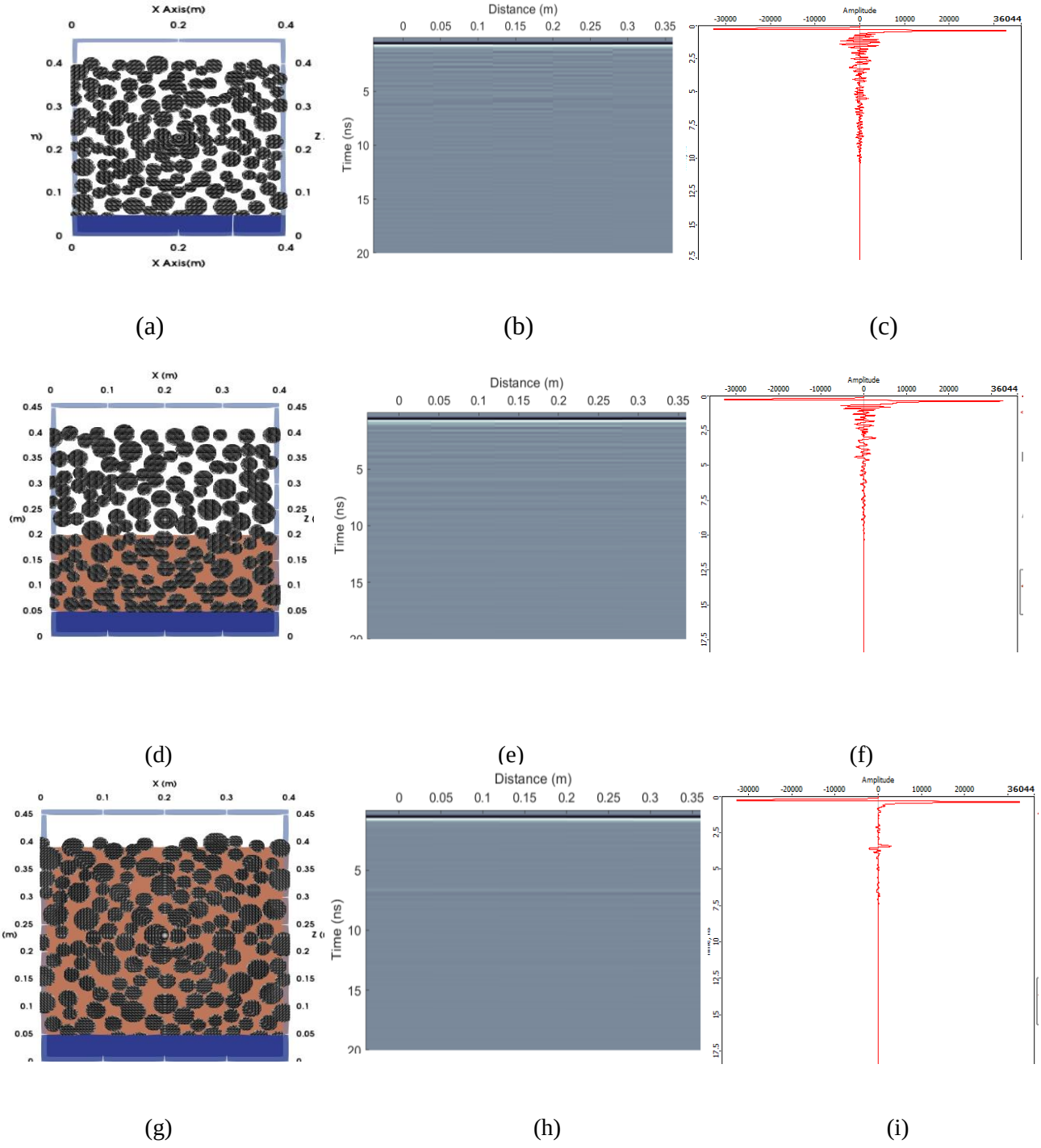

Figure 4.4 Forward simulation results of 1600Mhz Antenna (a,b, and c) are the outcomes of the gprmax simulation model of the .vti, B-scan, and A scan of clean ballast trace 1, (d,e,and f) are partially fouled ballast (g,h and i) are fully fouled ballast respectively.

From figure 4.4 it observed in clean ballast conditions, the GPR signal response will typically show a strong reflection from the ballast box. This reflection is caused by the contrast in electromagnetic properties between the air or pec below the ballast and the ballast itself. Secondly, when the ballast becomes partially fouled with materials like fines, the GPR signal response will change. The presence of these additional materials will cause scattering and absorption of the electromagnetic waves, resulting in a weaker and more diffuse signal response. Lastly, in cases where the ballast is fully fouled with fine particles, debris, or other contaminants, the GPR signal response will be significantly attenuated and scattered. The electromagnetic waves will be absorbed and scattered by the fouling material,

Using comparing the B-scan results of the 400MHz, 900MHz, and 1600 MHz antennas produced using prism2 software. And the MATLAB convert code on the gprmax tool's output file must be changed to a GISS (.dzt) file in order to use the fit prism2 software (Appendix C). And Compare A-scan single trace data on MATLAB to show how antennas with higher signal axis crossings perform better than others in terms of signal characteristics.

Preprocessing of B-Scan

1. Gain Function: - Using a gain function of 50db, which is inversely proportional to the signal strength, aims to equalize the amplitudes of all GPR signals. When defining continuity of reflecting occurrences, this kind of gain is most helpful.
2. Time-zero correction; - A time-zero adjustment was made prior to beginning the data processing process. It entails modifying the response so that the reflection from the ground's surface equals time-zero. Accurate depth determination depends on this operation.
3. Background removal: - The background in GPR data can arise from various sources, including environmental factors, instrument artifacts, or reflections from nearby objects. Background removal techniques aim to minimize or eliminate these unwanted signals to enhance the clarity and accuracy of the subsurface information. However, in our instance there is no background noise because it is a simulation.
4. Hilbert Transform: - The Hilbert transform is a mathematical operation that can be applied to GPR data to obtain the analytic signal. The analytic signal represents the complex envelope of the GPR data and contains information about the amplitude and phase of the

signal.

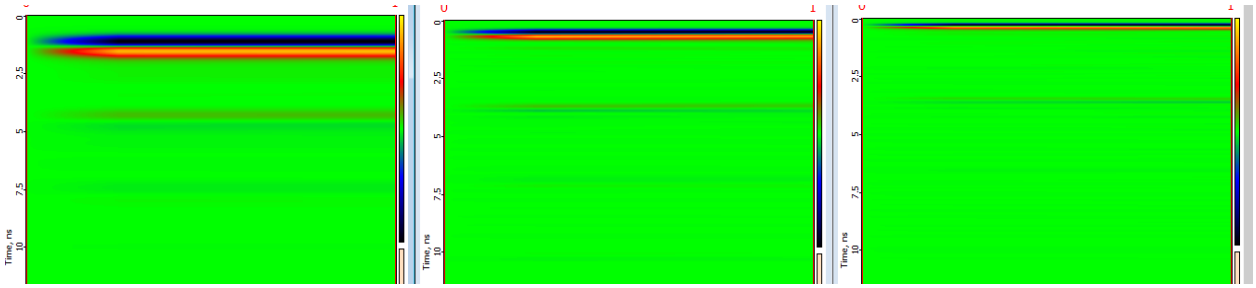

(a) 400MHz (b) 900MHz (C) 1600MHz

(d) 400MHz (e) 900MHz (f) 1600MHz

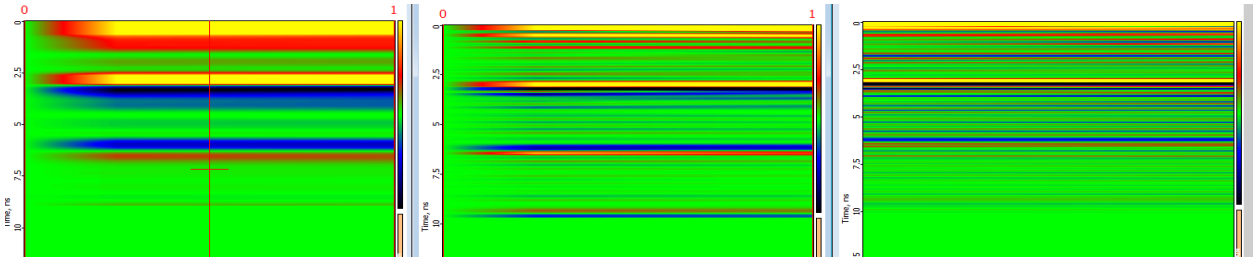

(g) 400MHz (h) 900MHz (i) 1600MHz

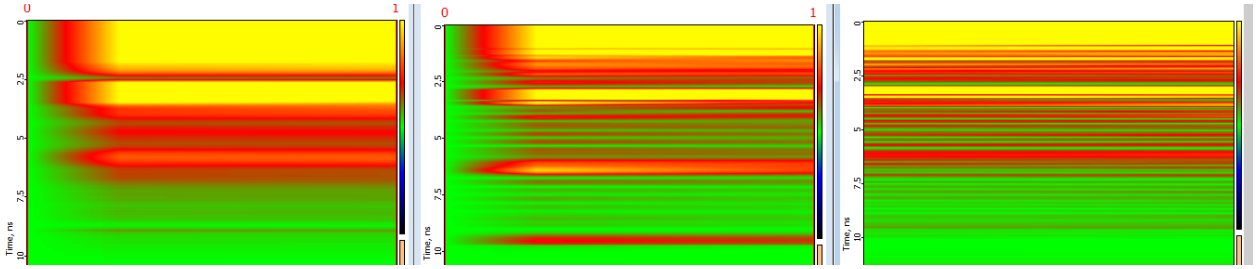

(j) 400MHz (k) 900MHz (l) 1600MHz

Figure 4.5 B-scan of foully fouled ballast on different antenna frequency (a, b, and c) are the raw data of simulation output. (d, e, and f) are Time-zero correction, (g, h, and i) are applying 50db gain function, (j, k and l) are Hilbert Transform process.

The 1600MHz signal axis crossings shown in the below Figure 4.6 A-scan perform better than

others in terms of antenna signal characteristics. Furthermore, based on the B-scan raw data preprocessing method, 1600MHz antenna has more data on a given shallow depth than 400MHz and 900MHz antenna. Additional output data are depicted on (Appendix B2)

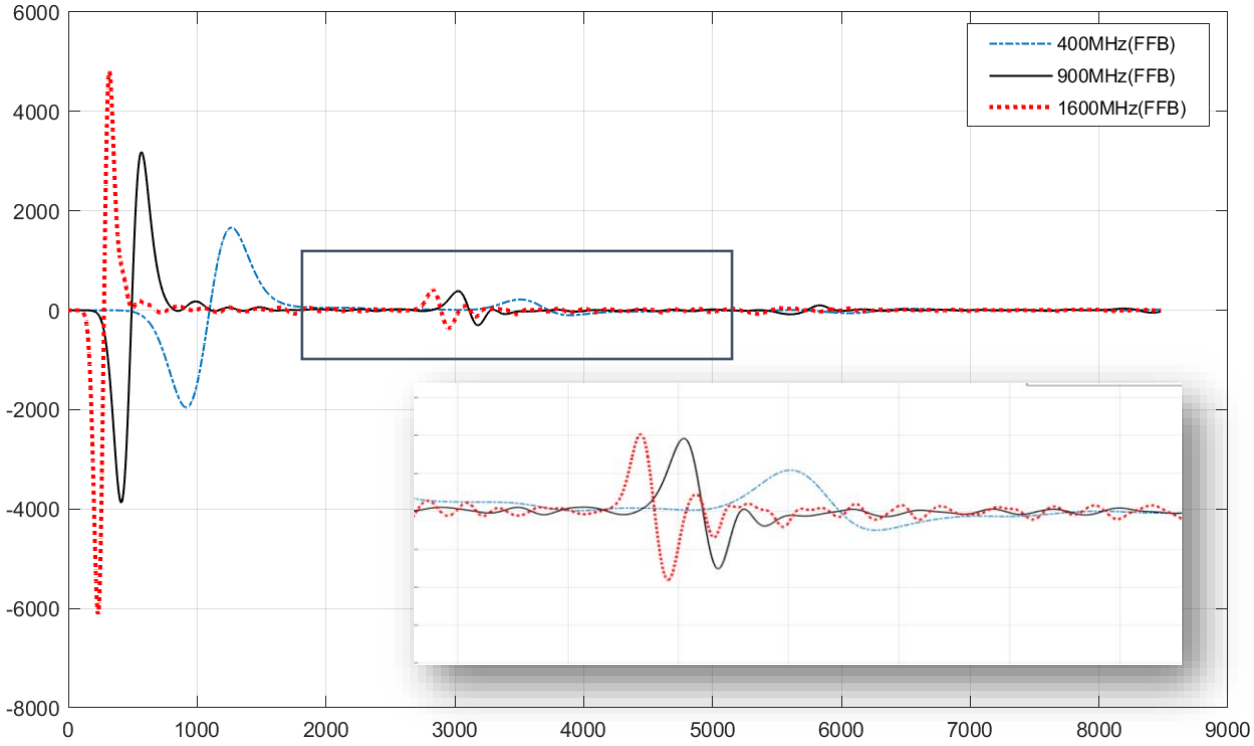

Figure 4.6 A- scan foully fouled ballast on different antenna frequency on a single trace.

As of right now, using 900MHz A-scan to estimate the dielectric constant of CB, PFB, and FFB is effective because using 1600MHz would result in a high bottom reflection of a Pec material are distorted the data in the case of CB and PFB ballast conditions.

4.2.2. Layer Thickness Estimation:

Create a text file with the extension ".in" (e.g., "input_file.in") and specify the necessary parameters for the gprMax simulation. This includes setting up the antenna parameters, material properties, and simulation settings. After the simulation is complete, i can process the output data to estimate the layer thickness. The output data is typically saved in an ".out" file (e.g., "output_file.out"). i can use Python's file handling capabilities to read and analyze the data. Additionally, using a MatLab to convert ".out" to ".dtz" Depending on the specific analysis i want to perform, the .dzt file may need to extract relevant information from the output file and apply

appropriate algorithms or techniques by using prism2 software.

A comparison was performed between 400MHz, and 1600MHz frequency antenna and three railway track bed layer of dielectric properties of the material on heterogeneous model environment. Clean ballast, sub-ballast, and subgrade are all present in the track bed layer, as shown in figure 3.5.

Here is figure 4.7 B-scan Preprocessing of 400MHz and 1600MHz antenna on the left and right respectively:-

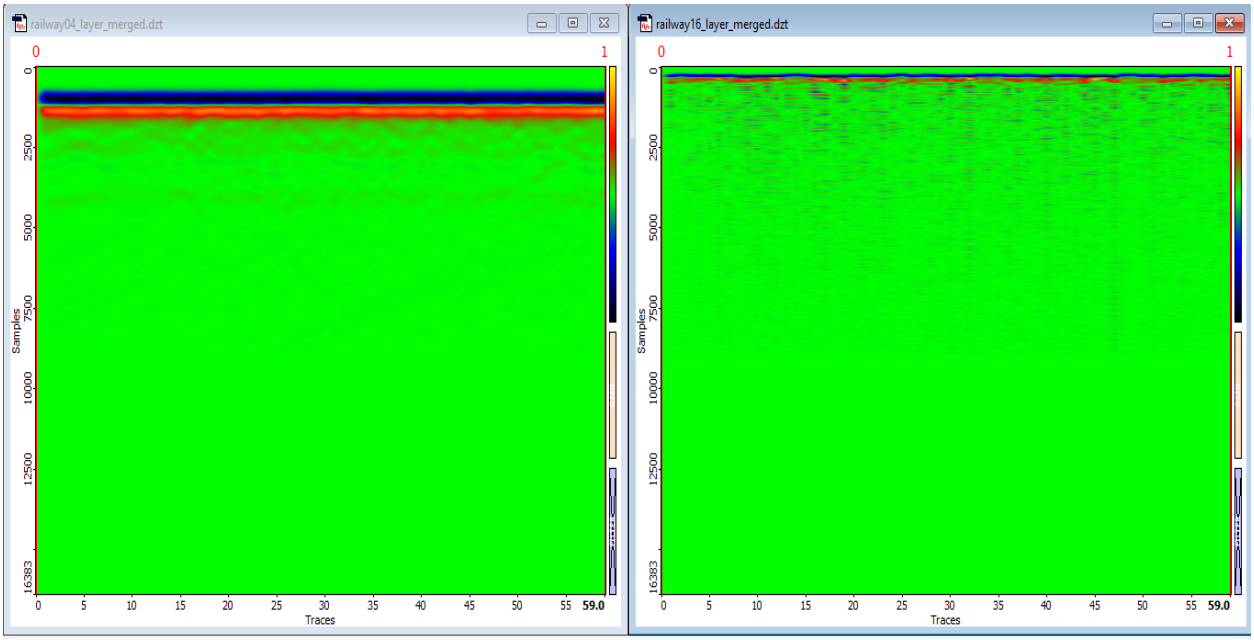

(a)

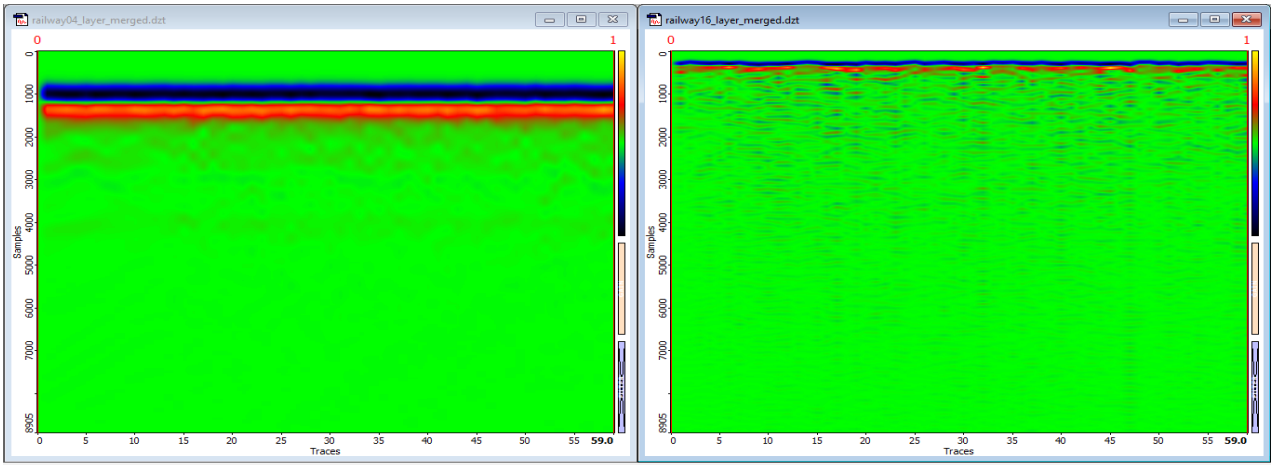

(b)

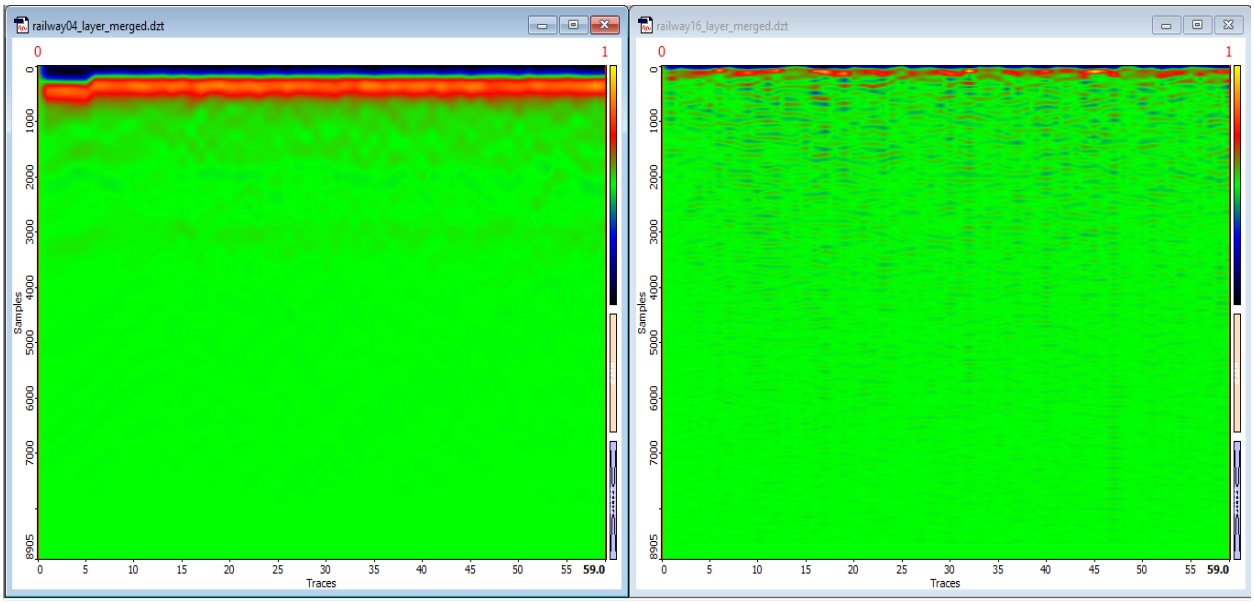

©

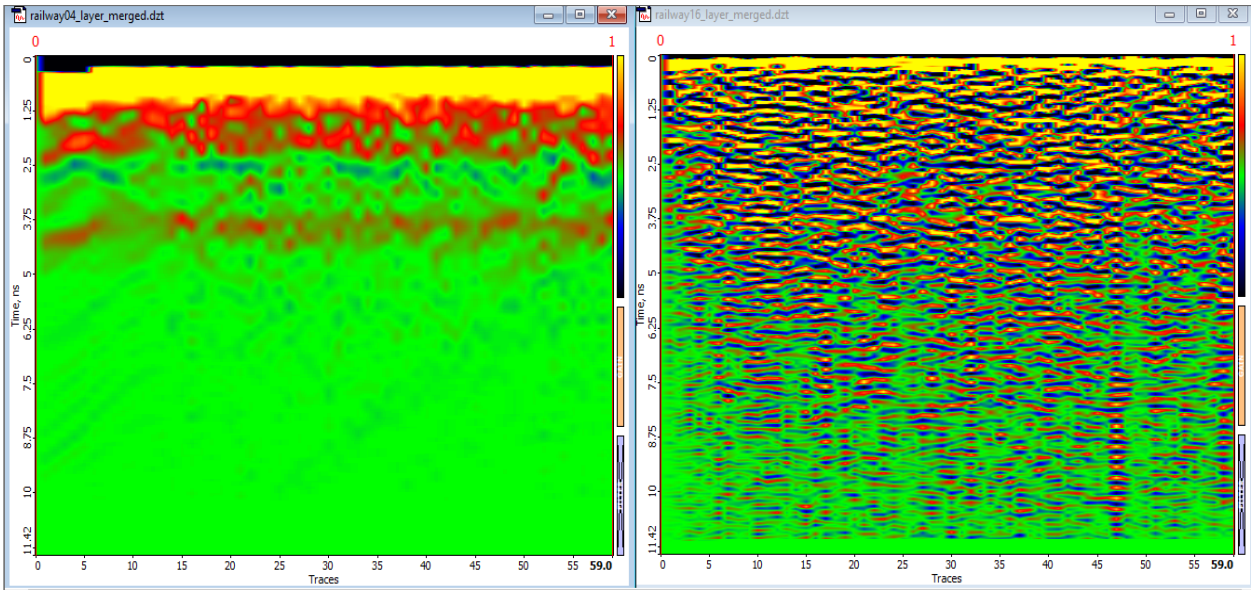

(d)

Figure 4.7 B-scan Preprocessing of 400MHz and 1600MHz antenna (a) Raw Data (simulation output), (b) trimming sample size, (c) time zero flittering (d) applying 50dB gain

Through seeing the above B-scan output processing 400MHz antenna is better layer thickness

detection than 1600MHz. therefore taking the processed output of 400 MHz antenna simulation to continue the next step of estimation of each layer dielectric constant?

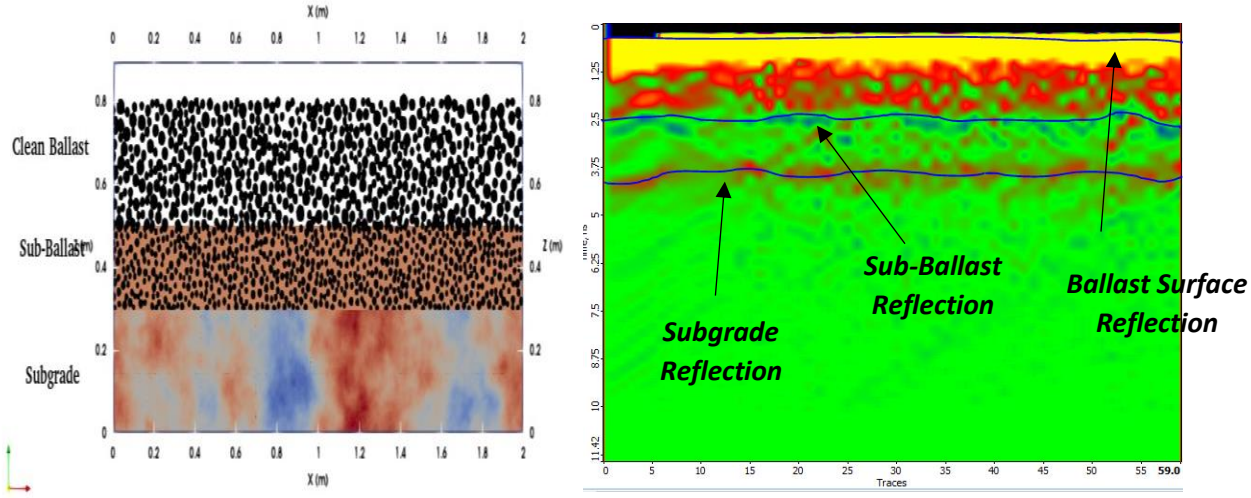

Figure 4.8. On the left model simulation of track bed layer, on the right processed output data of 400MHz antenna with lining by blue marker layer reflection

From the above figure 4.8 layer reflection compute dielectric constant of 5 random trace each A-scan by surface reflection coefficient method on equation (3.4). Here is the equation:-

$$E_{r,1} = \frac{(1+R_0)^2}{(1-R_0)^2} = \frac{(1+\frac{A_0}{A_{calib}})^2}{(1-\frac{A_0}{A_{calib}})^2}$$

In order to determine the value of $A\text{-}calib$, the 400MHz antenna is first calibrated. Recently, thicknesses have been calculated using simulation environments for multi-offset techniques like the common midpoint (CMP) method.

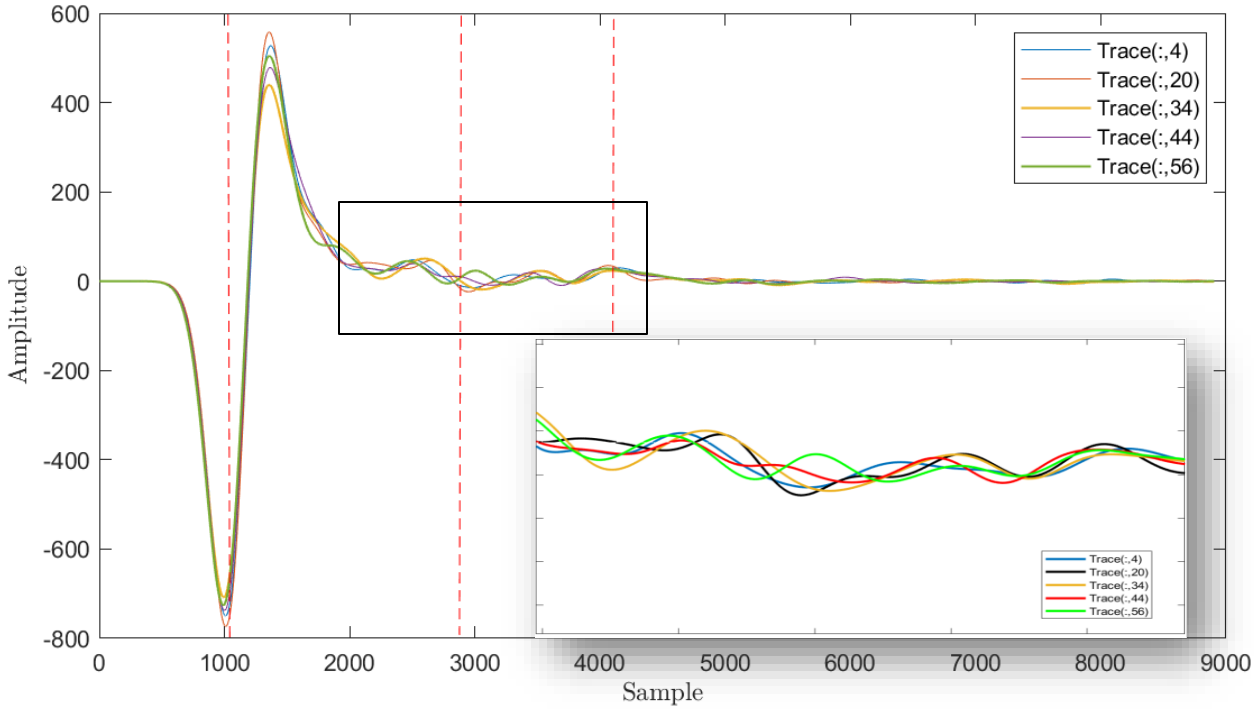

(a)

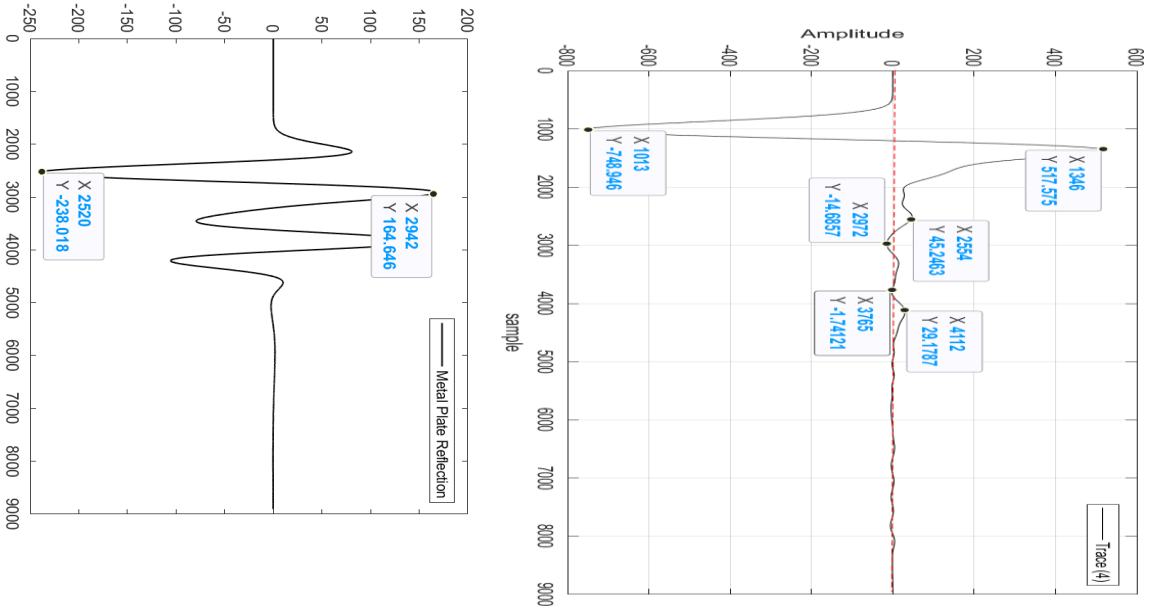

(b)

(c)

Figure 4.9 Measuring result of A-Scan output data (a) five random trace output (b) calibrated Amplitude of metal *plate (c) Matlab Measurement Trace 4 A-Scan output data.*

Sample dates are shifting to time windows on gprMax. To determine the travel time of a single sample, divide the time frame used in the input file by the number of samples that were produced by the simulation. That means ($\frac{21*10^{-9}}{8905} = 0.00236ns$) 1 sample = 0.00236ns)

My estimation of the dielectric characteristics and layer thickness is shown in the table below using equations (3.3), (3.4), and (3.5). Without mentioning the subgrade, the ballast and sub ballast layer are described.

Ballast Layer										
Trace	***(+A0)***	***(-A0)***	***Acalib***	***A0***	***Er1***	***t1***	***t0***	***Δt***	***c***	***h***
Trace 4	515	749	402	1264	*3.735*	6.52E-09	2.76E-09	3.76E-09	3E+08	*0.29181*
Trace 20	551	767	402	1318	*3.526*	6.44E-09	2.76E-09	3.68E-09	3E+08	*0.29397*
Trace 34	494	726	402	1220	*3.932*	7.07E-09	2.76E-09	4.31E-09	3E+08	*0.32604*
Trace 44	478	737	402	1215	*3.956*	7.36E-09	2.76E-09	4.6E-09	3E+08	*0.34692*
Trace 56	485	727	402	1212	*3.97*	6.75E-09	2.76E-09	3.99E-09	3E+08	*0.30036*

Table 4.1 Result of dielectric constant and thickness of ballast layer.

Sub Ballast Layer										
Trace	***(A0)***	***(A1)***	***Acalib***	***Er1***	***Er2***	***t2***	***t1***	***Δt***	***c***	***h***
Trace 4	1264	26	402	3.7354	6.62362	9.745E-09	6.52E-09	3.225E-09	3E+08	0.18796
Trace 20	1318	69	402	3.5259	7.84101	9.99E-09	6.44E-09	3.55E-09	3E+08	0.19016
Trace 34	1220	68	402	3.9318	9.59344	1.138E-08	7.07E-09	4.31E-09	3E+08	0.20872
Trace 44	1215	36	402	3.9558	7.81482	1.196E-08	7.36E-09	4.6E-09	3E+08	0.24682
Trace 56	1212	27	402	3.9704	7.40257	1.074E-08	6.75E-09	3.99E-09	3E+08	0.21997

Table 4.2 Result of dielectric constant and thickness of Sub-ballast layer.

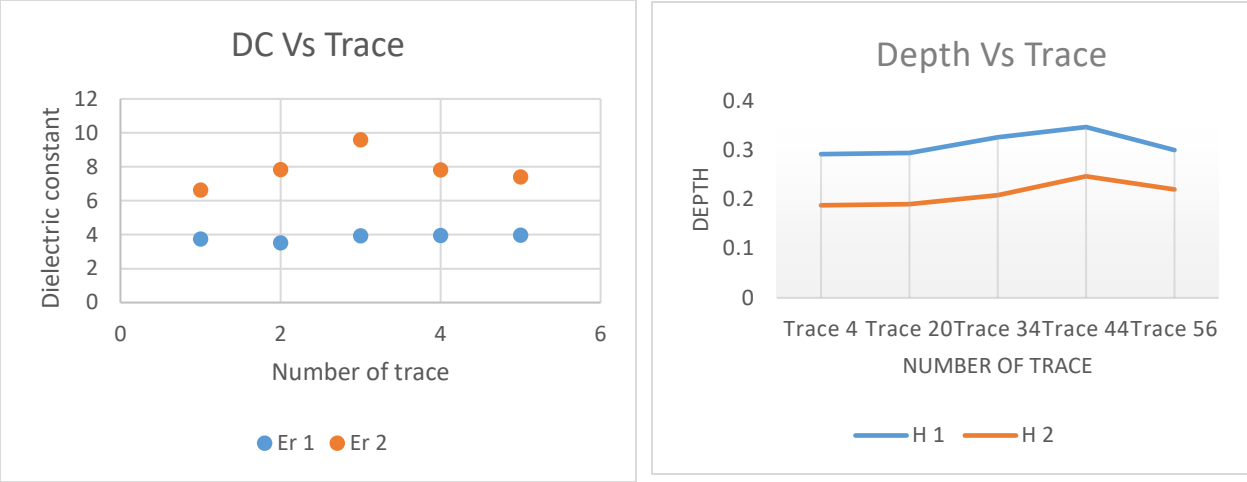

(a) (b)

Figure 4.10 a) dielectric constant Vs Trace and b) depth of track bed Vs Trace.

CRIM CB Er Value	Estimation Er value	Absolute Error	Er Relative Error	Actual depth	Estimation Depth	Absolute Error	Depth Relative Error
3.24	3.735	-0.495	-15.290	0.3	0.292	0.008	2.727
3.24	3.526	-0.286	-8.823	0.3	0.294	0.006	2.009
3.24	3.932	-0.692	-21.353	0.3	0.326	-0.026	-8.680
3.24	3.956	-0.716	-22.094	0.3	0.347	-0.047	-15.640
3.24	3.970	-0.730	-22.544	0.3	0.300	0.000	-0.121

Table 4.3 relative Error clean ballast dielectric constant and ballast depth

4.2.3 Different ballast layer thickness

Analyzing the effects of various parameters, including layer thickness, on the Ground Penetrating Radar (GPR) simulation results is known as a parametric research in GprMax. The effect of ballast layer thickness (300, 200, and 100 mm) on GPR simulations using GprMax in this instance. This is how it can go about this. :

From the above simulation setups where the only varying parameter is the thickness of the ballast layer. For example:

Simulation 1: Ballast layer thickness = 300mm

Simulation 2: Ballast layer thickness = 200mm

Simulation 3: Ballast layer thickness = 100mm

When evaluating the output raw data from GprMax simulations in terms of B-scan and A-scan, it

is essentially analyzing how the electromagnetic waves interact with the layered structure (including ballast layers of different thicknesses) and how this interaction manifests in the recorded data.

Here is below figure the comparison study of A-scan and B-scan.

A-scan (Amplitude scan):

Figure 4.11 A-scan shows the received signal's amplitude, or intensity, as a function of depth or time at a single location, or single trace, on the scan line for three distinct ballast layer conditions. The top of the ballast layer and other subsurface layer interfaces are examples of common reflections from underlying features. The thickness of the ballast layer is evidently influenced by the temporal reflection of the top of the sub ballast which clearly visible on the figure, and the top of subgrade reflection still the same number of sample reflection.

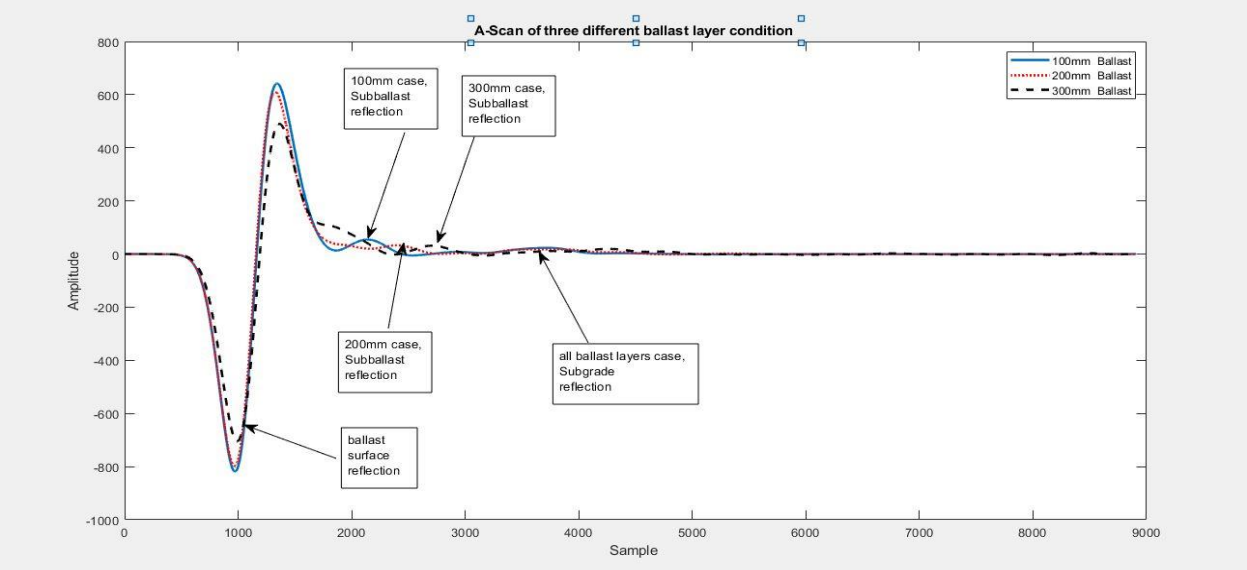

Figure 4.11 A-scan of three different ballast layer condition

B-scan (Depth profile scan):

Figure 4.12 B-scan displays a vertical cross-sectional view along a scan line, showing how the amplitude varies with depth at different lateral positions of ballast and sub-ballast thickness. It helps visualize the distribution of reflections across the entire scan line (60 traces), revealing the structure beneath the surface, including layer interfaces and anomalies. Here the figure outlines 300mm, 200mm, and 100mm ballast layer thickness from left to right, and each ballast layer is

visible. The figure has different boundary conditions, which are marked by a blue line. The first line is the top of the ballast surface reflection, the second line is sub-ballast reflection, and the last one is the top of subgrade reflection.

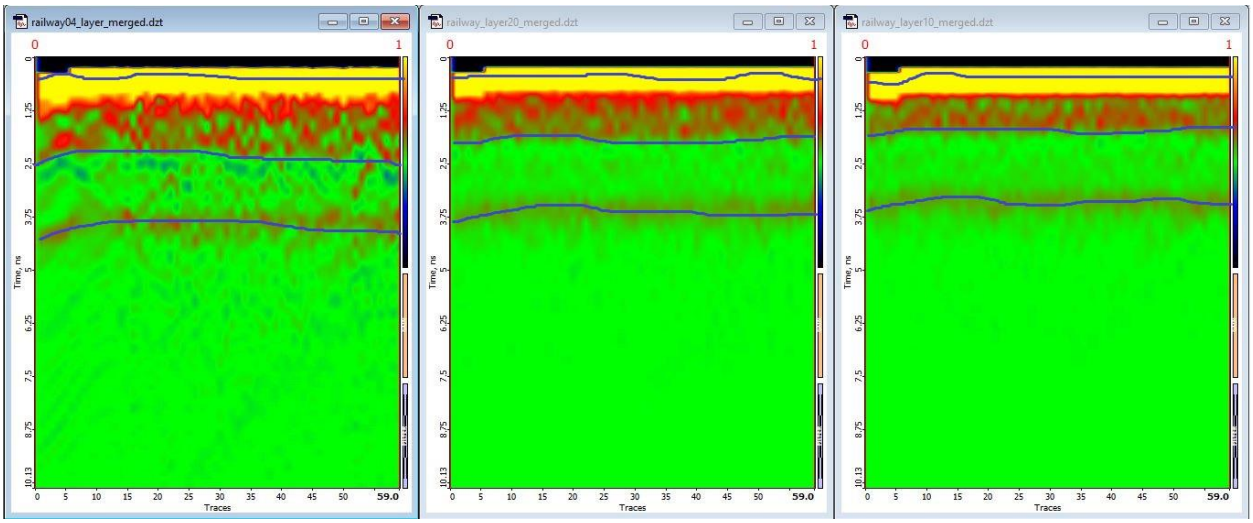

Figure 4.12 B-scan of three different ballast layer condition

In summary, the thickness of the different ballast layer thickness directly influences the effectiveness of GPR surveys. It affects signal attenuation, reflection strength, resolution, and depth penetration, all of which are crucial factors in interpreting subsurface conditions and features. Understanding these effects helps in optimizing GPR surveys and improving the reliability of subsurface assessments in various engineering and geological applications

4.2.3. Ballast Water Content/Anomaly Investigation

The quantity of ballast fouling and the moisture content are two important components of ballast quality that affect how stiff the track bed is. This is demonstrated by comparing two GPR antennas (400MHz and 1600MHz in this case) for the railway track bed water content and anomaly inquiry. Because the composition of track bed materials can vary greatly, it might be challenging to extract pertinent information from GPR data alone.

This model simulation thoroughly examines the ways in which the electromagnetic characteristics of rail bed materials, which are connected to varying levels of moisture content and ballast fouling, impact the qualities produced by reflected and scattered GPR signals. It is shown that because of the inherent uncertainties in the way GPR responds to fouling and moisture in the track bed, neither can be reliably anticipated by the technique. This is a B-scan using the same preprocessing

techniques for layer thickness estimation. Preprocessing of the 400 MHz and 1600 MHz antennas on the left and right, respectively:-

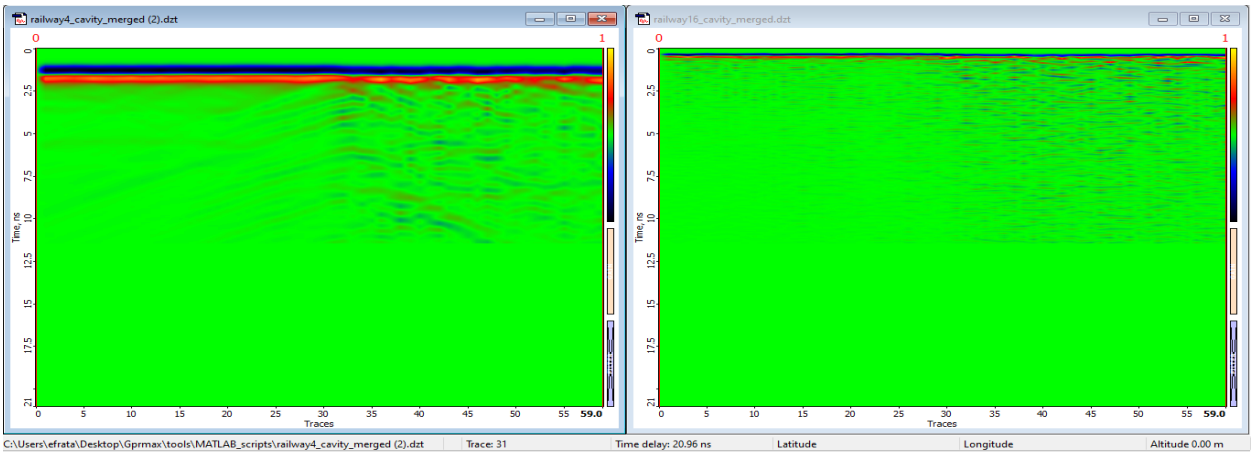

(a)

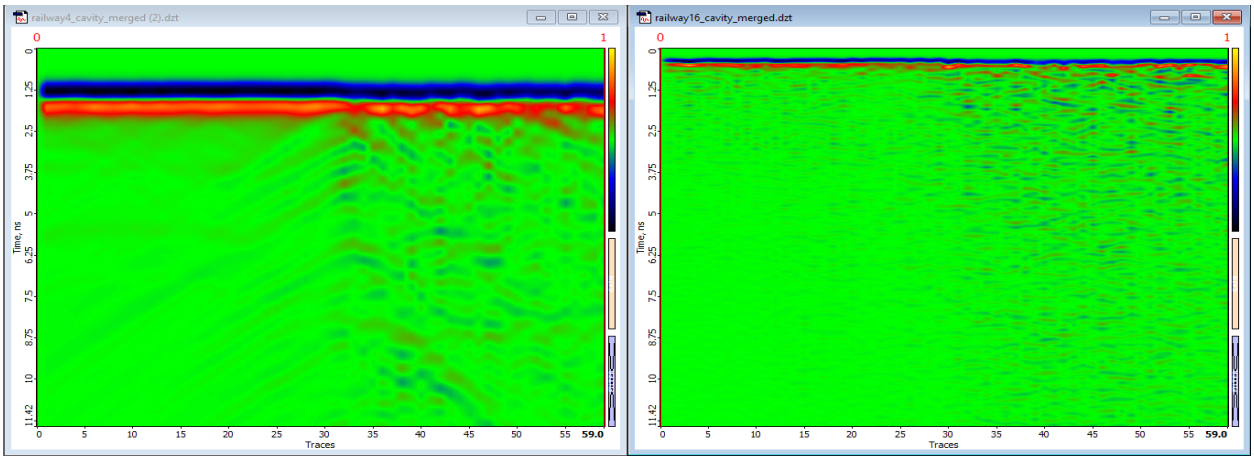

(b)

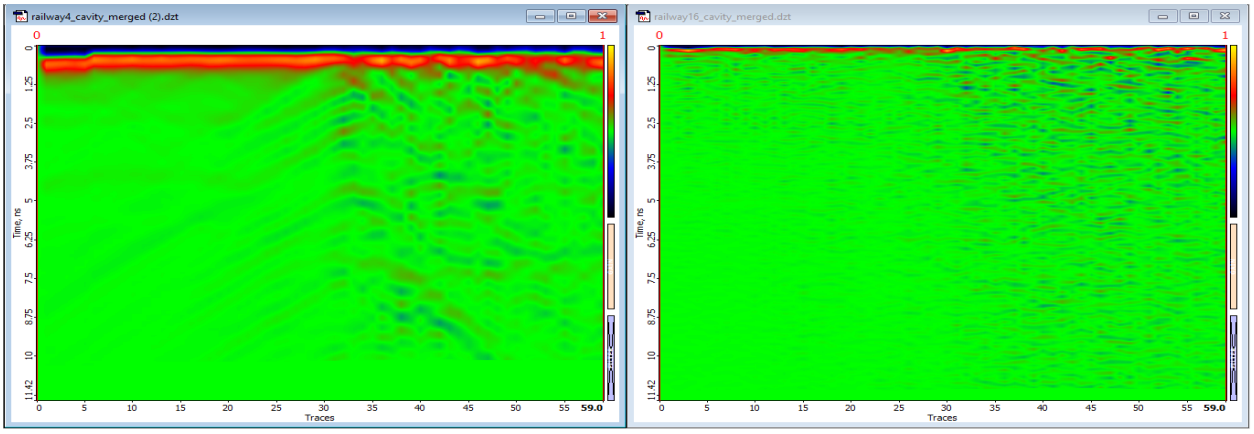

(c)

Figure 4.13 B-scan Preprocessing of 400MHz and 1600MHz antenna (a) Raw Data (simulation output), (b) trimming sample size, (c) time zero flittering

Through seeing the above B-scan output processing 400MHz and 1600MHz is holding something different but not enough to interpret, so to change in the color plate to gray scale. Color plates are often used to represent the GPR data and enhance the interpretation process. It is typically involve assigning different colors to specific amplitudes or reflections in the GPR data. This allows for easier visualization and identification of subsurface features.

By examining the color plate, I can identify various subsurface features such as geological layers and voids, or anomalies. The interpretation process involves analyzing the shape, depth, continuity, and spatial relationships of these features to understand their significance and potential implications.

After changing the color plate applying a gain function which is Signal-to-Noise Ratio (SNR) measures the strength of the desired signal relative to the background noise.

Below is a figure showing the output result and a discussion of an observation It made.

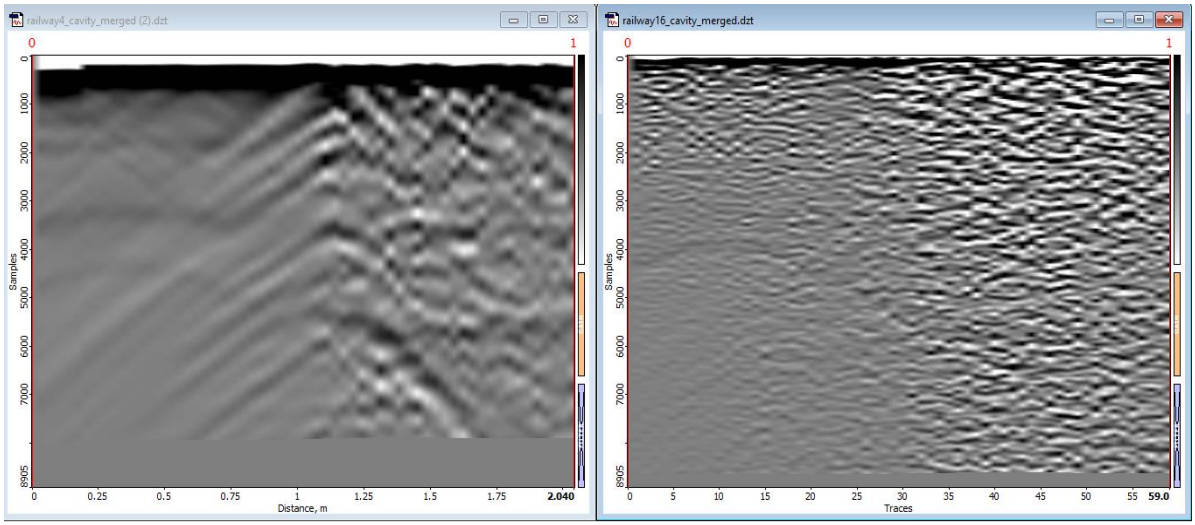

(a)

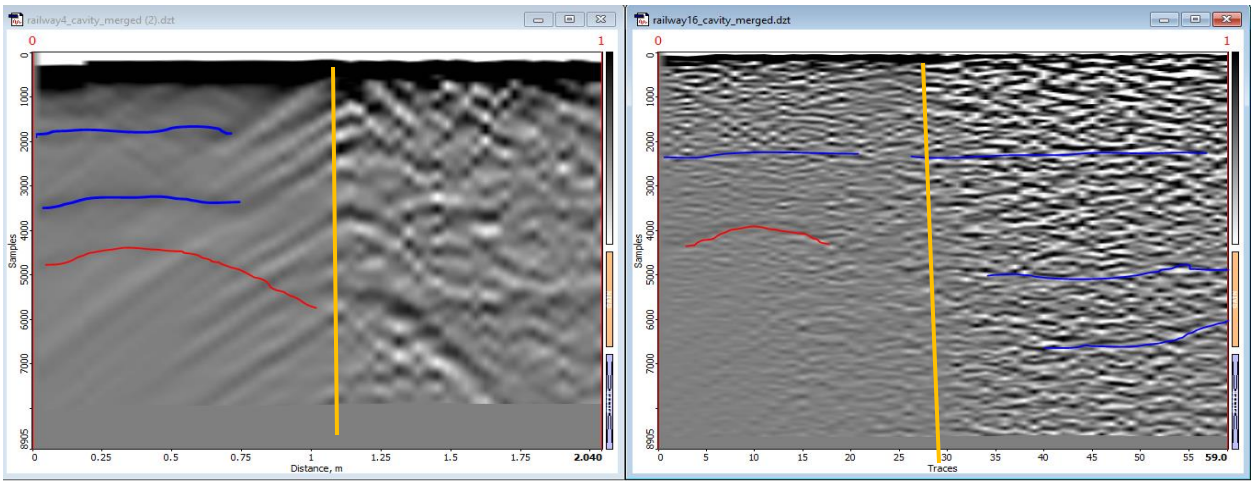

b)

Figure 4.14 a) gray scale color plate with adding 50dB, b) Lining the observing data

- The intersection (yellow line) of dry and wet fouling ballast is clearly visible, but the reflection of the 400 MHz antenna creates a huge parabola between them that either provides false information or is caused by the connection of materials with wildly divergent dielectric properties and a small signal frequency antenna response. However, clear signal responses are obtained from a 1600 MHz antenna without harming various material components reflection.
- The 400 MHz antenna can be seen well on the dry side but not as well on the wet one due to its good layer detection. The red line that resembles a parabola in figure 4.14 (b) is a cavity (void) reflection, and the two blue lines in figure 4.14 (b) on the left side of the dry section are sub-ballast and subgrade reflections, respectively. Additionally, it is challenging to identify the layer and void in the moist part. On the other hand, in the 1600 MHz antenna figure 4.14 (b), a single line that is blue-lined and represents subgrade reflection is seen on the right side of the dry area. Due to their comparable dielectric property behavior, it is challenging to see the junction of the bottom ballast and top of the sub ballast; the red lines represent reflections of the cavity (void). Because of the high dielectric property of the material composition, there is some reflection (blue line) in a wet condition, but it is difficult to determine which one is a suitable representative of the layer. A wet condition also alters the depth of the reflection. This is due to the fact that high-dielectric materials have a long two-way traveling time (TWTT).

5. VERIFICATION STUDY THROUGH LABORATORY EXPERIMENTS

The process and outcome of the Ground Penetrating Radar simulation for determining the thickness of the track bed and characterizing the material are detailed in Chapters 3 and 4. This chapter contains experimental work that validates the work done in earlier chapters. A number of lab tests were conducted to replicate the work done using numerical modeling. The validity and accuracy of the framework were assessed by comparing the outcomes of the simulated experiments and the laboratory investigations. For both lab and modeling studies, the A KRRI (Korea Railroad Research Institute, Uiwang-si, South Korea) 0.5 GHz antenna was utilized. .

5.1 Experimental setup

"Three ballast boxes with different fouling levels were used in the lab to imitate the ballast rails. According to figure 5.2, the three ballast boxes stand in for the phases of fouling on a ballast track: (1) clean (Box 1), (2) slightly fouled (Box 2), and (3) totally fouled (Box 3). Before the boxes are filled, the fouling material is always combined with the ballast aggregate in specified ratios." [42].

"Wooden frames measuring 2 m by 2 m by 0.6 m made up the ballast tracks. To make visual inspections easier, the front side wall was made of a translucent material. The ballast box manufacturing process is shown in Figure 5.1. The gravel and fouling materials were combined with an excavator. The boxes were subsequently filled with this mixture, as seen in Figure 5.2."

(a) (b) (c)

Figure 5.1. Construction of ballast boxes. (a) Build wooden box (b) Mix with fouled materials (c) Construct ballast layer [42]

(a) (b) (c)

Figure 5.2 fouling ballast condition (a) Box 1, (b) Box 2 and (c) Box 3. [42]

A 500 MHz GPR instrument made by the Korea Railroad Research Institute (KRRI) in Uiwang-si, South Korea, for laboratory testing and surveys of ballast fouling conditions.

"In order to avoid the boundary impacts of the ballast boxes, the centerlines of the boxes were surveyed. Figure 5.3 shows how the KRRI devices are set up and used during the test. There are eight channels on the KRRI device: four on the left and four on the right. Therefore, during the lab test, just one side antenna (channel-0) was employed to scan the centerline (pleases see Figure 5.3b)" [42].

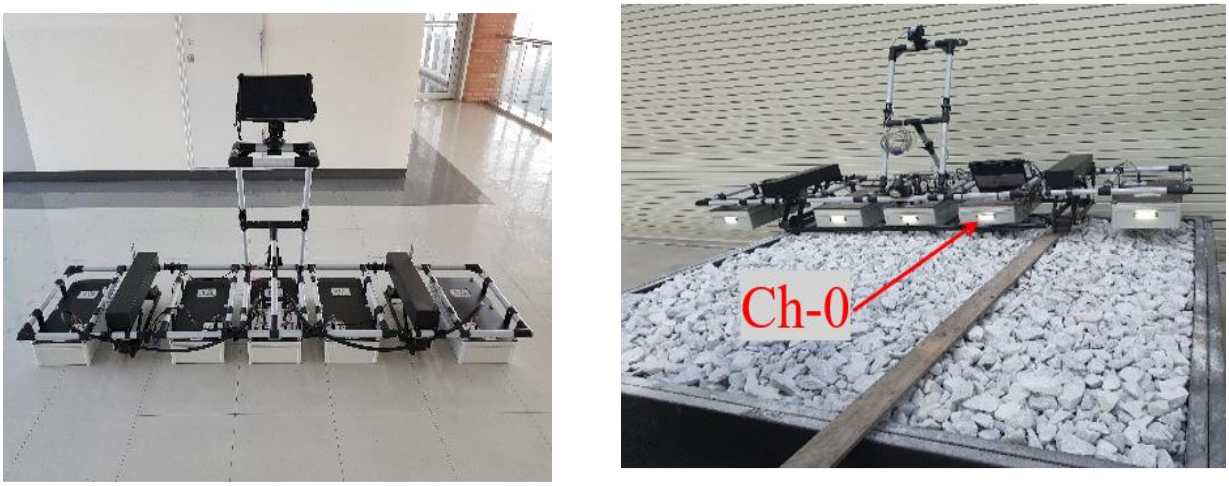

(a) (b)

Figure 5.3. "(a) KRRI GPR device; (b) KRRI ballast survey in the lab" [42]

"(Birhane, F.N.; Choi, Y.T.; Lee, S.J. Development of Condition Assessment Index of Ballast Track Using Ground-Penetrating Radar (GPR). Sensors 2021, 21, 6875.) Note that the experimental model mentioned above is based on this work. https://doi.org/10.3390/s21206875" and the actual GPR data availability is obtained through a request

5.2. Simulator and Environment Setup

The design of the ballast fouling situation and the simulation environment were created simultaneously. This was to guarantee that the simulation model would most nearly resemble the actual environment in order to properly validate the results. In the x, y, and z dimensions, the environment was spatially separated into 2 mm cells. By reducing the y dimension to a single cell, the world was made simpler as a 2D environment. .

Because solving a three-dimensional environment required exponentially large computation times, the 2D Simplification was implemented. In early software testing, resolving 200mm of horizontal scans in a 3D environment took about three days of computation time, while resolving 2m in an identical (bar y) 2D environment took about thirty minutes with little variation in results. Additionally, the random access memory (RAM) of a computer affects how long it takes to compute a 3D or 2D problem.

Modeled dimensions for the simulation environment were 2 m (x) by 680 mm (z). The lower 600mm depth is occupied by the ballast fouling condition medium, with the remaining 80mm being modeled as air. As in the lab experiment, three ballast fouling conditions are modeled. Figure 2 shows a geometric representation of a different ballast fouling scenario. In order to match the actual GPR hardware, the transmitter and receiver are placed right on the air-ballast interface and are set to perform a scan every 2 mm in a horizontal manner. A 40ns time window was selected in order to better align with hardware specs. The GPR hardware only obtains 256 samples during this time, compared to 4092 samples produced by the simulator. Consequently, the simulator's output was down-sampled to correspond.

According to the nominal manufacturer requirements, the transmitter source wave was originally supposed to be a Hertzian dipole excitation with a Ricker waveform with a central frequency of 0.5GHz. However, preliminary tests revealed that the resulting radar graphs were too clean and basic because the simulator was unable to reproduce noise and other flaws such antenna ringing effects. This is mostly because the 2D simulator is idealized and simplified. .

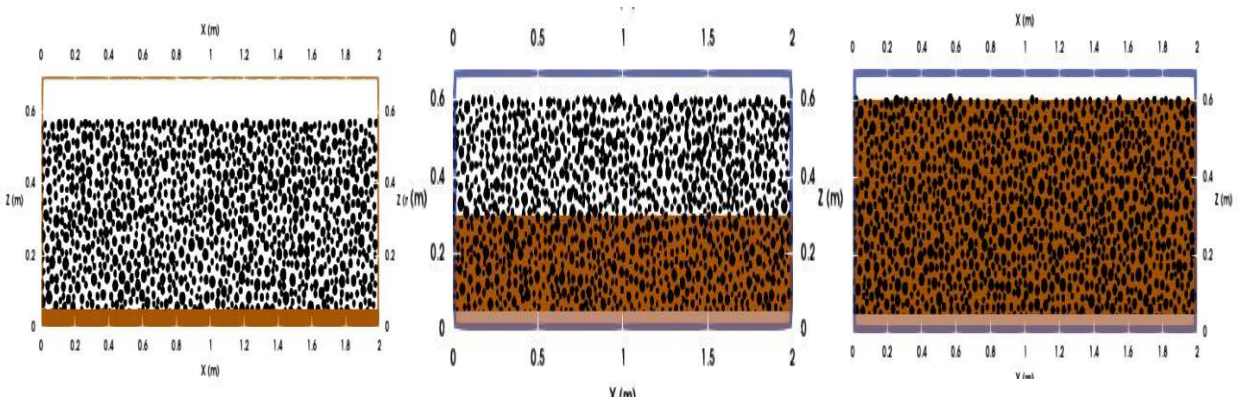

(a) (b) (c)

Figure 5.4. 2D geometry view of ballast fouling condition for simulation model (a) CB; (b) PFB and (c) FFB.

5.3 Real and Simulated Data Comparison

Figure 5.5 shows preprocessed B-scan images from the KRRI devices and the GprMax simulation. As the chart shows, it is difficult to ascertain the ballast's fouling level only from the B-scan image. Both the computer model and the KRRI devices are able to identify the border between the sublayer and the ballast layer. . It would be presumed that the boundary in Figure 5 is located where the GPR signal jumps. The only information that B-scan images can provide is the boundary. Only the boundary top of the ballast surface (red) and the bottom ballast reflection of the ground surface and wood plate are detectable.

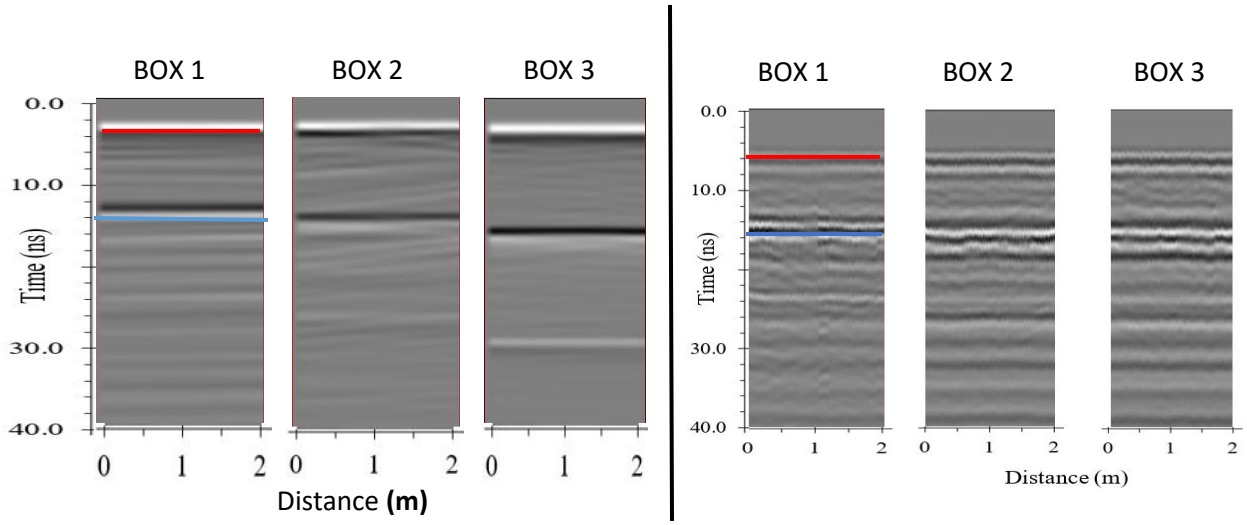

Figure 5.5. "(a) B-scan 500 MHz GprMax Simulation, and (b) B-scan 500 MHz KRRI device using Channel 0."

Figure 5.6 compares the shape, phase, and field strength of various wavelets between the real and simulated data. The model makes use of a look-alike KRRI model, whereas the real wavelet was generated by the actual KRRI device's 500 MHz antenna. A wood box with a distinct permittivity ballast fouling condition—such as clear ballast or ballast mix with fine particles—was the aim in both situations.

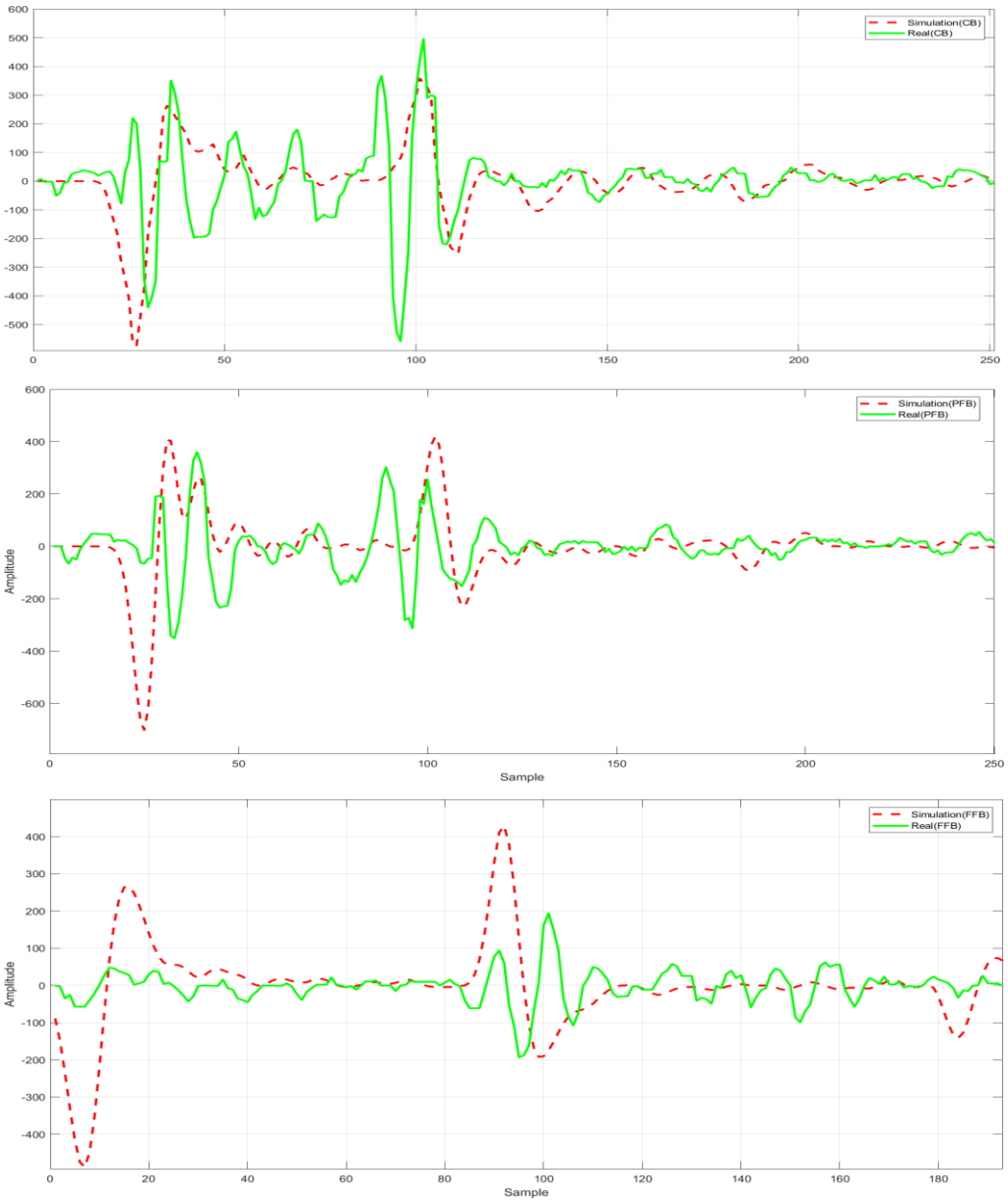

Figure 5.6 comparison result of the A-Scan at the center point of the domain (A) CB; (B) PFB and (C) FFB.

- As shown the above the model specimen conditions considered in this study (Fig. 5.6 A-scan results calculated from the center of the domain according to three ballast condition are presented. and showed the results compared with the model test results. A little bit about the A-scan results of the analysis and experiment under each test condition. It can be seen that there is an error of a 2D numerical analysis model is used to describe the antenna's 3D shape. Because each receiver was considered a point, It is believed that it occurred. More reliable A-scan data In order to secure the shape of the future antenna, It was determined that expansion into a 3D analysis model would be necessary.
- Clean ballast typically has a higher frequency response both simulated and experimental case, compared to fouling ballast on ground penetrating radar (GPR). This is because clean ballast is more homogeneous and uniform, allowing the radar waves to penetrate and reflect back with minimal interference. On the other hand, fouling ballast may contain various materials such as fine particle, which can scatter and attenuate the radar waves, resulting in a lower frequency response.
- As shown the above figure in the green signal of Real GPR response has limitations due to factors like signal attenuation, scattering, and interference from surrounding objects. Simulations can help understand these limitations and develop strategies to overcome them. But the ground truth of Real GPR data can be validated by comparing it with information obtained through excavation or other means.

Generally, simulations can provide valuable insights and aid in system development and optimization, it cannot fully replace real GPR data for accurate subsurface imaging and detection. Combining both real and simulated data can enhance the understanding and interpretation of GPR results.

6. CONCLUS ION AND RECOMMENDATIONS

This chapter's objective is to present the thesis's overarching conclusions and a summary of each chapter's output. In light of this findings, certain suggestions are made for additional study and advancement.

6.1 Conclusions

This thesis' primary goal is to develop a numerical model. For material characterization and track bed thickness estimation, ground penetrating radar simulation is used. The following conclusions could be made in light of this research:

- The study successfully demonstrated that varying degrees of ballast fouling significantly affect GPR signal penetration and reflection characteristics. Advanced numerical models were developed, closely mimicking real-world conditions, which enhance the understanding of ballast fouling impacts on GPR performance. These models can serve as reliable tools for predicting fouling conditions, aiding in the maintenance and management of railway infrastructure.
- The research revealed that changes in ballast layer thicknesses have a notable impact on GPR detection capabilities. The comparison of different antennas indicated that specific antennas are better suited for particular layer thicknesses, optimizing the accuracy of GPR measurements. These findings can guide the selection of appropriate antennas for varied trackbed conditions, improving the reliability of GPR in railway applications.
- The investigation into ballast moisture content showed that wet and dry conditions significantly influence GPR signal propagation and reflection characteristics. The study highlighted the necessity to account for moisture content variations when interpreting GPR data, as it affects the accuracy of trackbed assessments. Understanding these effects ensures more precise monitoring and maintenance of railway infrastructure under different environmental conditions.
- The capability of GPR simulations to accurately predict trackbed layer thicknesses under varying conditions was slightly verified. The simulations provided some reliable results that matched real-world scenarios, confirming their validity as a tool for railway infrastructure analysis. This verification supports the use of GPR simulations in practical applications, reducing the need for extensive physical testing.

- The study highlighted the potential of GPR simulations in GprMax to eliminate the need for cost-intensive physical models. By enabling professionals and academics to conduct mathematical experiments on their computers, the research promotes a cost-effective approach to studying railway trackbeds. This advancement allows for more efficient resource allocation and fosters innovation in railway infrastructure management.

6.2 Recommendation and Future Work

A more precise and reliable simulation of ground penetrating radar for forecasting track bed thickness and material characterization techniques, as well as an improved form factor for the "CRIM model and SRC" approach , are the results of this study. Even if the aforementioned has been thoroughly examined, more research may be required to improve the models' accuracy and dependability as well as to apply them to new study areas. Here are a few chances to conduct additional research. :

- Increasing the models' realistic geometry may improve the dependability of the results, depending on computing power. .
- Instead of having a single shape factor for all materials, heterogeneous models contain distinct shape factor values for each material. This could improve the shape factor's accuracy and forecast improved bulk permittivity. .
- Simulating 3D Model ballast fouling condition and using real antenna model with various commercial antenna structures including the MALA 1.2GHz, GSSI 400MHz, and GSSI 1.5GHz (Model 5100). In this study filed investigation is not considered which is recommended for validation the real and synthetic data.
- Compare Synthetic and Real Data on Machin Learning Models for a good interpretation and findings.
- For Sim vs Exp, In order to increase the reliability of the analysis results, the actual antenna expansion into a 3D model that can reflect the shape as it is required.

REFERENCE

[1] L. B. Ciampoli, A. Calvi, and F. D'Amico, "Railway ballast monitoring by GPR: A test-site investigation," Remote Sens., vol. 11, no. 20, pp. 1–14, 2019, doi: 10.3390/rs11202381.

[2] "Ground Penetrating Radar Theory and Applications. Chapter 2. Electrical and Magnetic Properties of Rocks, Soils and Fluids". Cassidy, N. J. (2009). Elsevier. Editor: HarryM.Jol.

[3] "Ground Penetrating Radar Theory and Applications. Chapter 1. Electromagnetic Principles of Ground Penetrating Radar". Elsevier. Editor: Harry M. Jol , Annan, A. P. (2009)..

[4] Goodman, D., Piro, S. (2013). Understanding GPR via a Simulator. In: GPR Remote Sensing in Archaeology. Geo technologies and the Environment, vol 9. Springer, Berlin, Heidelberg. https://doi.org/10.1007/978-3-642-31857-3_2

[5] Rail Tracks and Track Beds in Tunnels. 2013. [Online]. Available: http://www.aftes.asso.fr/contenus/upload/File/Publications/Recommandations/GT40R2A1.pdf AFTES (2013),. [Accessed 21 July 2014].

[6] Non-destructive technologies for sustainable assessment and monitoring of railway infrastructure: a focus on GPR and InSAR methods. Ferrante, C., Bianchini Ciampoli, L., Benedetto, A. et al. Environ Earth Sci 80, 806 (2021). https://doi.org/10.1007/s12665-021-10068

[7] "Analysis and Evaluation of Railway Track Systems on Soft Soil: Trackbed Thickness Design and Dynamic Track-Soil Interaction" Puguh B. Prakoso, 2017., TECHNISCHE UNIVERSITÄT MÜNCHEN

[8] Track Geotechnology and Substructure Management. Selig, E. and Waters, J. (1984).

[9] Track Substructure Maintenance–From Theory to Practice. Technical report,, Selig, E. T. and Cantrell, D. D. (2001). AREMA 2001.

[10] Advanced Rail Geo technology- Ballasted Track. CRC Press/Balkema Indraratna, B., Salim, W., and Rujikiatkamjorn, C. (2011)..

[11] The Railway Track and Its Long Term Behaviour. Springer Tzanakakis, K. (2013)..

[12] Geophysical prospection of underground water in the desert by means of electromagnetic interference fringes El Said, M. A. H. (1956)..

[13] Ground Penetrating Radar Principles, Procedures & Applications. Sensors & Software Inc Annan, A. P. (2003)..

[14] Scanlan KM, Hendry MT, Martin CD, Schmitt DR. Evaluating the sensitivity of low-frequency ground-penetrating radar attributes to estimate ballast fines in the presence of variable track foundations through simulation. Proceedings of the Institution of Mechanical Engineers, Part F: Journal of Rail and Rapid Transit. 2018;232(4):1168-1181. doi:10.1177/0954409717710408

[15] Inspection of railroad ballast using geophysical method. International Journal of Pavement Engineering, Plati, C., Loizos, A., and Papavasiliou, V. (2010). 11.

[16] The application of time domain ground penetrating radar to evaluate railway track ballast. NDT & E International Gallagher, G. P., Leiper, Q., Williamson, R., Clark, M. R., and Forde, M. C. (1999)., 32.

[17] An Integrated System for Accurate Tie and Ballast Condition Assessment. AREMA Conference Keogh, T., Mesher, D. E., and Keegan, T. R. (2006)..

[18] Imaging attributes of railway track formation and ballast using ground probing radar. NDT & E International, Jack, R. and Jackson, P. (1999)., 32.

[19] Lawrence B Conyers. "Analysis and interpretation of GPR datasets for integrated archaeological mapping." In: Near Surface Geophysics 13.6 (2015), pp. 645–651

[20] GPR Antenna Array for the Inspection of Railway Ballast. Proceedings of the National Seminar & Exhibition on Non-Destructive Evaluation, Kind, T. (2011)..
[21] Evaluation of ballast fouling using GPR. Technical report. 15th International Conference on Ground Penetrating Radar, Fontul, S., Fortunato, E., and De Chiara, F. (2014)..
[22] Railroad Ballast Evaluation Using Ground-Penetrating Radar. Journal of the Transportation Research Board Leng, Z. and Al-Qadi, I. L. (2010)., 2159.
[23] Ground Penetrating Radar, 2nd Edition. The Institution of Electrical Engineers, Daniels, D. J. (2004)..
[24] Benchmarking large scale GPR experiments on railway ballast. Construction and Building Materials De Bold, R., O'Connor, G., Morrissey, J. P., and Forde, M. C. (2015)., 92.
[25] Non-destructive and geotechnical testing of railway track bed ballast. PhD thesis, University of Edinburgh. Clark, M. (2001).
[26] Non-destructive assessment of rail track condition using ground penetrating radar. Technical report Su, L., Indraratna, B., and Rujikiatkamjorn, C. (2011). , IACMAG 2011.
[27] Identification of type and degree of railway ballast fouling using ground coupled GPR antennas P. Anbazhagan Journal of Applied Geophysics, ISSN: 0926-9851, Vol: 126, Page: 183-190, 2016.
[28] "Development of a time-frequency approach to quantify railroad ballast fouling condition using ultra-wide band ground- penetrating radar data. International Journal of Pavement Engineering" Al-Qadi, I., Xie, W., Jones, D., and Roberts, R. (2010a)., 11.
[29] "Data Analysis Techniques for GPR used for Assessing Railroad Ballast in High-Frequency Environment. Journal of Transportation Engineering" Al-Qadi, I., Xie, W., Roberts, R., and Leng, Z. (2010b)., 136.
[30] "Railroad Bal- last Fouling Detection using Ground Penetrating Radar - A New Approach Based on Scattering from Voids. Technical report Roberts", R., Rudy, J., Al-Qadi, I., Tutumluer, E., and Boyle, J. (2006)..
[31] "An inspection of railway ballast quality using ground penetrating radar in Finland. Journal of Rail and Rapid Transit" Silvast, M., Nurmikolu, A., Wiljanen, B., and Lavomäki, M. (2010a)., 224.
[32] "Development of Wavelet Technique to Interpret Ground-Penetrating Radar Data for Quantifying Railroad Ballast Conditions. Transportation Research Journal",Shangguan, P., Al-Qadi, I., and Leng, Z. (2012)., 2289.
[33] "A Complete FDTD Simulation of a Real GPR Antenna System Operating Above Lossy and Dispersive Grounds. Progress in Electromagnetics Research" Uduwawala, D., Norgren, M., Fuks, P., and Gunawardena, A. (2005)..
[34] "Railway track inspection using GPR" Hugenschmidt, J. (2000).. Journal of Applied Geo- physics, 43.
[35] "Use of Ground Penetrating Radar for Transportation Infrastructure Maintenance. PhD thesis, Norwegian University of Science and Technology" Lalagüe, A. (2015)..
[36] "Geo radar-model and in-situ investigations for inspection of railway tracks. Technical report, Fifth International Conferential on Ground Penetrating Radar" Göbel, C., Hellmann, R., and Petzold, H. (1994)..
[37] "Ground Penetrating Radar for Railroad Track Substructure Evaluation. Technical report. U.S. Department of Transportation" Hyslip, J. P., Olhoeft, G. R., Smith, S. S., and Selig, E. T. (2005)..
[38] "Railroad Track Monitoring Using Ground Penetrating Radar: Simulation Study and Field Measurements." SPIE Confer- ence on Subsurface Sensors and Applications, Denver, Colorado Narayanan, R. M., Kumke, C. J., and Li, D. (1999).
[39] Ayala-Cabrera, D., Campbell, E., Carreño Alvarado, E. P., and Izquierdo, J. (2014). Water Leakage Evolution Based on GPR Interpretations. Procedia Engineering, 89..
[40] Giannopoulos A. (1997) gprMax User Guide Release 3.0.0b20. https://docs.gprmax.com/en/latest/

[41] “gprMax: Open source software to simulate electromagnetic wave propagation for Ground Penetrating Radar, Computer Physics Communications” Warren, C., Giannopoulos, A., & Giannakis I. (2016). (http://dx.doi.org/10.1016/j.cpc.2016.08.020)
[42] “Development of Condition Assessment Index of Ballast Track Using Ground-Penetrating Radar” (GPR)Birhane, F.N.; Choi, Y.T.;Lee, S.J.. Sensors 2021, 21, 6875. https://doi.org/10.3390/s21206875
[43] “Optimising the Complex Refractive Index Model for Estimating the Permittivity of Heterogeneous Concrete Models” Zadhoush, H.; Giannopoulos, A.; Giannakis, I.. Remote Sens. 2021, 13, 723.
[44] Albéric De Coster , Evaluation of pavement layer thicknesses using GPR: A comparison between full-wave inversion and the straight-ray method. 0950-0618/ 2018 Elsevier Ltd. All rights reserved.
[45] “In situ measurements of hot-mix asphalt dielectric properties” Al-Qadi, I.L.; Lahouar, S.; Loulizi, A.. NDT E Int. 2001, 34, 427–434.

APPENDIX A

A1 Homogeneous clean ballast of input data for GPRMax Software.

```
#title: Homogeneous_Clean_Ballast_2D
#domain: 0.4 0.001 0.45
#dx_dy_dz: 0.001 0.001 0.001
#time_window: 20e-9
#material: 3.24 0 1 0 Clean_Ballast
#box: 0 0 0.05 0.4 0.001 0.35 Clean_Ballast
#box: 0 0 0 0.4 0.001 0.05 pec n
#waveform: gaussian 1 0.4e9 my_gaussian
#hertzian_dipole: y 0.2 0 0.35 my_gaussian
#rx: 0.2 0 0.35
#src_steps: 0.004 0 0
#rx_steps: 0.004 0 0
#box: 0 0 0 0.4 0.001 0.05 pec n
#geometry_view: 0 0 0 0.4 0.001 0.45 0.001 0.001 0.001 Homogeneous_Clean_Ballast_2D n
```

A2 Heterogeneous clean ballast of input data for GPRMax Software.

```
#title: Hetrogeneous_Clean_Ballast_2D
#domain: 0.4 0.001 0.46
#dx_dy_dz: 0.001 0.001 0.001
#time_window: 20e-9
#material: 6 0 1 0 aggregate
#python:
import random
import math
from gprMax.input_cmd_funcs import cylinder
from gprMax.input_cmd_funcs import box
from gprMax.input_cmd_funcs import sphere
class Aggregate():
    def __init__(self, p_aggregate):
```

```
        self.z = random.uniform(0.005, 0.40)
        if p_aggregate > 0.60:
            lower = 0.004
            upper = 0.008
        if p_aggregate > 0.80:
            lower = 0.006
            upper = 0.010
        else:
            lower = 0.010
            upper = 0.020
        radius = random.uniform(lower, upper)
        self.r = radius
    def check_collision(self, aggregate, agg):
        j = 0
        no_coll = False
        while j < len(aggregate) and no_coll is False:
            other = aggregate[j]
            point_dist = math.sqrt((agg.x - other.x)**2 + (agg.z - other.z)**2)
            j += 1
            if point_dist <= agg.r + other.r:
                no_coll = True
        return no_coll
area_sum = 0
p_aggregate = 0
area_box = 0.39 *  0.39
aggregate = []
while p_aggregate < 0.6:
    agg = Aggregate(p_aggregate)
    if agg.check_collision(aggregate, agg) is False:
        aggregate.append(agg)
        area_sum +=  math.pi * agg.r**2
```

```
        p_aggregate = area_sum / area_box
    for i in range(0, len(aggregate)):
        agg = aggregate[i]
        sphere(agg.x, 0.001, agg.z, agg.r, 'aggregate', 'n')
    #end_python:
    #waveform: gaussian 1 0.4e9 my_gaussian
    #hertzian_dipole: y 0.20 0 0.40 my_gaussian
    #rx: 0.20 0 0.40
    #src_steps: 0.04 0 0
    #rx_steps: 0.04 0 0
    #box: 0 0 0 0.4 0.001 0.05 pec n
    #geometry_view: 0 0 0 0.4 0.001 0.46 0.001 0.001 0.001 Hetrogeneous_Clean_Ballast_2D n
```

A3 Railway track bed layer of input data for GPRMax Software.

```
#title: Railway_Layer_2D
#domain: 2 0.001 0.9
#dx_dy_dz: 0.001 0.001 0.001
#time_window: 21e-9
#material: 6 0 1 0 aggregate
#material: 6 0 1 0 aggregateg
#material: 4 0 1 0 dry_sand
#box: 0 0 0.3 2 0.001 0.5 dry_sand n
#python:
import random
import math
from gprMax.input_cmd_funcs import cylinder
from gprMax.input_cmd_funcs import box
from gprMax.input_cmd_funcs import sphere
class Aggregate():
    def __init__(self, p_aggregate):
        self.x = random.uniform(0.001, 1.99)
        self.z = random.uniform(0.5, 0.8)
```

```
        if p_aggregate > 0.60:
            lower = 0.004
            upper = 0.008
        if p_aggregate > 0.80:
            lower = 0.006
            upper = 0.010
        else:
            lower = 0.010
            upper = 0.020
        radius = random.uniform(lower, upper)
        self.r = radius
    def check_collision(self, aggregate, agg):
        j = 0
        no_coll = False
        while j < len(aggregate) and no_coll is False:
            other = aggregate[j]
            point_dist = math.sqrt((agg.x - other.x)**2 + (agg.z - other.z)**2)
            j += 1
            if point_dist <= agg.r + other.r:
                no_coll = True
        return no_coll
area_sum = 0
p_aggregate = 0
area_box = 1.95 *  0.29
aggregate = []
while p_aggregate < 0.6:
    agg = Aggregate(p_aggregate)
    if agg.check_collision(aggregate, agg) is False:
        aggregate.append(agg)
        area_sum +=  math.pi * agg.r**2
        p_aggregate = area_sum / area_box
for i in range(0, len(aggregate)):
```

```
    agg = aggregate[i]
    sphere(agg.x, 0.001, agg.z, agg.r, 'aggregate', 'n')
class Aggregateg():
    def __init__(self, p_aggregateg):
        self.x = random.uniform(0.001, 1.99)
        self.z = random.uniform(0.3, 0.5)
        if p_aggregateg > 0.60:
            lower = 0.002
            upper = 0.003
        if p_aggregate > 0.80:
            lower = 0.001
            upper = 0.002
        else:
            lower = 0.008
            upper = 0.012
        radius = random.uniform(lower, upper)
        self.r = radius
    def check_collision(self, aggregateg, agg):
        j = 0
        no_coll = False
        while j < len(aggregateg) and no_coll is False:
            other = aggregateg[j]
            point_dist = math.sqrt((agg.x - other.x)**2 + (agg.z - other.z)**2)
            j += 1
            if point_dist <= agg.r + other.r:
                no_coll = True
        return no_coll
area_sum = 0
p_aggregateg = 0
area_box = 1.95 *  0.17
aggregateg = []
while p_aggregateg < 0.6:
```

```
        agg = Aggregateg(p_aggregateg)
        if agg.check_collision(aggregateg, agg) is False:
            aggregateg.append(agg)
            area_sum +=  math.pi * agg.r**2
            p_aggregateg = area_sum / area_box
    for i in range(0, len(aggregateg)):
        agg = aggregateg[i]
        sphere(agg.x, 0.001, agg.z, agg.r, 'aggregateg', 'n')
    #end_python:
```

```
#soil_peplinski: 0.73 0.27 2.0 2.66 0.001 0.1 my_soil
#fractal_box: 0 0 0 2 0.001 0.3 1.5 1 1 1 50 my_soil my_soil_box
#waveform: gaussian 1 1.6e9 my_gaussian
#hertzian_dipole: y 0.04 0 0.8 my_gaussian
#rx: 0.06 0 0.8
#src_steps: 0.03 0 0
#rx_steps: 0.03 0 0
```

A4 Railway water content and cavity with in the track bed layer of input data for GPRMax Software.

```
#title: Railway_Cavity_2D
#domain: 2 0.001 0.9
#dx_dy_dz: 0.001 0.001 0.001
#time_window: 21e-9
#material: 6 0 1 0 aggregate
#material: 6 0 1 0 aggregateg
#material: 5 0 1 0 dry_sand
#material: 3 0 1 0 dry_clay
#material: 20 0 1 0 wet_sand
#material: 30 0 1 0 wet_clay
#material: 1 0 1 0 Air
#box: 0 0 0.3 1 0.001 0.5 dry_sand n
#box: 0 0 0.5 1 0.001 0.8 dry_clay n
#box: 1 0 0.3 2 0.001 0.5 wet_sand n
#box: 1 0 0.5 2 0.001 0.8 wet_clay n
```

```
#python:
import random
import math
import numpy as np
from gprMax.input_cmd_funcs import cylinder
from gprMax.input_cmd_funcs import box
from gprMax.input_cmd_funcs import sphere
class Aggregate():
    def __init__(self, p_aggregate):
        self.x = random.uniform(0.001, 1.99)
        self.z = random.uniform(0.5, 0.8)
        if p_aggregate > 0.60:
            lower = 0.004
            upper = 0.008
        if p_aggregate > 0.80:
            lower = 0.006
            upper = 0.010
        else:
            lower = 0.010
            upper = 0.020
        radius = random.uniform(lower, upper)
        self.r = radius
    def check_collision(self, aggregate, agg):
        j = 0
        no_coll = False
        while j < len(aggregate) and no_coll is False:
            other = aggregate[j]
            point_dist = math.sqrt((agg.x - other.x)**2 + (agg.z - other.z)**2)
            j += 1
            if point_dist <= agg.r + other.r:
                no_coll = True
        return no_coll
```

```
area_sum = 0
p_aggregate = 0
area_box = 1.95 *  0.29
aggregate = []
while p_aggregate < 0.6:
    agg = Aggregate(p_aggregate)
    if agg.check_collision(aggregate, agg) is False:
        aggregate.append(agg)
        area_sum +=  math.pi * agg.r**2
        p_aggregate = area_sum / area_box
for i in range(0, len(aggregate)):
    agg = aggregate[i]
    sphere(agg.x, 0.001, agg.z, agg.r, 'aggregate', 'n')
class Aggregateg():
    def __init__(self, p_aggregateg):
        self.x = random.uniform(0.001, 1.99)
        self.z = random.uniform(0.3, 0.5)
        if p_aggregateg > 0.60:
            lower = 0.002
            upper = 0.003
        if p_aggregate > 0.80:
            lower = 0.001
            upper = 0.002
        else:
            lower = 0.008
            upper = 0.012
        radius = random.uniform(lower, upper)
        self.r = radius
    def check_collision(self, aggregateg, agg):
        j = 0
        no_coll = False
        while j < len(aggregateg) and no_coll is False:
```

```
            other = aggregateg[j]
            point_dist = math.sqrt((agg.x - other.x)**2 + (agg.z - other.z)**2)
            j += 1
            if point_dist <= agg.r + other.r:
                no_coll = True
        return no_coll
area_sum = 0
p_aggregateg = 0
area_box = 1.95 *  0.17
aggregateg = []
while p_aggregateg < 0.6:
    agg = Aggregateg(p_aggregateg)
    if agg.check_collision(aggregateg, agg) is False:
        aggregateg.append(agg)
        area_sum +=  math.pi * agg.r**2
        p_aggregateg = area_sum / area_box
for i in range(0, len(aggregateg)):
    agg = aggregateg[i]
    sphere(agg.x, 0.001, agg.z, agg.r, 'aggregateg', 'n')
#end_python:
```

```
#soil_peplinski: 0.73 0.27 2.0 2.66 0.001 0.05 my_soil
#fractal_box: 0 0 0 2 0.001 0.3 1.5 1 1 1 50 my_soil my_soil_box
#cylinder: 0.332 0 0.138 0.332 0.001 0.138 0.040 Air
#cylinder: 1.618 0 0.138 1.618 0.001 0.138 0.040 Air
#waveform: gaussian 1 0.4e9 my_gaussian
#hertzian_dipole: y 0.040 0 0.80 my_gaussian
#rx: 0.060 0 0.80
#src_steps: 0.03 0 0
#rx_steps: 0.03 0 0
#snapshot: 0 0 0 2 0.001 0.9 0.001 0.001 0.001 21e-9 snap_cavity
#geometry_view: 0 0 0 2 0.001 0.9 0.001 0.001 0.001 Railway_Cavity n
```

APPENDIX B

B1, Homogenous model simulation result of B-Scan, frequency spectrum and A-scan of each ballast condition with respect to 400MHz, and 1600MHz antenna.

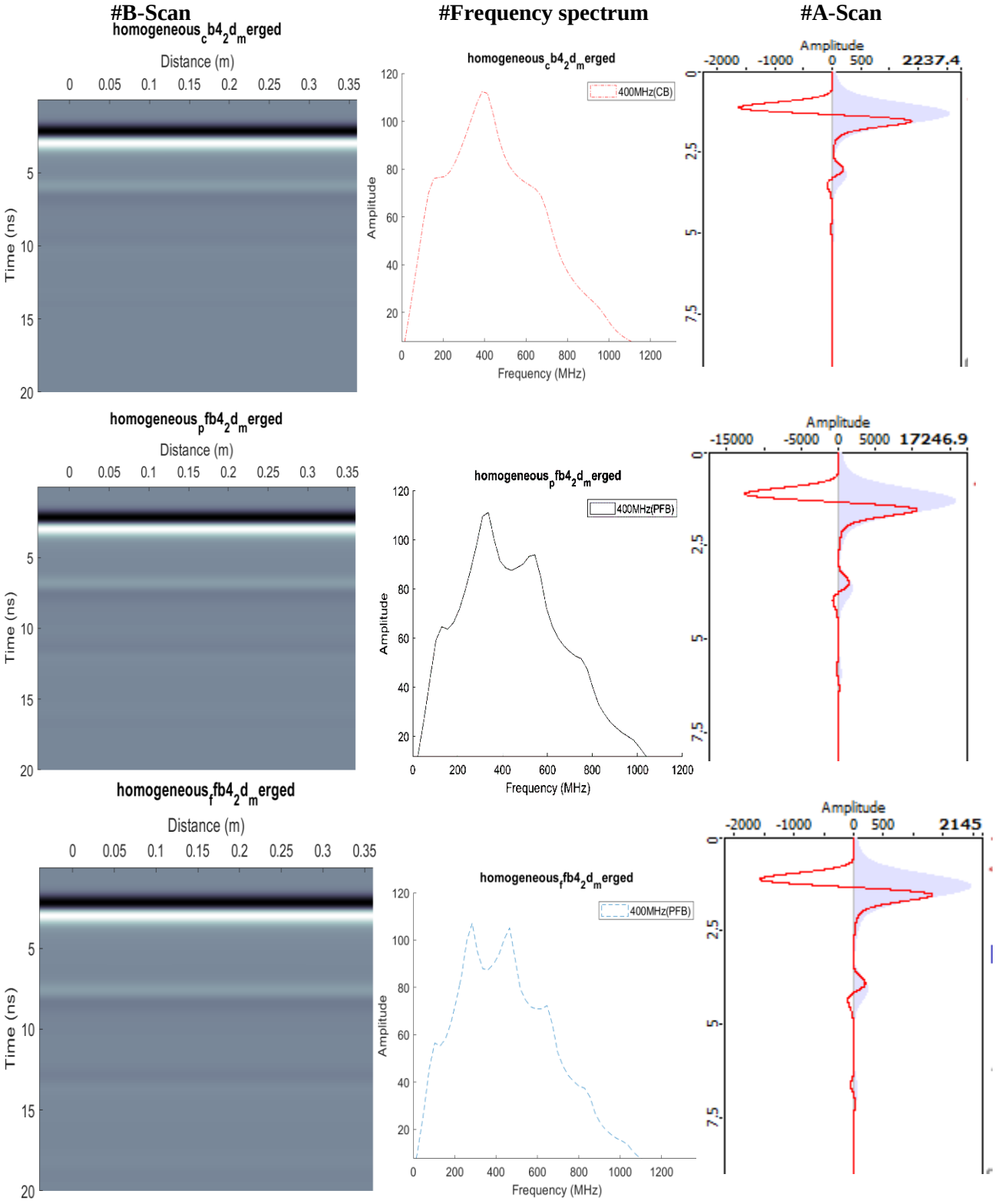

Output of 1600MHz frequency Antenna

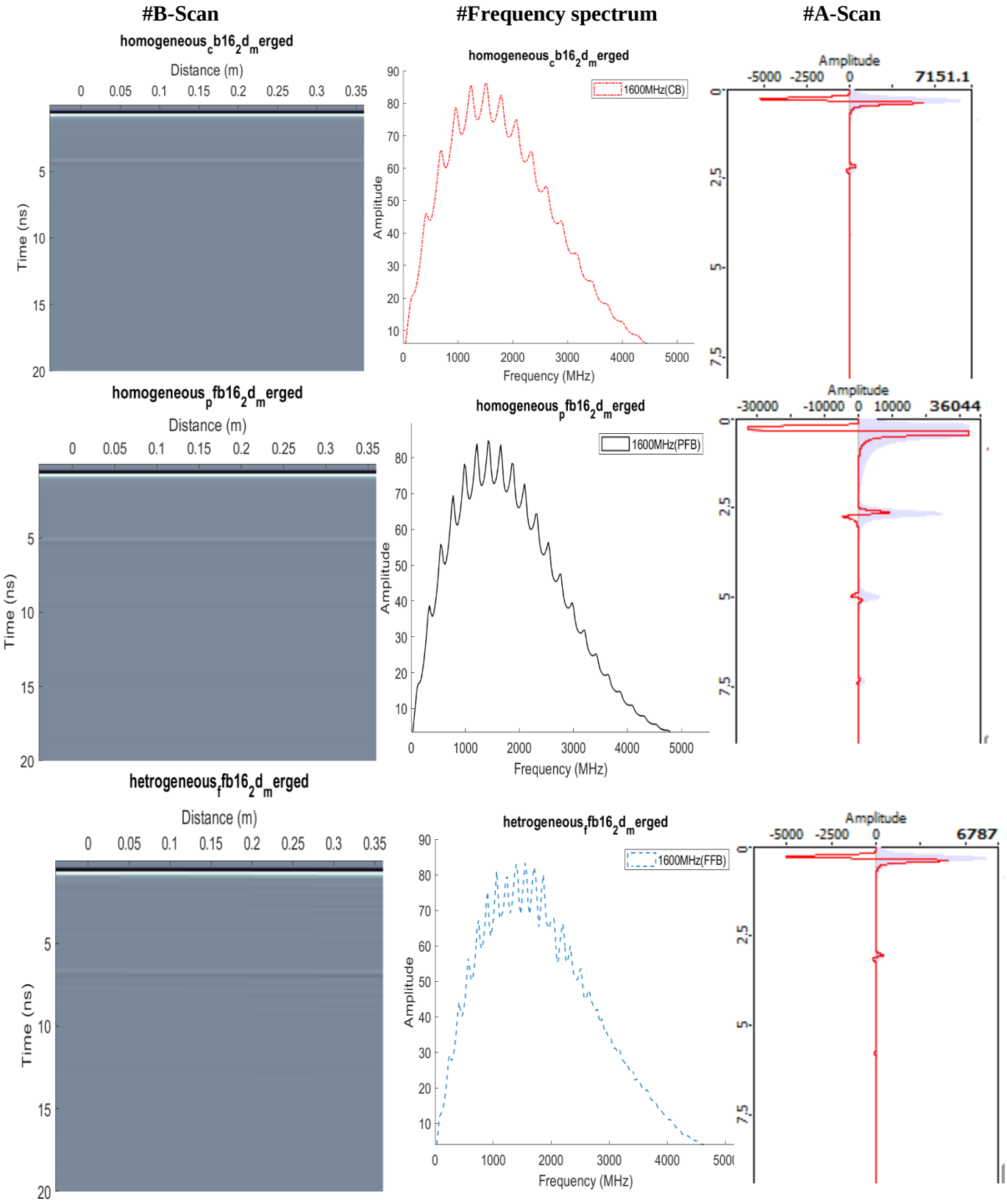

B2, Heterogeneous model simulation result of B-Scan, frequency spectrum and A-scan of each ballast condition with respect to 400MHz, 900MHz and 1600MHz antenna.

- 400MHz Antenna

#B-Scan **#Frequency spectrum** **#A-Scan**

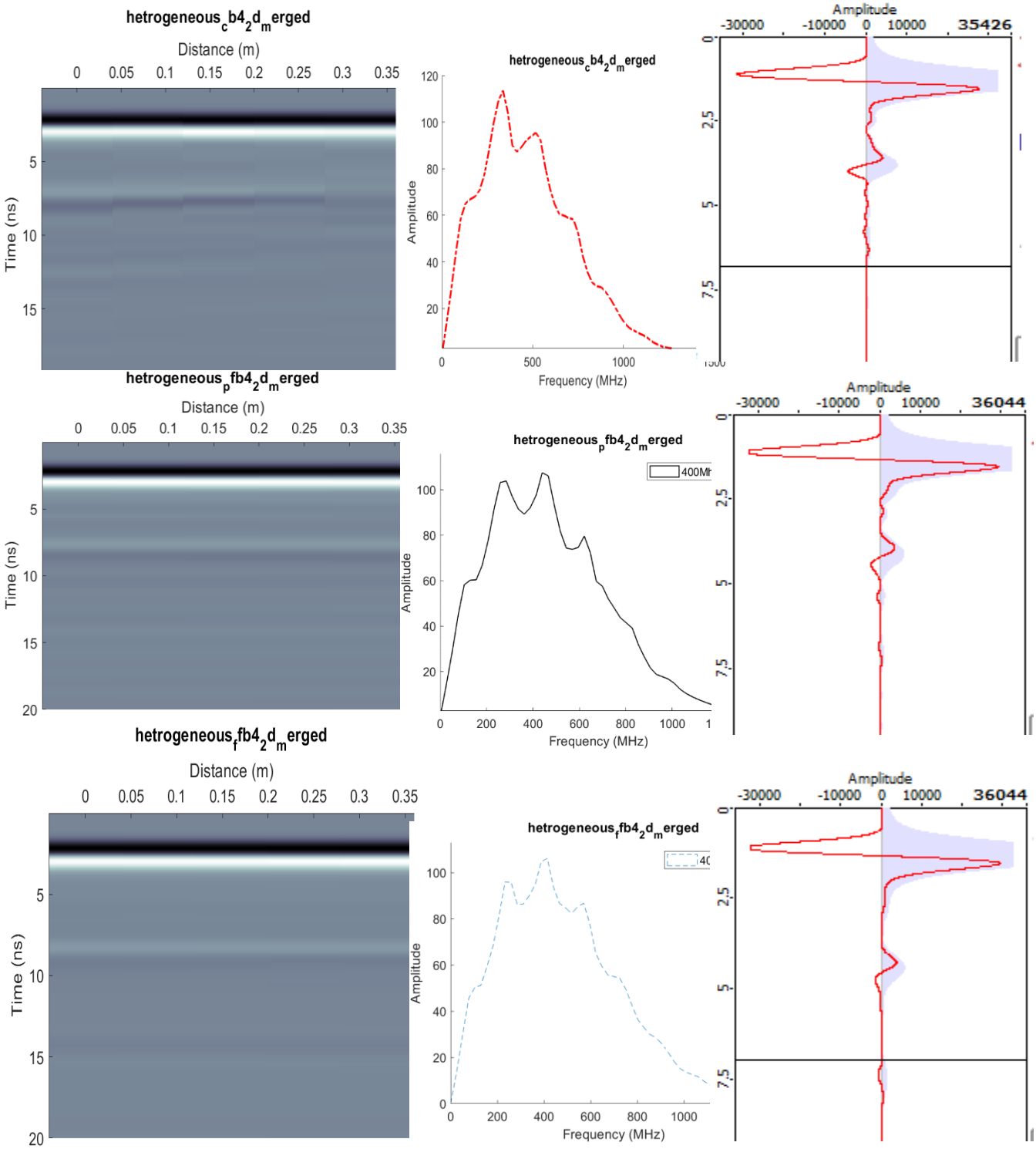

- 900MHz Antenna

#B-Scan **#Frequency spectrum** **#A-Scan**

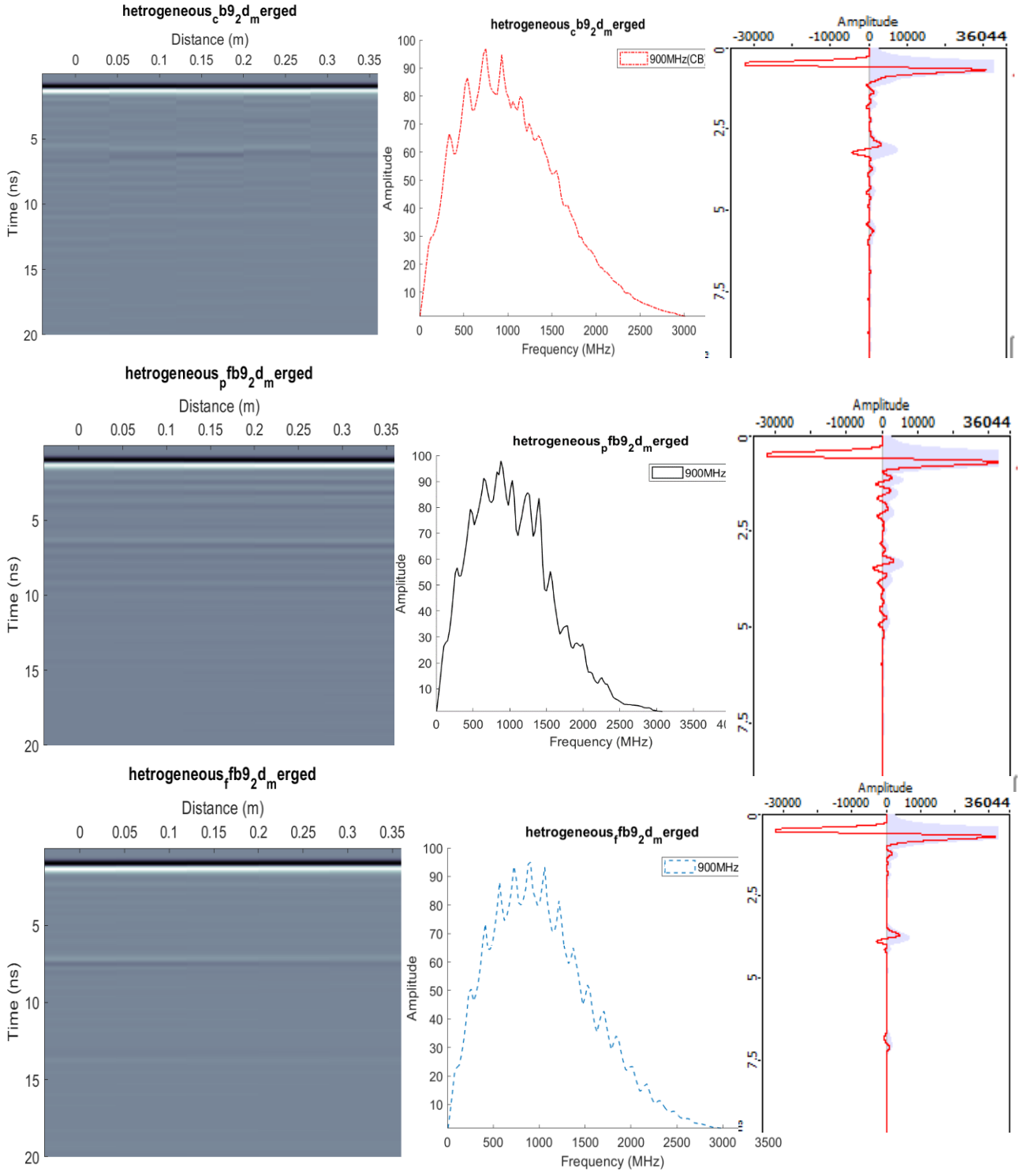

- 1600MHz Antenna

#B-Scan **#Frequency spectrum** **#A-Scan**

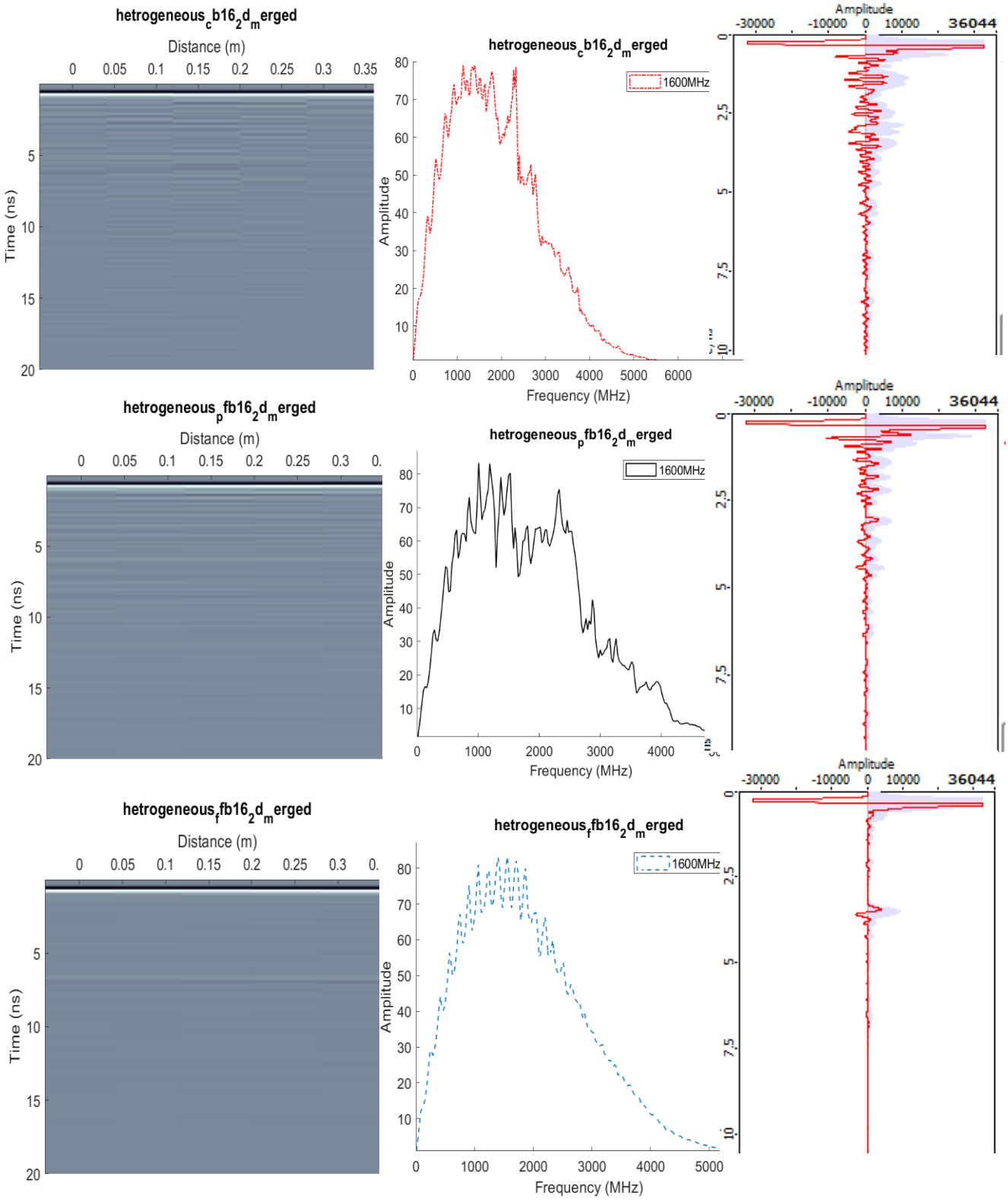

APPENDIX C

ParaView 5.11.3 Software

ParaView is an open-source, multi-platform scientific data analysis and visualization tool that enables analysis and visualization of extremely large datasets. ParaView is both a general purpose, end-user application with a distributed architecture that can be seamlessly leveraged by your desktop or other remote parallel computing resources and an extensible framework with a collection of tools and libraries for various applications including scripting (using Python), web visualization (through ParaViewWeb), or in-situ analysis (with Catalyst).

You can also show the data in a view to produce images or renderings. Just as there are several types of filters, each performing different operations and types of processing, there are several kinds of views for generating various types of renderings including 3D surface views, 2D bar and line views, parallel coordinate views, etc.

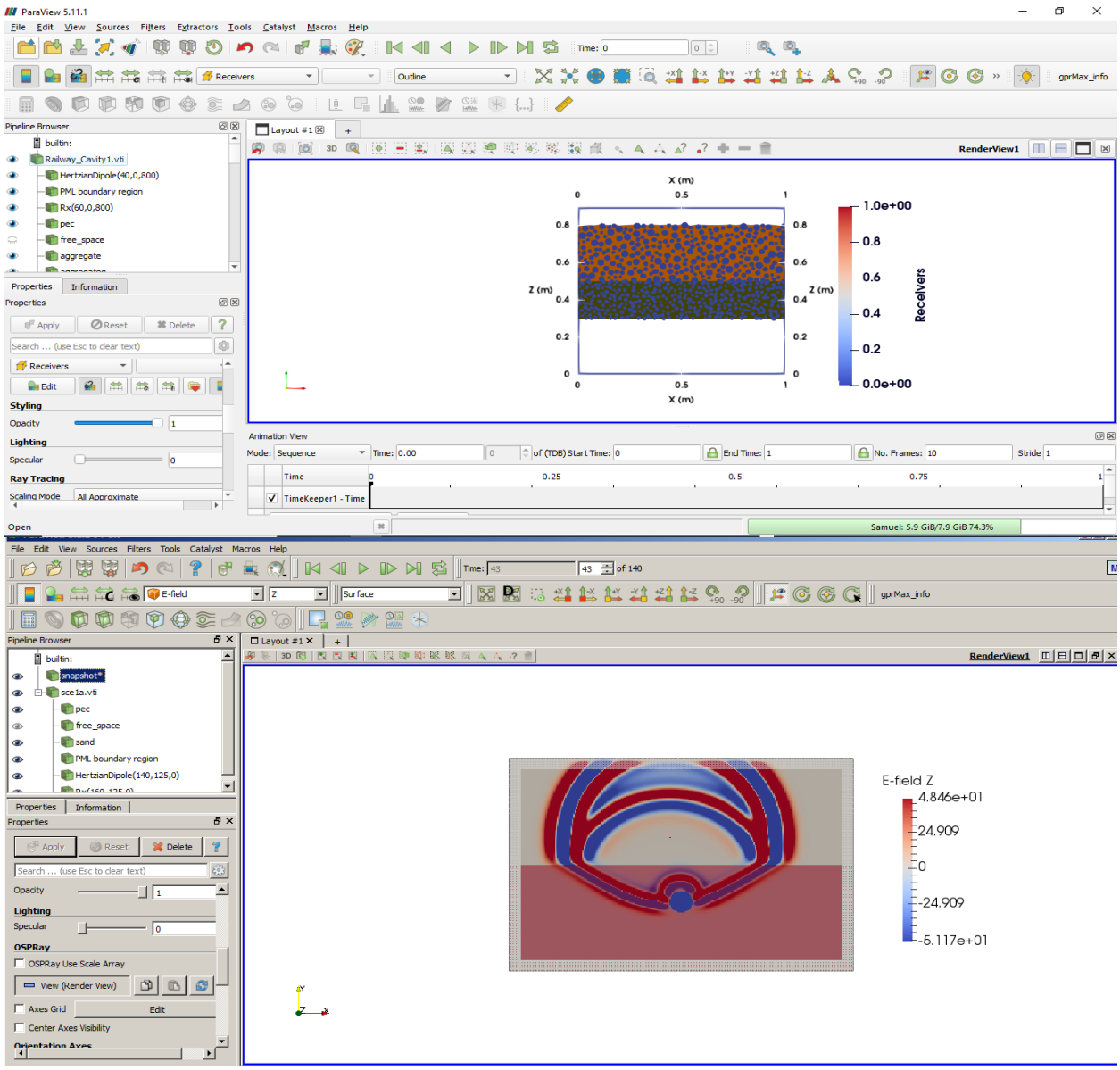

Prisim2 Software

Prism2 software is designed for geo radar parameter control, sounding data reception with simultaneous computer display and hard disc file record as well as for file processing and printout.

All of the geo radar parameters (except the on/off function) are controlled via a computer which facilitates operation of the hardware. In the course of tuning the radar and performing the sounding, the software outputs error messages if parameter settings are incorrect, and suggests proper steps to be taken. Useful keyboard-oriented interface for geo radar management and data acquisition. You don't need touch mouse (trackball, touchpad...) on your Notebook when work in field condition.

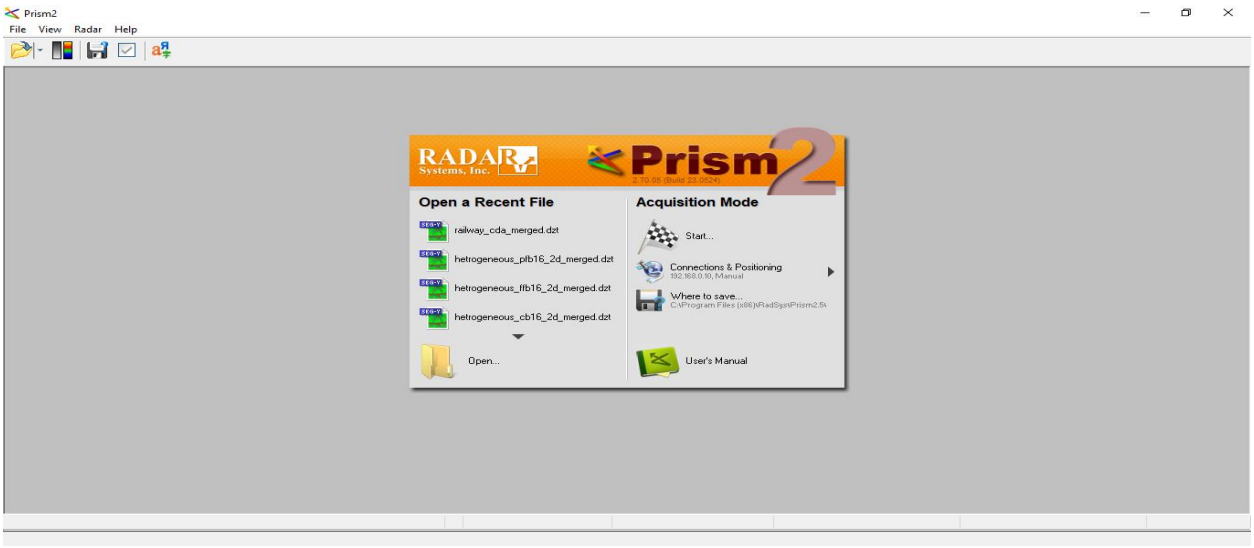

MATLAB R2023a Software

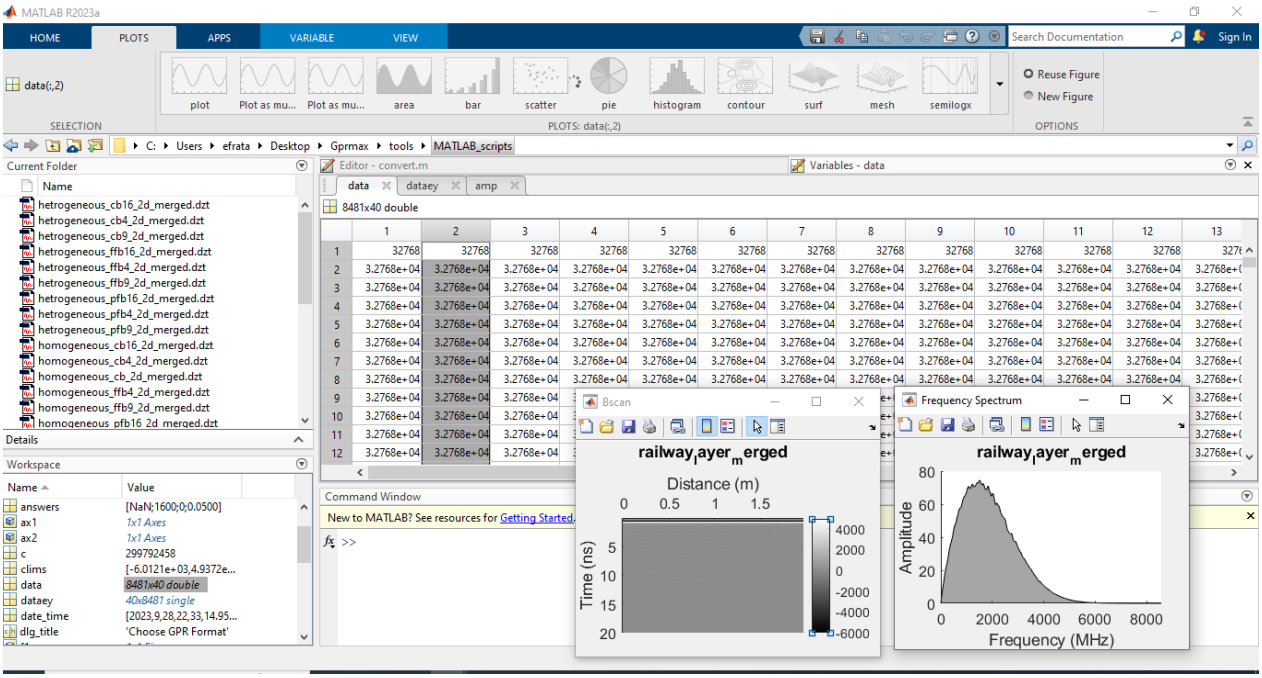

GPRMax Open Source Software

gprMax is open source software that simulates electromagnetic wave propagation. It solves Maxwell's equations in 3D using the Finite-Difference Time-Domain (FDTD) method. gprMax was designed for modelling Ground Penetrating Radar (GPR) but can also be used to model electromagnetic wave propagation for many other applications.

gprMax is principally written in Python 3 with performance-critical parts written in Cython. It includes a CPU-based solver parallelised using OpenMP, and a GPU-based solver written using the NVIDIA CUDA programming model.

Alongside improvements to the input file there is a new output file format – HDF5 – to manage the larger and more complex data sets that are being generated. HDF5 is a robust, portable and extensible format with a number of free readers available.

User guide https://www.gprmax.com and https://docs.gprmax.com/en/latest

Picture indicate simulation process on CMD(command Prompt) .